


Center for Advanced Biomaterials for Health Care,
Università Federico II di Napoli, NAPOLI

Ph.D. course in
Industrial product and process Engineering

Ph.D Thesis

Engineered Extracellular Vesicles: Processing and testing of cell-derived Exos

Coordinator:

Prof. Andrea D'Anna

Supervisors:

Prof. Paolo Antonio Netti

Prof.Enza Torino

Candidate:

Eugenia Romano

Contents

Introduction

More than 40 years ago, vesicle structures, similar to “cytoplasmic fragments” physiologically released, were identified in the cellular matrix. Their peculiarity was their ability to contain various materials, including ribosomes, which are involved in several pathological and physiological activities. After being initially considered as part of the lysosomal degradation pathway [1] through which the cell ejected its waste, they are now recognized as important messengers involved in proximal and distal intercellular communication. These systems were defined as extracellular vesicles (EVs), and they include a wide variety of vesicles (from 30 nm to 5 μm) released from the plasma membrane (PM) of many different cell types into several bodily fluids, including plasma, milk, saliva, sweat, tears, semen, and urine [2, 3].

All EVs present a lipid bilayer membrane that surrounds a pool of genetic material, cytosolic proteins, or cellular debris [4]. However, they significantly differ in terms of size, biogenesis, mechanisms, and function. For this reason, they are generally categorized into three subtypes: exosomes (Exos), ectosomes, or Shedding MicroVesicles (SMVs) and apoptotic bodies [5, 6].

Exos have sizes ranging between 30 and 150 nm and represent a homogenous population of EVs released from cells when multivesicular bodies (MVBs) are fused with the membrane through inward budding in a highly regulated process [7].

In contrast, SMVs are a more heterogeneous population of EVs, with a size ranging from 50 nm to 1 μm, which are formed under specific physiological stimuli, such as calcium-dependent signaling, by the budding and shedding of PM [5, 6].

Consequently, Exos and SMVs are currently believed to have endosomal and PM origins, respectively [8].

Finally, apoptotic bodies, composed of cytoplasmic organelles and fragmented nuclei, are EVs 1–5 μm in diameter. They are formed when a cell is dying via apoptosis. After the disruption of PM, the cytoplasmic content is divided into different membrane-enclosed vesicles [9].

Among these membrane vesicles, the role of Exos in cancer research has been rapidly growing over the last two decades. Cancer cells release a high number of Exos containing many functional biomolecules in the extracellular space. EVs transfer proteins, receptors, and small RNAs that regulate both physiological and pathological processes. Moreover, the lipid bilayer membrane protects the exosome cargo from degradation in the bloodstream, allowing crossing different physiological barriers, such as the Blood–Brain Barrier (BBB) [10].

BBB is one of the most complex and selective barriers in the human organism. Its principal role is to preserve the homeostasis of the central nervous system and protect the brain parenchyma against the invasion of inflammatory mediators, which may interrupt its critical function [11]. The BBB, together with pericytes, perivascular astrocytes, microglia, and neurons, forms a functional unit called the neurovascular unit. Interestingly, EVs regulate the communication between cells in short or long distances within the neurovascular unit [12]. Furthermore, Exos cargo such as miRNAs, proteins, and other physiological compounds reflect different brain disease progression stages, allowing their use as a “window to the brain” [11].

As natural carrier systems, EVs present low immunogenicity, low toxicity, stability in the bloodstream, and efficient cell uptake due to their endogenous cellular tropism [13]. Their ability to

mediate intercellular communication, especially in tumor progression, allows their use as a promising therapeutic and diagnostic tool [14-21].

Biogenesis of Exos: A Spontaneous Formation

The biogenesis and release of Exos in the extracellular space initiate an endocytic pathway at the PM [9]. Even though this event is not entirely clarified, it begins with the formation and progressive accumulation of intraluminal vesicles (ILVs) in MVBs. These late vesicles elude the lysosomal digestive system and, after the fusion with the PM, are finally secreted into the extracellular space [22].

The physiological mechanism related to exosome formation and secretion is mediated via an Endosomal Sorting Complex Required for Transport (ESCRT)-dependent and/or ESCRT-independent pathway [23] (Figure 1).

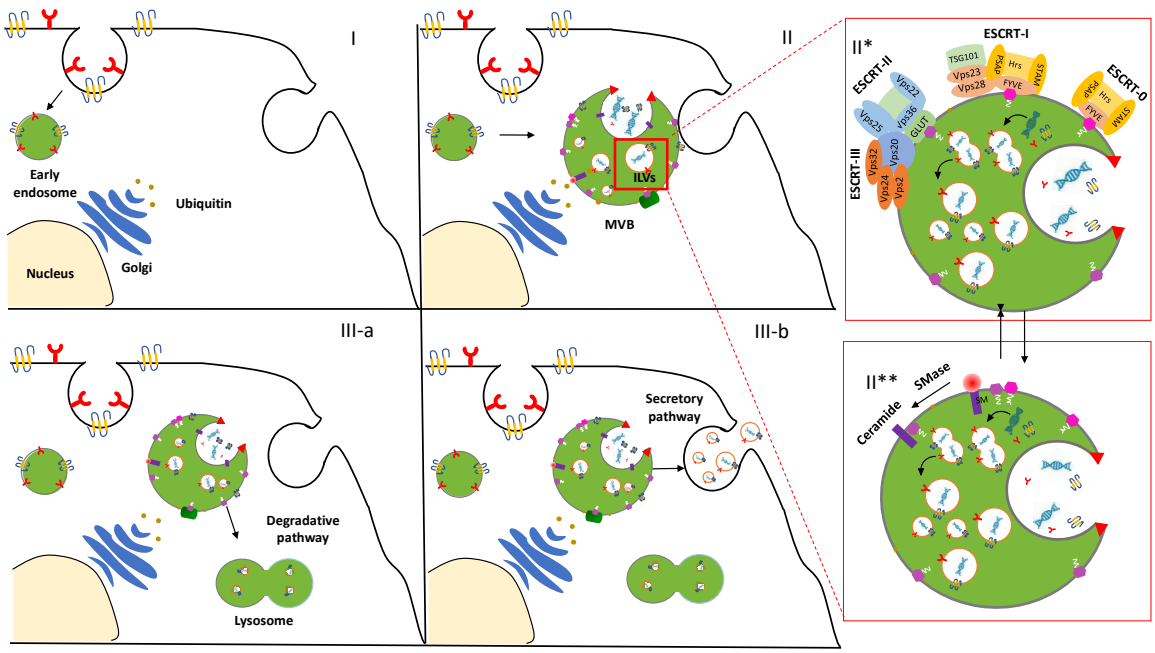

Figure 1. Biogenesis and secretion of Exos. After the endocytosis of the plasma membrane, the transmembrane proteins are sorted into the vesicles that bud from the cellular membrane into "early endosomes" (I). The biogenesis of the Exos begins with the progressive formation and accumulation of ILVs inside MVBs (II). This process is mediated via an ESCRT-dependent (II*) and/or independent (II**) pathway. Then, the MVBs may follow a degradation pathway fusing with lysosomes or are destined to release the ILVs as Exos to the extracellular space by exocytosis (III).

ESCRT-Dependent Pathway

ESCRT machinery, conserved throughout eukaryotic and yeast cells, consists of four complexes—ESCRT-0, -I, -II, and -III—which act sequentially to bind and cluster ubiquitinylated proteins in the late endosome [24]. In particular, ESCRT-0 is involved in cargo clustering, ESCRT-I and ESCRT-II induce bud formation, and ESCRT-III drives vesicle scission. ILVs formation begins with the

interaction between ESCRT-0—in particular, the two subunits hepatocyte growth-factor-regulated tyrosine kinase substrate (Hrs) and Signal Transducing Adaptor Molecule (STAM) in eukaryotic cells—and the region of the FYVE domain [25, 26] of the endosomal lipid PhosphatidylInositol 3-Phosphate (PtdIns(3)P). Subsequently, the PSAP sequence (residues 348–351) in Hrs interacts with the Ubiquitin E2 Variant (UEV domains) of Tsg101 and Vps23 expressed in ESCRT-I, making possible both the formation of the ESCRT-0/ESCRT-I complex and the recruitment of ESCRT-I to endosomal membranes [27].

Then, the Vps36 subunit of ESCRT-II binds the ESCRT-I Vps28 C-terminal domain [28] through its GLUE N-terminal domain. ESCRT-III, the most ancient and preserved of the ESCRTs [29], consists of a core complex that contains the subunits Vps20, Vps32, Vps24, and Vps2, assembled in a highly ordered manner. However, these metastable subunits are present as inactive monomeric forms and, only after their conformational changes, the autoinhibition mechanism allows interactions with other ESCRT-III subunits. However, even though the activation of the assembly is not fully understood,it might happen in a directional order, so, one activated, the ESCRT-III subunit activates the next one [30, 31]. The subunit that nucleates the ESCRT-III assembly on membranes is a N-terminally myristoylated subunit (Vps20). Vps20 from ESCRT-III binds to the Vps25 subunit of ESCRT-II. Finally, through the formation of this new complex, nascent ILVs results in the closing of the cargo-containing vesicle and the pinching off of the vesicles, even though how ESCRT-III oligomerization induces membrane curvature remains still elusive [30].

ESCRT-Independent Pathway

Conversely, a recent study of mammalian cells [32] showed, through the depletion of all four ESCRT key subunits, that, despite a dramatic alteration in the morphology of cellular components, early and late endosomes remain unaffected. Evidence of an ESCRT-independent pathway was shown also for melanosomes [33], lysosome-related organelles that contain melanin-producing enzymes and produce melanin. They are assembled within melanocytes, and their biogenesis involves a series of protein sorting and vesicular trafficking events: melanosomal protein Pmel17 is sorted into ILVs by a mechanism independent of lumenal determinants, and it is not affected by the functional inhibition of Hrs and ESCRT complexes [34]. These observations led to the conclusion that eukaryotes utilize mostly the established ESCRT system, as is already understood in yeast, and, probably, additional ESCRT-independent pathways to form ILVs. Indeed, an unconventional pathway seems to be driven by the presence of certain lipids such as ceramides, as confirmed in the membrane trafficking of the proteolipid content in the oligodendroglial murine cell line [35]. These data provided evidence for an alternative pathway depending on raft-based microdomains that may contain high concentrations of sphingomyelina (SM). Therefore, the hydrolytic removal of the phosphocholine moiety of SM by sphingomyelinases (SMases) induces ceramide formation that sequentially allows the coalescence of the small microdomains into larger ones. Finally, another protein that has been suggested to play a role in exosome formation is the Small Integral Membrane Protein of the Lysosome/late Endosome (SIMPLE, also called lipopolysaccharide-induced TNF factor, LITAF) [36]. After the transfection of cells with SIMPLE, an increased secretion of Exos was observed, while SIMPLE mutation causes the loss of MVBs' proper formation and exosome biogenesis [37].

Currently, it is possible to confirm that exosome biogenesis is a complex mechanism in which several compounds are involved. Structural and biochemical analyses of the upstream components and detailed studies of all the steps involved in the assembly and disassembly of the ESCRT complex contributed to its consideration as the main one implicated in EV biogenesis and clarified insights about EV formation and function. However, several studies have proved that biogenesis was not inhibited by the depletion of ESCRT subunits. This result increased evidence that other lipids and proteins play a key role in the membrane-invagination process.

Reinforcing this point, some features have to be considered. To date, it is legitimate to describe the presence of these two distinct processes as ESCRT-dependent or ESCRT-independent mechanisms. However, the activation of these alternative pathways is not fully elucidated and some aberrant ILV morphologies were observed while the early and late endosome remained differentiated [22]. Thus, we may hypothesize that the pathways are not entirely separated. They might work synergistically or influence each other. The cell type and/or cellular homeostasis could be an essential factor in controlling Exos secretion [38].

Isolation Techniques for the Collection of the Exos

To date, Exos purification is essentially based on size exclusion [39], polymeric precipitation [40, 41], ultracentrifugation [42], and microfluidics [43, 44] techniques. An ideal purification method should isolate Exos from various biological sources in appreciable quantity and purity, but, due to their small size and heterogeneity, their isolation from interfering components, such as cellular debris and aggregated proteins, can be challenging.

Centrifugation-Based Isolation Techniques

Ultracentrifugation (UC)-based isolation is the most commonly used technique [42, 45-50] according to a worldwide International Society for Extracellular Vesicles (ISEV) survey [51].

Currently, there is a standard protocol that includes several cleaning steps before the recovery of the exosomal sample [44], despite the fact that the final purity and concentration are extremely variable (Table 1).

Generally, 3×10^{12} particles per mg (p/mg) of protein has to be considered as a high purity value. Preparations with lower ratios, around three times lower (1×10^{10} p/mg), can be achieved readily by simple pellet and wash protocols. These are naturally inferior purifications containing significantly higher levels of contaminating proteins [52].

Cell Source	Source Amount	Isolation Method	Exosome Yield	Reference
Non-Small-Lung Cancer (SK-MES-1)	150 mL Cell culture medium (CCM)	UC UF	1.3×10^{12} particles/mL 2×10^{12} particles/mL	[42]
Human colon carcinoma (LIM186)	2×10^{9} cells	UC Density gradient Immunoaffinity	375 μg protein 75 μg protein 195 μg protein	[45]
Murine melanoma (B16BL6)	-	UC	6×10^{11} particles/mL	[46]
Mouse mammary carcinoma (4T1) Human mammary adenocarcinoma (MCF-7)	2×10^{8} cells	Density gradient	-	[47]

Human prostate adenocarcinoma (PC3)				
Macrophages (Raw 264.7)	2×10^8 cells	UC	10^{11}–10^{12} Exosome/flask–1 mg/mL total protein	[48]
Human primary GBM (U-87 MG)	280 mL CCM	UC	10^{12} particles/mL	[49]
Melanoma (B16F10)	72 mL CCM	UC	$2.04 \times 10^{13} \pm 3.9 \times 10^{12}$ p/mL 451.15 ± 71.5 μg/mL $4.52 \times 10^{10} \pm 1.26 \times 10^{10}$ p/μg	[50]
Raw264.7	5×10^8 cells	UC	1 mg	[48, 53]
Mice Blood	10 mL CCM	UC	18 μg/mL protein 7.49×10^{10} particles/mL	[54]
Mesenchymal stem cells (MSC)	2×10^6 cells 10 mL CCM	UC	10 μg/mL	[55]

Table 1. Exos quantification in term of particles and μg of protein per mL significantly changes according to the isolation method, cell source, and source amount. This highlights the absence of a standardized method to obtain a homogeneous sample.

The initial centrifugations of a culture supernatant or a biological fluid at lower speeds allows, first, the removal of larger contaminants, generally at 300× g for 10 min, then of dead cells at 2000× g 10 min, and finally of cell debris at 10,000× g 30 min. In some cases, these passages are followed by supernatant filtering using a 0.2 μm syringe filter [48] to remove all particles larger than 200 nm, including residual apoptotic bodies and biological aggregates. These first pre-processing steps of culture medium are followed by proper Exos isolation. Exos pellet recovery is performed after treatments at a high speed (in a range from 100,000 to 120,000× g), resuspending it in phosphate-buffered saline (PBS). All the centrifugation steps are always performed at 4 °C to avoid the aggregation of proteins.

A valid alternative to standard UC is the density gradient UC (DG). In this case, the separation of Exos is based on their size, mass, and density in medium with a progressively decreased density from the bottom to the top of the tube. Samples are layered as a narrow band on the top of the density gradient medium and are subjected to an extended round of UC [44]. A discontinuous iodixanol gradient consisting of 40% w/v, 20% w/v, 10% w/v, and 5% w/v solutions is prepared by diluting a stock solution of OptiPrep™ in 0.25 M of sucrose/10 mM of Tris at pH 7.5. The gradient is set up in a polyallomer tube by the subsequent layering of 3 mL fractions of 40%, 20%, and 10% iodixanol solution, and 2.8 mL of 5% iodixanol solution. DG fractions of 1 mL each are collected from the top of the gradient and resuspended in PBS for a further 90 min of UC at 100,000 g [42].

The comparison of dUC, immunoaffinity, and OptiPrep™ DG revealed that this method isolated the pure population of Exos from blood plasma [4]. It allowed the elimination of contaminants and enhanced the quality of EVs analysis [56], despite the fact that it may co-isolate EVs and certain lipoproteins [57]. However, DG is a laborious and time-consuming method. Unlike differential ultracentrifugation, a downside of density gradient ultracentrifugation is that its capacity is largely limited by the narrow load zone [58] density gradients.

Polymer-Based Precipitation

The isolation of Exos by a polymer solution is relatively new, indeed, its principle was applied for the first time more than 50 years ago by Hebert [59] to isolate viruses. Prevalent results in exosome

purification mainly ensue from the use of a less time-consuming commercial kit (ExoQuickt from System Bioscience or the Total Exosome Isolation Kit from Life Technologies). This method is based on the formation of a polymer network—generally consisting of polyethylene glycol (PEG) with a molecular weight of 8000 Da—that extracts water and forces less soluble components out of the solution. Although this method has a high scalability, it requires pre and post-cleanup. Indeed, the recovery of the precipitated sample is performed after incubation at 4 °C overnight, but the final collection in PBS [44, 60] requires low-speed centrifugation or filtration.

A recent study from Chang et al. [61] presented a novel method for exosome isolation using Fe_3O_4 magnetic nanoparticles (MNPs) coated with polyethylene glycol (PEG). PEG chains can form reticular structures that allow the entrapping of proteins, aggregates, and impurities in the holes of MNP. Therefore, Exos can be purified by removing the proteins using a permanent magnet. Unfortunately, the presence of residual magnetic material can cause the necessity of a time-consuming post-purification procedure.

Indeed, most studies [62] demonstrated that polymer-based precipitation is not a specific method because of the recovery of contaminants as protein aggregates, lipoproteins, and small cellular debris. Secondly, once isolated, the presence of the polymer material may not be compatible with downstream analyses. Nevertheless, the use of polymer-based precipitation may be appropriate to achieve an initial enrichment of Exos, where the presence of contaminating non-exosomal materials can be problematic [63].

Size-Based Isolation Technique

The separation of Exos based on size exclusion can be realized using ultrafiltration (UF) membranes and/or size exclusion chromatography (SEC).

UF allows the separation of Exos from other soluble proteins and aggregates using matrices with defined molecular weight or size exclusion limits (Vivaspins® or Amicons®). These vesicles can, for example, be selectively isolated based on a molecular weight greater than 200 kDa, followed by isolation with a diameter less than 200 nm [64, 65].

UF is faster than UC and does not require special equipment. Furthermore, one or multistep concentrations can be efficient for large volume samples. However, a potential drawback could be the clogging and particle trapping due to the use of mechanical forces [44].

In SEC, the separation of Exos is due to their small dimensions compared to other cellular debris and residual impurity or protein aggregates. A sample is loaded onto a packed column and passes through a selective porous resin: larger molecules are entrapped in the network structure while small molecules can pass faster through the pores and are eluted earlier [42]. Thus, in SEC separation, it is possible to underline several advantages such as the low contamination and high purity of the final sample, whose biological activity is preserved with superior reproducibility. Nevertheless, the procedure requires a long run time, and it is not simple to scale up.

Microfluidic Technology for the Separation of the Exos

Although the development is still at an early stage, microfluidic technology is emerging as an efficient and rapid alternative to conventional isolation methods.

The techniques developed for microfluidic-based exosomal purification can be classified into two categories: chips with or without the application of external sources. The first ones allow an active sorting of the final sample due to the application of external sources such as an electric or magnetic field. Chips with no external forces achieve a passive sorting of nano-size objects through the integration of microfluidic components that drive Exos into specific streamlines and immunoaffinity/size exclusion entrapping principles [66].

Immunoaffinity isolation exploits a specific interaction between characteristic surface proteins, membrane-bound antigens expressed by a specific subtype of EV, and immobilized antibodies. The isolation of the desired EV population could be obtained with an immuno-enrichment positive trapping or a negative selection of the unwanted exosome population (immuno-depletion) [67]. In 2010, Chen et al. demonstrated the rapid recovery of small EVs from both serum and conditioned culture medium with a microfluidic device containing antibody-coated surfaces [43].

The first example of size-based separation was reported by Davies et al. [68]. They sieved EVs directly from mouse blood through a pressure-driven filtration process on a membrane. Porous polymer monoliths were integrated into poly (methyl methacrylate) microfluidic chips as membranes with a proper size for the extraction of vesicles [68].

Wang and colleagues [69] designed a ciliated micropillar structure forming a microporous silicon nanowire. This nanowire-on-micropillar structure was able to trap particles selectively in the range of 40–100 nm. Silicon pillars were designed to have a distance too narrow (900 nm) to allow the passage of cells larger than 1 μm; at the same time, smaller cell debris can enter the micropillar area but is excluded by the ciliated nanostructure, which forms pores with diameters ranging between 30 and 200 nm in order to trap Exos and small EVs selectively [70]. This method allows the selective sorting of vesicles with dimensions of less than 100 nm. However, even though the trapping step is relatively fast (10 min), the final recovery of the exosomal sample requires dissolving the ciliated part of the silicon nanowire in PBS buffer overnight. Furthermore, active sorting mechanisms, such as acoustic separation and electromagnetic activation, could represent a valid alternative to usual microfluidics approaches. An acoustic nanofilter, as shown by Lee at al. [71] could use ultrasound standing waves to exert radiation forces on the biological fluid and allow the vesicles' separation according to their mechanical properties such as their size and density.

All microfluidic technologies present important advantages compared to standard isolation techniques: they are not very time consuming, have high reproducibility, and allow the sorting of an EV subtype population. Nevertheless, generally, further off-chip additional steps for sample preparation are required, such as plasma extraction or reagent mixing [70], and these techniques are restricted to low sample volumes.

For this reason, all the mentioned techniques are not always mutually exclusive, and it is possible to combine them or apply slight variations to the protocols within each group in order to overcome limitations in the purification processes.

It seems evident that technologies for the quality control and mass production of Exos are desperately needed to achieve fast, highly efficient extraction procedures. Indeed, to overcome this invalidating drawback, recent studies seem to address more the molecular engineering of EVs.

Architectures of Exos and Their Biological Composition

An enormous heterogeneity characterizes the Exos architecture in terms of proteins, lipids, and genetic material, including messenger RNAs (mRNAs), microRNAs (miRNAs), other small non-coding RNAs, and genomic DNA (gDNA) expressed on the EV surface [72]. Regarding their biological composition, to date, a few studies have been conducted on specific cell lines highlighting this complex aspect. Among these studies, the highest cholesterol concentration (41–46%) was interestingly found in Exos obtained from reticulocytes and human prostate cancer cells (PC-3). Even though Exos secreted from oligodendrocytes only contain 2.2% cholesterol, they are highly enriched in phosphatidylcholine (40%), phosphatidylserine (25%), and phosphatidylethanolamine (20%). In contrast, 50% of the lipids found in B-cell-derived Exos are ceramides [73].

The lipidomes of Huh7 Exos showed a marked enriching of cardiolipins and lyso-derivatives (where one fatty acid tail is removed by hydrolysis) of phosphatidylserines, phosphatidylglycerols, and phosphatidylinositols. Meanwhile, lyso-phosphatidylethanolamines are rather enriched in U-87 MG Exos. These lyso-derivatives are also enriched in Marrow Stromal Cell MVs but depleted from U-87 MG and Huh7 MVs [74]. Thus, the variety of the lipidic composition characterizes not only the EVs derived from different progenitor cells but also those derived from the same population.

Likewise, EVs' proteome data suggests that the exosomal and MV proteomes of the same source-cell type are not directly comparable. Traditional Exos markers CD81 and CD9 are present both in MSC Exos and MVs, but the level of enrichment seems to be higher in Exos, while the PLP2 enrichment is unique to MVs.

Secondly, also the proteome profile of Exos obtained from different source-cell types seems to be quite different. For example, Exos isolated from cerebrospinal fluid (CSF) have specific proteins related to their tissue of origin. Tissue expression mapping according to the Database for Annotation, Visualization and Integrated Discovery (DAVID) knowledge base showed the presence of 373 brain-derived proteins; several markers of specific brain cell types, such as the typical microglia marker integrin alpha-M (ITGAM) and the receptor-type tyrosine-protein phosphatase C (PTPRC); and also neuron-specific markers such as enolase 2 (ENO2), dihydropyrimidinase-related protein 2 (DPYSL2), and vesicle-associated membrane protein 2 (VAMP2), which is a component of the soluble N-ethylmaleimide-sensitive factor attachment protein receptors (SNARE) complex [75].

Otherwise, Tsg101, PDCD6IP (Alix), and CD82 are only enriched in U-87 MG Exos, while Flotillin-1 and tetraspanin-4 are highly enriched in all U-87 MG and Huh7 EVs [74]. Despite the variable composition, Immuno-Electron Microscopy localization studies, Western blot analysis, and the mapping of exosomal proteins have identified some common proteins located on the surface or in the lumen of nearly all Exos (exosomal markers). Notably, Exos are highly enriched in cytoplasmic proteins with various functions. Most Exos contain MHC class I molecules and heat-shock proteins such as Hsp70 and Hsp90 as part of the stress response [76]. A significant number of proteins, such as tetraspanins (CD9, CD63, CD81) and Rab proteins (Rab11, Rab27a, Rab27b), are involved in their biogenesis process [77], while tubulin, actin, actin-binding proteins, and annexins proteins are responsible for membrane transport and fusion. Signal transduction and exosome release are instead mediated by protein kinases, heterotrimeric G-proteins, and molecules such as Alix and TSG101 [78].

Since Exos have been discovered in almost all body fluids, including blood, urine, saliva, breast milk, cerebrospinal fluid, semen, amniotic fluid, and ascites [79], their specific profile (miRs, proteins, and lipids) can mirror the cellular origin and its physiological state as a “fingerprint” [80].
The application of Exos in liquid biopsy could represent a valid alternative to traditional invasive methods in clinical diagnosis. However, although these markers are often enriched in specific Exos, they are also present in EVs released by other progenitor cells.

Mechanism of Interaction in the Biological Environment

The rising interest in EVs is due to their capacity to induce phenotypic changes in acceptor cells [81]. Exos play a key role in the systemic propagation of patho-physiological mechanisms, including development, homeostasis, and immune surveillance/pathogen response [82]. EVs’ internalization and regulatory properties depend on factors such as the maturation, physiological and environmental conditions of target cells, or even on the vesicular proteomic and lipidomic profile generally determined by the progenitor cell type [83]. The fact that EVs’ cargo reflects their tissue of origin is relevant, since cancer cells are known to produce greater numbers of EVs containing signaling molecules compared to healthy cells.
First of all, tumor-derived EVs at hypoxic conditions stimulate the neo-vascularization and propagation of the angiogenic phenotype to endothelial cells [84]. EVs’ angiogenic cargo includes a wide range of molecules such as tissue factors, cytokines, tetraspanin, oncoproteins, sphingomyelin, and miRNAs [85]. As an example, a recent mass spectrometry analysis of GBM Exos identified over 1000 proteins that exert angiogenic and tumor-invasive characteristics [85]. Pro-angiogenic factors include angiogenin, IL-6, IL-8, TIMP-1,and TIMP-2 that stimulate an angiogenic phenotype in normal brain endothelial cells and increase malignancy in a hypoxia-dependent manner [86].
Furthermore, tumor-derived EVs modulate the extracellular matrix through the proteolytic degradation of collagens, LNs, and fibronectin [87]. Matrix degradation has severe consequences on the tumor microenvironment, such as promoting host cell adhesion, motility, invasiveness, and apoptosis resistance. As an example, malignant ovarian ascites samples from patients with stage-I to -IV ovarian cancer contain matrix metalloproteases MMP-2-, MMP-9-, and uPA-loaded EVs with highly invasive properties [88]. Hallal et al. [89] reported increased podosome formation and extracellular matrix degradation in astrocytes cultured with GBM Exos. Interestingly, this phenomenon seems to strongly correlate with tumorigenesis through decreased p53 levels. As consequence, EVs modify neighboring astrocytes to induce tumor-supportive functions and, moreover, drive peritumoral astrocytes to become tumorigenic themselves.
Conversely, in normal circumstances EVs are important in tissue homeostasis and organogenesis [90].
For example, platelet-derived EVs induce angiogenesis in vivo by facilitating the formation of endothelial capillaries [91]. Relevant studies show that Exos produced by neurons, oligodendrocytes, astrocytes, and microglia have a key role in the protection and repair of brain tissue [92]. They could protect neurons by inhibiting neuronal apoptosis, modulate axon reconstruction and neurogenesis through vascular regeneration, and increase synaptic vesicle release [90]. For example, microglia-derived EVs can alleviate acute inflammatory responses by converting immature IL-1b into a

biologically active molecule; regulate the excitation inhibition balance via the endocannabinoids content; and reduce the levels of amyloid-β, a neurotoxic peptide linked to Alzheimer's disease [93]. Once released in the extracellular space, Exos internalization in a recipient cell occurs via two different mechanisms: direct interaction resulting in EV fusion with PM or endocytic uptake.

Endocytosis seems the principal pathway. It can involve multiple routes: the clathrin-dependent or independent pathway, the caveolin-mediated mechanism, micropinocytosis, phagocytosis, or lipid raft-mediated uptake [94]. Lipid composition is heavily involved in intracellular trafficking. The phosphatidylserine enrichment of oligodendrocyte-derived Exos activated pinocytosis in a subset of microglia macrophages without antigen-presenting capability [95]. Additionally, the sphingolipids within the EV have an important role in binding and endocytosis, possibly through cholesterol-rich microdomains in dendritic cells [94]. Additionally, surface and cytoplasmic proteins anchored to the vesicle lipid bilayer membrane are involved in specific ligand-receptor type interactions. They include tetraspanins, TNF, TRAIL, FasL, integrins, or T cell immunoglobulin [96]. For example, tetraspanins are highly abundant on Exos' surfaces and notably have been shown to be involved in several processes, including vesicular and cellular fusion. The treatment of recipient cells with antibodies against the tetraspanins CD81 or CD9 can reduce the uptake of EVs by dendritic cells [97]. Cells over-expressing Tspan8 released EVs bearing a Tspan8-CD49d complex, the presence of which contributed to EV uptake by rat aortic endothelial cells [98].

Although there are several types of proteins capable of interacting specifically with a cellular target, none have been established as sufficient and necessary for EV internalization. Many EV subtypes share common surface proteins, and it is possible that one of them acts as a general ligand for a receptor, enabling vesicle internalization.

One unresolved question currently vexing the EV field is whether EV uptake is a cell type–specific process or whether the process is unspecific. The mechanisms of EV uptake into the cytosol of the recipient cell are still unclear and seem to act both in a generic and a specific manner.

Applications of Exos for Diagnosis and the Therapy

In the last few decades, evidence about the role that Exos secreted by healthy and tumor cells have in the growth and spread of such a complex environment suggested their use as a diagnostic and prognostic indicator of tumor progression [75], even for brain malignancies such as glioma (Table 2). Unmodified Exos can cross BBB thanks to their small size, flexibility, and the presence of adhesive proteins on their surface, while their endogenous origin and the presence of a cellular lipidic bilayer minimize immunogenicity and toxicity, supporting their stabilization in blood circulation [99]. Furthermore, the application of Exos both as diagnostic and therapeutic tools is deeply correlated to their long in vivo blood circulation and biodistribution [100]. Exogenous blood circulating Exos are enriched in proteins and genetic material, which should allow an earlier and more accurate diagnosis. On the other hand, EVs artificially introduced into circulation with a prolonged half-life at the target site could achieve a lower and more efficient therapeutic dosage of the active substance carried. Unfortunately, to the best of our knowledge, Exos in vivo biodistribution studies seem to be very controversial. Establishing a unique biodistribution mechanism seems to be impossible due to the numerous variables involved; the route of administration, the progress of the disease, the exosomal

parent cell source, as well as the different target cell types available to internalize the circulating EVs are just the main parameters to keep in consideration.

Direct intravenous, intraperitoneal, or subcutaneous injection of breast 4T1, MCF-7, and prostatic PC3 tumoral Exos, for example, result in rapid clearance from the blood circulation and accumulation in the liver, spleen, lung, and gastrointestinal tract [47]. The intravenous injection of blood cell-derived EVs showed an uptake by the liver (44.9%), bone (22.5%), skin (9.7%), muscle (5.8%), spleen (3.4%), kidney (2.7%), and lung (1.8%) [101]. In contrast, B16 melanoma-derived EVs were mainly taken up by lungs and spleen [102]. Regardless of the delivery route and cell source, the half-life of the majority of systemically injected Exos seems often to be very short due to the macrophage uptake in the reticuloendothelial system [103], and this could lead to a rapid clearance. However, their hemodynamic is still debated. Indeed, differently derived Exos exhibit different circulation, biodistribution, and clearance properties compared to their normal counterparts, with additional changes associated with tumor progression and response to treatment [102].

As for traditional nanovectors, it seems clear that even for Exos, the engineering of nanovesicular structures through post-isolation modifications can be helpful for diagnostic and moreover therapeutic application [104]. For example, in addition to naturally expressed protein, the conjugation of specific targeting ligands, such as antibodies and peptides, may enable specific interactions with target cells. Further advantages can be achieved through the pre- or post-isolation loading of unmodified EVs with molecules of interest [105].

Cell Source	Cargo	Application	Models	Reference
Raw264.7	SPIONs/Curcumin/RGE peptide	Imaging and anti-tumor therapy	In vitro (U251) In vivo glioma mice model xenograft	[53]
MSC	miRNA-584	Anti-tumor miRNA therapy Inhibition glioma growth	In vitro (U-87 MG) In vivo U-87 MG xenograft nude mouse mode	[106]
MSC	miR-199	Inhibition glioma growth Chemosensitivity	In vitro (U251) Ex vivo immunohistochemistry tumor-bearing nude mice	[107]
MSC	miR-146b	Anti-tumor miRNA therapy Inhibition glioma growth	In vitro (9L glioma) Ex vivo rodent model (9L glioma) xenograft	[55]
U-87 MG X12 cells	miR-1	Anti-tumor miRNA therapy Inhibition glioma growth	In vitro (U87 and X12 GBM) In vivo xenograft nude mouse model	[108]
MSC	anti-miR-9	Chemosensitivity	In vitro (U-87 MG T98G)	[109]
U-87 MG Brain endothelial cell (bEND.3)	PTX/DXR	Delivery anticancer drugs	In vitro (U-87 MG) In vivo brain imaging of embryos zebrafish model	[110]
Mouse fibroblast cell line (L929)	KLA peptide LDL/MTX	Delivery of anticancer drug and therapeutic targeted peptides	In vitro (U-87 MG) In vivo glioma mice xenograft	[18]
MSC	miR-124	Anti-tumor miRNA therapy Dysregulation of cellular metabolism	In vitro (GSC26-28 GSC6-27) In vivo glioma mice xenograft	[111]
Natural killer-92MI	-	Immunotherapy Inhibition Glioblastoma growth	In vitro (U-87 MG) In vivo glioma mice xenograft	[112]
CSF	miR-21	Diagnostic biomarker	-	[113]
Serum	miR-21/miR-222/miR-124-3p	Diagnostic biomarker	-	[114]
CSF	miR-21 miR-103, miR-24, and miR-125	Diagnostic biomarker	-	[115]

Serum	miR-320/miR-574-3p/RNU6-1	Diagnostic biomarker Tumorigenesis factors	-	[116]
Serum	miR-301a	Diagnostic biomarker	In vitro (H4)	[117]
T98G cell line	L1CAM	Tumorigenesis factor	Chick embryo brain tumor model	[118]
Plasma	CAV1 IL-8	Hypoxia-induced, proangiogenic proteins	In vivo glioma mice xenograft	[119]
Blood	EGFR/EGFRvIII	Diagnostic biomarker	μNMR	[120]
Blood	PTRF	Diagnostic biomarker	In vitro (LN229 U-87 MG U251) In vivo mouse model xenograft	[121]

Table 2. Summary of the literature assessing Exos as a drug delivery system and diagnostic biomarkers in in vitro and in vivo glioma models.

Encapsulation Techniques

For the encapsulation of exosomal carriers with therapeutic cargo, several methods can be utilized. These may be divided in two main categories:

- loading/transfecting parental cells with DNA encoding therapeutically active compounds which are then released in Exos, thus before Exos isolation;
- loading naïve Exos isolated from parental cells ex vitro, so after Exos isolation.

Each methodology has its advantages and limitations and may be dictated by the type of therapeutic cargo, conditions suitable for a specific type of Exos-encapsulated cargo, and site of the disease.

Loading before Exos isolation

This approach consists into loading of therapeutics into cells from which the Exos are derived, that, using the endogenous loading machinery of the cells, may result in subsequent Exos loading with the drug, protein or oligonucleotide of interest.

More specifically, in order to attain the encapsulation with genetic material such as siRNAs and microRNAs miRNAs, transfection-based strategies that employ vector induced expression in cells have been proposed [61, 62].

Alternatively, siRNAs or a drug may be used directly to transfect Exos donor cells by incubation at 37 °C. For example, Shtam, Tatyana A., et al. [122] showed that transfection of HeLa and HT1080 human fibrosarcoma cells with a vector for expression of two different siRNAs against RAD51 and RAD52 resulted effective at causing post-transcriptional gene silencing in recipient cells. Pascucci et al. [123] showed that MSCs-secreted Exos were loaded with paclitaxel (PTX) by incubating the parental cells with the drug.

However, the main drawback of these strategies is that the amount of RNA/drug incorporated into Exos by transfection depends on drug characteristics and RNA sequence.

Loading after Exos isolation

Regarding ex vitro loading of naïve Exos, several techniques have been suggested.

In most cases, Exos encapsulation of small hydrophobic molecules is achieved through direct mixing. Indeed, in several studies anticancer agents, Doxorubicin and Paclitaxel (PTX) [124], a model drug Rhodamine 123 [125], and low molecular antioxidant, curcumin [126, 127], were passively loaded into Exos by simple incubation at room temperature (RT). However, this method suffers from very low encapsulation efficacy – from 7.2% for PTX to 11.7% for Dox [8].

For the encapsulation of hydrophilic compounds, such as exogenous RNAs, the major hurdle is represented by the vesicle membrane, restricting the possibility of passive loading.

One utilized strategy is electroporation after Exos isolation. This approach relies on the spontaneous pore formation in membranes to compensate for variations in voltage after stimulation with an electrical signal. The first to report apparent successful siRNA loading into EVs by electroporation were Alvarez-Erviti et al. [128]. Successively, several other studies have confirmed the possibility of loading Exos by electroporation without affecting Exos integrity and function. Nevertheless, it should be considered that, when loading Exos with siRNAs by this technique, extensive siRNA aggregate formation was reported [129] and suggested to cause overestimation of the amount of siRNA actually loaded into Exos. Moreover, electroporation might cause aggregation or fusion of Exos themselves.

In attempt to encapsulate large molecules, as catalase, as well as other therapeutics and imaging agents, methods as saponin-mediated permeabilization, extrusion, freeze-thaw cycles were compared [130, 131] or explored singularly in distinct studies. More precisely, extrusion and sonication are techniques creating extensive reshaping and reformation of Exos, thus aiding the diffusion across the vesicle lipid bilayer. These strategies result in higher loading efficacy than the aforementioned ones (20%–26% loading capacity [130]).

However, it is worth noting that neither of these strategies is a satisfactory, scalable and cost-effective procedure for the efficient encapsulation of Exos.

Cellular membrane: dynamic of the lipidic bilayer

Cell membranes are highly dynamic, fluid structures, which are made functional by lipid–lipid, lipid–protein, and protein–protein interactions [132]. The first insight into the general structural organization of biological membranes was proposed in the early 1970s [133]. In its initial form, the celebrated Singer–Nicolson fluid mosaic model considers the cell membrane as a two-dimensional sea of lipid molecules with integral proteins, floating in it [134]. It is now admitted that the membrane constituents do not diffuse freely in the two-dimensional lipid matrix but are structured in 3D domains [135].

So, the cell lipid bilayer could be considered as a 3D assembly with a rich variety of physical features that modulate cell signaling and protein function.

Cell membrane tends to maintain a specific lipid packaging density and therefore an optimal surface pressure on the order of 30 mN m^{-1} [136]. This is principally due to some relevant physical features of proteins and lipids present in the PM.

The local shape of a membrane depends on which lipids are present and on how they are spatially distributed. Insertion or removal of lipids into the inner or outer leaflet leads to area mismatches that also alter curvature.

Most of the lipid species have not a cylindrical structure and contribute to a spontaneous curvature to the membrane [137]. An example detergent molecule, lysophospholipids and polyphosphoinositides, form structures with a positive curvature, such as micelles [136]. Cylindrical-shaped lipid molecules, such as phosphatidylcholine and sphingomyelin, preferentially form flat bilayer structures [138]. Lipid molecules that have an overall conical shape, such as diacylglycerol, with a small hydrophilic cross-section, form structures with a negative curvature, such as the inverted hexagonal phase of tubes with headgroups inside and hydrophobic tails outside [139]. So, lateral Pressure stress depends sensitively on lipid composition.

Furthermore, cell membrane packaging is based on equilibrium between its hydrophobic and hydrophilic parts (Figure 2). Even though the bilayer as a whole might be stable, each part of it is highly stressed and the maintenance of the entropy in the system is allowed by interfacial tension. Indeed, in cell membrane the hydrophobic and hydrophilic parts are in a very high energy configuration due to their chemical incompatibility.. The hydrophilic headgroups at the surface of the membrane are crowded together more tightly than they would be if free in solution [140].

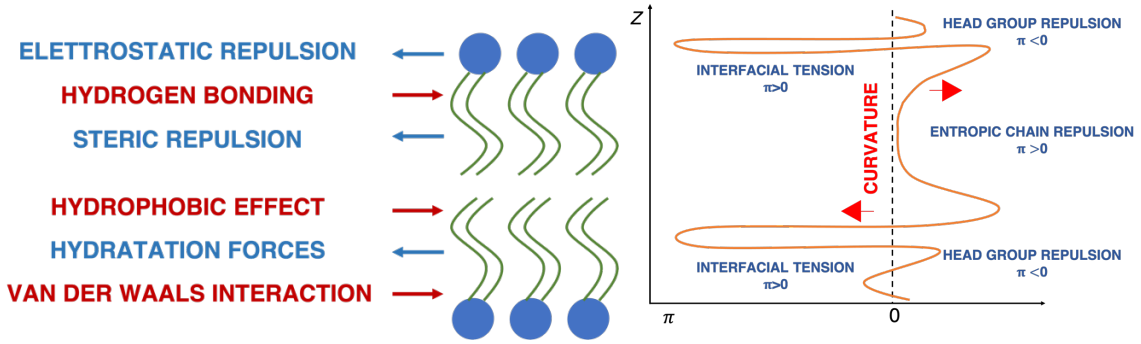

Figure 2. The forces that act within the bilayer and how they act on the corresponding lateral pressure, p(z), at different distances (z) across the bilayer thickness.

In this scenario, the lipidic bilayer of nanovesicles could behave as cell membrane on small scale.

A vesicle is a viscous droplet enclosed by a lipid bilayer. The bilayer membrane could be considered as an incompressible fluid in that it admits relative in-plane shear motion between lipid molecules without incurring any static shear stress [141].

Within the lipid bilayer, disorder is introduced by differences in chain length and saturation of the hydrophobic chains in the membrane interior and the lateral distribution of different lipids within each leaflet, which can alter the biophysical properties of the membrane. Proteins also constitute 50% of the cross-sectional area of the membrane, and peripheral proteins interact with both extracellular and cytoplasmic lipid [142].

If a lipid bilayer is discussed only in its liquid crystal state, it can be considered as a two-dimensional liquid. Consequently, the mechanical properties of such an object are characterized by its stretching and bending elastic moduli, lipid molecules can freely slide one to another and the shear elastic modulus is equal to zero. Evidently, in the case of natural membranes, containing a cytoskeleton, shear deformations cannot be neglected [135].

In order to understand the response of lipid membranes to an external force as Pressure stimuli several studies were conducted.

Weiner et al. [143] employed fully atomistic molecular dynamics simulations to investigate the effects of a high external Pressure of 1000 bar by comparing monounsaturated 1-palmitoyl-2-oleoyl-phosphatidylcholine (POPC) and unsaturated dioleoyl-phosphatidylcholine (DOPC) bilayers.
In line with literature [144], they find out that increased unsaturation results in a stronger resistance to structural change in response to high pressure.
Thus, it can be hypothesized that a change in external Pressure as simulated in this work will induce a conformational change in specific proteins embedded in a monounsaturated POPC bilayer, while a unsaturated DOPC bilayer would represent a control system where no conformational shift is expected. Peters, Judith, et al. [145] compared the effect of cholesterol at different concentrations on the phase behavior of DMPC (1,2-dimyristoyl-sn-glycero-3-phosphocholine) multilamellar vesicles. They used Pressure perturbation differential scanning calorimetry (PPC). Applying Pressure up to 600 bar they find out that the membrane order is increased and therefore the phase transition temperatures altered accordingly. Furthermore, the calorimetry data reveal a subsequent broadening of the heat capacity and the volume expansion with increasing amount of cholesterol.
Even though at date several studies involve simulations of lipidic multilamellar system, further experimental analysis is needed, aimed to quantifying high Pressure effects on specific biological processes in relation to lipid and protein membrane diversity in cellular and sub-cellular complex structures.

Aim of the work

Since the identification of EVs as exogenous intercellular communication tools, in the last few years the field of Exos-based drug delivery has greatly expanded because of their interesting properties: nanosized and specific compositions minimize recognition by the mononuclear phagocyte system; patient self-derived nature eludes immune system activation; low immunogenicity potentially delivers Exos in a cell type-specific manner; surface composed of GM3, sphingomyelin, and cholesterol supports the stabilization of the vesicles in the blood circulation and stimulates membrane fusion; surface proteins have likewise been linked to membrane fusion in cell–cell and virus–cell interactions; proteo-lipid architecture protects the encapsulated cargo.
Moreover, additional targeted functions have been developed arising from the engineering of the donor cells or the post-isolation modification of Exos' surfaces, always preserving their inherent properties. Furthermore, as Exos are structures encased in a lipid bilayer membrane with an aqueous core, they are capable of housing both hydrophilic and lipophilic drugs.
Despite early promising experimental results, the application of Exos for therapeutic drug delivery, for the treatment of several diseases is far from a clinical translation. First, a major limitation is the lack of standardized techniques for the isolation of Exos because of time-consuming procedures, poor reproducibility, and low production yield. Notably, protein aggregates and other cell debris can also affect Exos' purity. Once extracted from biological fluids, several distinct approaches could be applied for the loading of exosomal carriers with therapeutic cargo. However, it is worth noting that neither of these strategies is a satisfactory, scalable, and cost- effective procedure for the efficient encapsulation of nanovesicles.

With the present work we will investigate the high shear rates in turbulent flow to promote mixing by a high-pressure system as ground-breaking method for Exos production and encapsulation (Figure 3). The latter will be obtained through Microfluidizer, a lab-scale homogenizer, by exploiting the unique fixed-geometry interaction chamber technology capable of processing a wide variety of fluids in as few as one or two passes. This High-Pressure system works at the highest homogenization pressures possible and, consequently, in an extremely turbulent flow situation, thus creating very high shear forces on the fluid sample in the interaction chamber. It delivers a repeatable process that is guaranteed to scale up to pilot and/or production volumes. To date, biological applications of microfluidization are only aimed at cell lysis for the extraction of proteins or lipids of interest.

The rationale behind this whole new approach is to exploit pressure gradients along with both high shear and elongational stresses acting on cellular and vesicles membranes to induce the formation of transient pores or even the reformation of Exos without disrupting them, thus allowing inward diffusion of cargos from the surrounding media.

The goal will be the achievement of the desired stability and reproducibility for engineered Exos by optimizing the process parameters for both Exos' production and encapsulation with different compounds. So, aim of this work is the creation of a new platform for theranostic application through the improvement of production and loading capability of Exos.

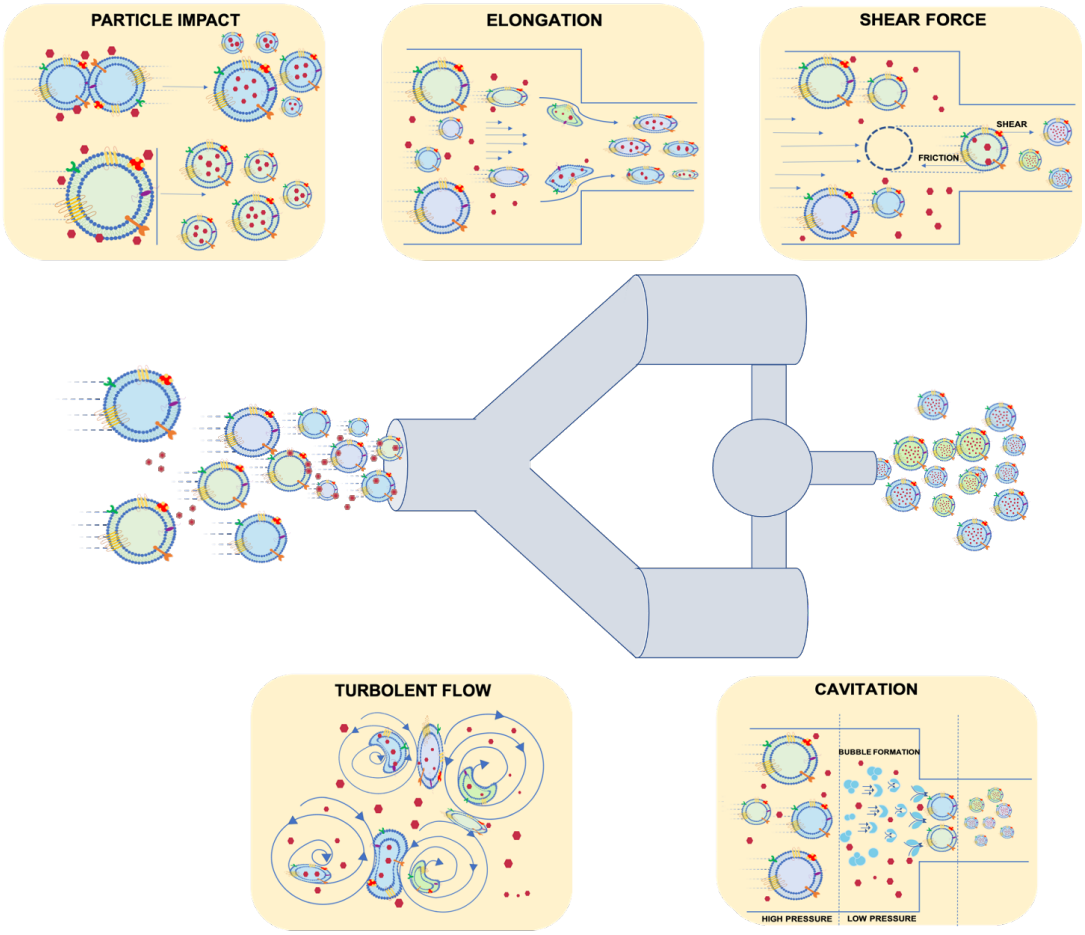

Figure 3. Phenomena acting on cellular lipidic bilayers in the High Hydrostatic Pressure system of the homogenization chamber.

References

1. Dörsam, B., K. S. Reiners and E. P. von Strandmann. "Cancer-derived extracellular vesicles: Friend and foe of tumour immunosurveillance." *Philosophical Transactions of the Royal Society B: Biological Sciences* 373 (2017): 20160481.
2. Keller, S., J. Ridinger, A. K. Rupp, J. W. G. Janssen and P. Altevogt. "Body fluid derived exosomes as a novel template for clinical diagnostics." *Journal of Translational Medicine* 9 (2011): 10.1186/1479-5876-9-86. <Go to ISI>://WOS:000291822700001.
3. Caby, M. P., D. Lankar, C. Vincendeau-Scherrer, G. Raposo and C. Bonnerot. "Exosomal-like vesicles are present in human blood plasma." *International Immunology* 17 (2005): 879-87. 10.1093/intimm/dxh267. <Go to ISI>://WOS:000230513700006.
4. Kalra, H., C. G. Adda, M. Liem, C. S. Ang, A. Mechler, R. J. Simpson, M. D. Hulett and S. Mathivanan. "Comparative proteomics evaluation of plasma exosome isolation techniques and assessment of the stability of exosomes in normal human blood plasma." *Proteomics* 13 (2013): 3354-64. 10.1002/pmic.201300282. <Go to ISI>://WOS:000327979600013.
5. Raposo, G. and W. Stoorvogel. "Extracellular vesicles: Exosomes, microvesicles, and friends." *Journal of Cell Biology* 200 (2013): 373-83. 10.1083/jcb.201211138. <Go to ISI>://WOS:000315157600002.
6. Cocucci, E. and J. Meldolesi. "Ectosomes and exosomes: Shedding the confusion between extracellular vesicles." *Trends in Cell Biology* 25 (2015): 364-72. 10.1016/j.tcb.2015.01.004. <Go to ISI>://WOS:000355708500007.
7. Lawson, C., J. M. Vicencio, D. M. Yellon and S. M. Davidson. "Microvesicles and exosomes: New players in metabolic and cardiovascular disease." *Journal of Endocrinology* 228 (2016): R57-R71. 10.1530/joe-15-0201. <Go to ISI>://WOS:000371155400003.
8. Batrakova, E. V. and M. S. Kim. "Using exosomes, naturally-equipped nanocarriers, for drug delivery." *Journal of Controlled Release* 219 (2015): 396-405. 10.1016/j.jconrel.2015.07.030. <Go to ISI>://WOS:000365587800032.
9. Keller, S., M. P. Sanderson, A. Stoeck and P. Altevogt. "Exosomes: From biogenesis and secretion to biological function." *Immunology Letters* 107 (2006): 102-08. 10.1016/j.imlet.2006.09.005. <Go to ISI>://WOS:000242958700004.
10. Sarko, D. K. and C. E. McKinney. "Exosomes: Origins and therapeutic potential for neurodegenerative disease." *Frontiers in Neuroscience* 11 (2017): 7. 10.3389/fnins.2017.00082. <Go to ISI>://WOS:000394683700001.
11. Shi, M., L. Sheng, T. Stewart, C. P. Zabetian and J. Zhang. "New windows into the brain: Central nervous system-derived extracellular vesicles in blood." *Progress in neurobiology* 175 (2019): 96-106.
12. András, I. E. and M. Toborek. "Extracellular vesicles of the blood-brain barrier." *Tissue barriers* 4 (2016): e1131804.
13. Mentkowski, K. I., J. D. Snitzer, S. Rusnak and J. K. Lang. "Therapeutic potential of engineered extracellular vesicles." *Aaps Journal* 20 (2018): 10.1208/s12248-018-0211-z. <Go to ISI>://WOS:000431135700010.
14. Zhang, X., C. Liu, Y. Pei, W. Song and S. Zhang. "Preparation of a novel raman probe and its application in the detection of circulating tumor cells and exosomes." *ACS applied materials & interfaces* 11 (2019): 28671-80.
15. Yang, Y., E. Kannisto, G. Yu, M. E. Reid, S. K. Patnaik and Y. Wu. "An immuno-biochip selectively captures tumor-derived exosomes and detects exosomal rnas for cancer diagnosis." *ACS applied materials & interfaces* 10 (2018): 43375-86.
16. Zhang, K., X. Zhao, X. Chen, Y. Wei, W. Du, Y. Wang, L. Liu, W. Zhao, Z. Han and D. Kong. "Enhanced therapeutic effects of mesenchymal stem cell-derived exosomes with an injectable hydrogel for hindlimb ischemia treatment." *ACS applied materials & interfaces* 10 (2018): 30081-91.

17. Shaikh, S., F. u. Rehman, T. Du, H. Jiang, L. Yin, X. Wang and R. Chai. "Real-time multimodal bioimaging of cancer cells and exosomes through biosynthesized iridium and iron nanoclusters." *ACS applied materials & interfaces* 10 (2018): 26056-63.
18. Ye, Z. L., T. Zhang, W. S. He, H. L. Jin, C. W. Liu, Z. Yang and J. H. Ren. "Methotrexate-loaded extracellular vesicles functionalized with therapeutic and targeted peptides for the treatment of glioblastoma multiforme." *Acs Applied Materials & Interfaces* 10 (2018): 12341-50. 10.1021/acsami.7b18135. <Go to ISI>://WOS:000430642100024.
19. Wang, J., W. Li, L. C. Zhang, L. Ban, P. Chen, W. Du, X. J. Feng and B. F. Liu. "Chemically edited exosomes with dual ligand purified by microfluidic device for active targeted drug delivery to tumor cells." *Acs Applied Materials & Interfaces* 9 (2017): 27441-52. 10.1021/acsami.7b06464. <Go to ISI>://WOS:000408518800015.
20. Chen, C., S. Zong, Z. Wang, J. Lu, D. Zhu, Y. Zhang and Y. Cui. "Imaging and intracellular tracking of cancer-derived exosomes using single-molecule localization-based super-resolution microscope." *ACS applied materials & interfaces* 8 (2016): 25825-33.
21. Singh, R. K., K. D. Patel, J.-J. Kim, T.-H. Kim, J.-H. Kim, U. S. Shin, E.-J. Lee, J. C. Knowles and H.-W. Kim. "Multifunctional hybrid nanocarrier: Magnetic cnts ensheathed with mesoporous silica for drug delivery and imaging system." *ACS applied materials & interfaces* 6 (2014): 2201-08.
22. Kalra, H., G. P. C. Drummen and S. Mathivanan. "Focus on extracellular vesicles: Introducing the next small big thing." *International Journal of Molecular Sciences* 17 (2016): 10.3390/ijms17020170. <Go to ISI>://WOS:000371830800123.
23. Munson, P. and A. Shukla. "Exosomes: Potential in cancer diagnosis and therapy." *Medicines* 2 (2015): 310-27.
24. Raiborg, C. and H. Stenmark. "The escrt machinery in endosomal sorting of ubiquitylated membrane proteins." *Nature* 458 (2009): 445-52. 10.1038/nature07961. <Go to ISI>://WOS:000264532400033.
25. Burd, C. G. and S. D. Emr. "Phosphatidylinositol(3)-phosphate signaling mediated by specific binding to ring fyve domains." *Molecular Cell* 2 (1998): 157-62. 10.1016/s1097-2765(00)80125-2. <Go to ISI>://WOS:000075174500018.
26. Raiborg, C., B. Bremnes, A. Mehlum, D. J. Gillooly, A. D'Arrigo, E. Stang and H. Stenmark. "Fyve and coiled-coil domains determine the specific localisation of hrs to early endosomes." *Journal of Cell Science* 114 (2001): 2255-63. <Go to ISI>://WOS:000169790400006.
27. Bache, K. G., A. Brech, A. Mehlum and H. Stenmark. "Hrs regulates multivesicular body formation via escrt recruitment to endosomes." *Journal of Cell Biology* 162 (2003): 435-42. 10.1083/jcb.200302131. <Go to ISI>://WOS:000184667900009.
28. Slagsvold, T., R. Aasland, S. Hirano, K. G. Bache, C. Raiborg, D. Trambaiolo, S. Wakatsuki and H. Stenmark. "Eap45 in mammalian escrt-ii binds ubiquitin via a phosphoinositide-interacting glue domain." *Journal of Biological Chemistry* 280 (2005): 19600-06. 10.1074/jbc.M501510200. <Go to ISI>://WOS:000229113700023.
29. Leung, K. F., J. B. Dacks and M. C. Field. "Evolution of the multivesicular body escrt machinery; retention across the eukaryotic lineage." *Traffic* 9 (2008): 1698-716. 10.1111/j.1600-0854.2008.00797.x. <Go to ISI>://WOS:000259238000013.
30. Teo, H., O. Perisic, B. Gonzalez and R. L. Williams. "Escrt-ii, an endosome-associated complex required for protein sorting: Crystal structure and interactions with escrt-iii and membranes." *Developmental Cell* 7 (2004): 559-69. 10.1016/j.devcel.2004.09.003. <Go to ISI>://WOS:000224671300014.
31. Adell, M. A. Y. and D. Teis. "Assembly and disassembly of the escrt-iii membrane scission complex." *FEBS letters* 585 (2011): 3191-96.
32. Stuffers, S., C. S. Wegner, H. Stenmark and A. Brech. "Multivesicular endosome biogenesis in the absence of escrts." *Traffic* 10 (2009): 925-37. 10.1111/j.1600-0854.2009.00920.x. <Go to ISI>://WOS:000266981700014.

33. Theos, A. C., S. T. Truschel, D. Tenza, I. Hurbain, D. C. Harper, J. F. Berson, P. C. Thomas, G. Raposo and M. S. Marks. "A lumenal domain-dependent pathway for sorting to intralumenal vesicles of multivesicular endosomes involved in organelle morphogenesis." *Developmental Cell* 10 (2006): 343-54. 10.1016/j.devcel.2006.01.012. <Go to ISI>://WOS:000236255500011.
34. D'Alba, L. and M. D. Shawkey. "Melanosomes: Biogenesis, properties, and evolution of an ancient organelle." *Physiological reviews* 99 (2019): 1-19.
35. Trajkovic, K., C. Hsu, S. Chiantia, L. Rajendran, D. Wenzel, F. Wieland, P. Schwille, B. Brugger and M. Simons. "Ceramide triggers budding of exosome vesicles into multivesicular endosomes." *Science* 319 (2008): 1244-47. 10.1126/science.1153124. <Go to ISI>://WOS:000253530600044.
36. Moriwaki, Y., Y. Ohno, T. Ishii, Y. Takamura, Y. Kita, K. Watabe, K. Sango, S. Tsuji and H. Misawa. "Simple binds specifically to pi4p through simple-like domain and participates in protein trafficking in the trans-golgi network and/or recycling endosomes." *PloS one* 13 (2018):
37. Wang, G. H., M. Dinkins, Q. He, G. Zhu, C. Poirier, A. Campbell, M. Mayer-Proschel and E. Bieberich. "Astrocytes secrete exosomes enriched with proapoptotic ceramide and prostate apoptosis response 4 (par-4) potential mechanism of apoptosis induction in alzheimer disease (ad)." *Journal of Biological Chemistry* 287 (2012): 21384-95. 10.1074/jbc.M112.340513. <Go to ISI>://WOS:000306416800056.
38. Hessvik, N. P. and A. Llorente. "Current knowledge on exosome biogenesis and release." *Cellular and Molecular Life Sciences* 75 (2018): 193-208. 10.1007/s00018-017-2595-9. <Go to ISI>://WOS:000419471500003.
39. Böing, A. N., E. Van Der Pol, A. E. Grootemaat, F. A. Coumans, A. Sturk and R. Nieuwland. "Single-step isolation of extracellular vesicles by size-exclusion chromatography." *Journal of extracellular vesicles* 3 (2014): 23430.
40. Deregibus, M. C., F. Figliolini, S. D'antico, P. M. Manzini, C. Pasquino, M. De Lena, C. Tetta, M. F. Brizzi and G. Camussi. "Charge-based precipitation of extracellular vesicles." *International journal of molecular medicine* 38 (2016): 1359-66.
41. Niu, Z., R. T. Pang, W. Liu, Q. Li, R. Cheng and W. S. Yeung. "Polymer-based precipitation preserves biological activities of extracellular vesicles from an endometrial cell line." *PloS one* 12 (2017): e0186534.
42. Lobb, R. J., M. Becker, S. W. Wen, C. S. F. Wong, A. P. Wiegmans, A. Leimgruber and A. Moller. "Optimized exosome isolation protocol for cell culture supernatant and human plasma." *Journal of Extracellular Vesicles* 4 (2015): 10.3402/jev.v4.27031. <Go to ISI>://WOS:000365076200001.
43. Chen, C., J. Skog, C. H. Hsu, R. T. Lessard, L. Balaj, T. Wurdinger, B. S. Carter, X. O. Breakefield, M. Toner and D. Irimia. "Microfluidic isolation and transcriptome analysis of serum microvesicles." *Lab on a Chip* 10 (2010): 505-11. 10.1039/b916199f. <Go to ISI>://WOS:000274207700014.
44. Li, P., M. Kaslan, S. H. Lee, J. Yao and Z. Q. Gao. "Progress in exosome isolation techniques." *Theranostics* 7 (2017): 789-804. 10.7150/thno.18133. <Go to ISI>://WOS:000396557300022.
45. Tauro, B. J., D. W. Greening, R. A. Mathias, H. Ji, S. Mathivanan, A. M. Scott and R. J. Simpson. "Comparison of ultracentrifugation, density gradient separation, and immunoaffinity capture methods for isolating human colon cancer cell line lim1863-derived exosomes." *Methods* 56 (2012): 293-304. 10.1016/j.ymeth.2012.01.002. <Go to ISI>://WOS:000302105400025.
46. Morishita, M., Y. Takahashi, M. Nishikawa, K. Sano, K. Kato, T. Yamashita, T. Imai, H. Saji and Y. Takakura. "Quantitative analysis of tissue distribution of the b16bl6-derived exosomes using a streptavidin-lactadherin fusion protein and iodine-125-labeled biotin derivative after

intravenous injection in mice." *Journal of Pharmaceutical Sciences* 104 (2015): 705-13. 10.1002/jps.24251. <Go to ISI>://WOS:000349089500043.
47. Smyth, T., M. Kullberg, N. Malik, P. Smith-Jones, M. W. Graner and T. J. Anchordoquy. "Biodistribution and delivery efficiency of unmodified tumor-derived exosomes." *Journal of Controlled Release* 199 (2015): 145-55.
48. Haney, M. J., N. L. Klyachko, Y. L. Zhaoa, R. Gupta, E. G. Plotnikova, Z. J. He, T. Patel, A. Piroyan, M. Sokolsky, A. V. Kabanov*, et al.* "Exosomes as drug delivery vehicles for parkinson's disease therapy." *Journal of Controlled Release* 207 (2015): 18-30. 10.1016/j.jconrel.2015.03.033. <Go to ISI>://WOS:000354060000003.
49. Didiot, M. C., L. M. Hall, A. H. Coles, R. A. Haraszti, B. Godinho, K. Chase, E. Sapp, S. Ly, J. F. Alterman, M. R. Hassler*, et al.* "Exosome-mediated delivery of hydrophobically modified sirna for huntingtin mrna silencing." *Molecular Therapy* 24 (2016): 1836-47. 10.1038/mt.2016.126. <Go to ISI>://WOS:000387256700013.
50. Faruqu, F. N., J. T.-W. Wang, L. Xu, L. McNickle, E. M.-Y. Chong, A. Walters, M. Gurney, A. Clayton, L. A. Smyth and R. Hider. "Membrane radiolabelling of exosomes for comparative biodistribution analysis in immunocompetent and immunodeficient mice-a novel and universal approach." *Theranostics* 9 (2019): 1666.
51. Gardiner, C., D. D. Vizio, S. Sahoo, C. Théry, K. W. Witwer, M. Wauben and A. F. Hill. "Techniques used for the isolation and characterization of extracellular vesicles: Results of a worldwide survey." *Journal of extracellular vesicles* 5 (2016): 32945.
52. Webber, J. and A. Clayton. "How pure are your vesicles?" *Journal of extracellular vesicles* 2 (2013): 19861.
53. Jia, G., Y. Han, Y. L. An, Y. A. Ding, C. He, X. H. Wang and Q. S. Tang. "Nrp-1 targeted and cargo-loaded exosomes facilitate simultaneous imaging and therapy of glioma in vitro and in vivo." *Biomaterials* 178 (2018): 302-16. 10.1016/j.biomaterials.2018.06.029. <Go to ISI>://WOS:000440959000021.
54. Qu, M., Q. Lin, L. Huang, Y. Fu, L. Wang, S. He, Y. Fu, S. Yang, Z. Zhang and L. Zhang. "Dopamine-loaded blood exosomes targeted to brain for better treatment of parkinson's disease." *Journal of controlled release* 287 (2018): 156-66.
55. Katakowski, M., B. Buller, X. G. Zheng, Y. Lu, T. Rogers, O. Osobamiro, W. Shu, F. Jiang and M. Chopp. "Exosomes from marrow stromal cells expressing mir-146b inhibit glioma growth." *Cancer Letters* 335 (2013): 201-04. 10.1016/j.canlet.2013.02.019. <Go to ISI>://WOS:000323853200025.
56. Arab, T., A. Raffo-Romero, C. Van Camp, Q. Lemaire, F. Le Marrec-Croq, F. Drago, S. Aboulouard, C. Slomianny, A. Lacoste and I. Guigon. "Proteomic characterisation of leech microglia extracellular vesicles (evs): Comparison between differential ultracentrifugation and optiprep™ density gradient isolation." *Journal of extracellular vesicles* 8 (2019): 1603048.
57. Mathivanan, S., M. Maugeri, L. Mcginnis, M. Mcvey, D. Meckes, K. Meehan, I. Mertens, V. Minciacchi, A. Moller and M. M. Jorgensen. "Minimal information for studies of extracellular vesicles 2018 (misev2018): A position statement of the international society for extracellular vesicles and update of the misev2014 guidelines." (2018):
58. Konoshenko, M. Y., E. A. Lekchnov, A. V. Vlassov and P. P. Laktionov. "Isolation of extracellular vesicles: General methodologies and latest trends." *BioMed research international* 2018 (2018):
59. Hebert, T. T. *Precipitation of plant viruses by polyethylene glycol.* 53. *Phytopathology* 1963
60. Tang, Y.-T., Y.-Y. Huang, L. Zheng, S.-H. Qin, X.-P. Xu, T.-X. An, Y. Xu, Y.-S. Wu, X.-M. Hu and B.-H. Ping. "Comparison of isolation methods of exosomes and exosomal rna from cell culture medium and serum." *International journal of molecular medicine* 40 (2017): 834-44.

61. Chang, M., Y. J. Chang, P. Y. Chao and Q. Yu. "Exosome purification based on peg-coated fe3o4 nanoparticles." *Plos One* 13 (2018): 10.1371/journal.pone.0199438. <Go to ISI>://WOS:000436076600025.
62. Posch, A. *Proteomic profiling*. Springer, 2015,
63. Taylor, D. D. and S. Shah. "Methods of isolating extracellular vesicles impact down-stream analyses of their cargoes." *Methods* 87 (2015): 3-10.
64. Bunggulawa, E. J., W. Wang, T. Yin, N. Wang, C. Durkan, Y. Wang and G. Wang. "Recent advancements in the use of exosomes as drug delivery systems." *Journal of nanobiotechnology* 16 (2018): 1-13.
65. Kim, G., C. E. Yoo, M. Kim, H. J. Kang, D. Park, M. Lee and N. Huh. "Noble polymeric surface conjugated with zwitterionic moieties and antibodies for the isolation of exosomes from human serum." *Bioconjugate Chemistry* 23 (2012): 2114-20. 10.1021/bc300339b. <Go to ISI>://WOS:000309855000015.
66. Liu, C., J. Guo, F. Tian, N. Yang, F. Yan, Y. Ding, J. Wei, G. Hu, G. Nie and J. Sun. "Field-free isolation of exosomes from extracellular vesicles by microfluidic viscoelastic flows." *ACS nano* 11 (2017): 6968-76.
67. Buschmann, D., B. Kirchner, S. Hermann, M. Märte, C. Wurmser, F. Brandes, S. Kotschote, M. Bonin, O. K. Steinlein and M. W. Pfaffl. "Evaluation of serum extracellular vesicle isolation methods for profiling mirnas by next-generation sequencing." *Journal of extracellular vesicles* 7 (2018): 1481321.
68. Davies, R. T., J. Kim, S. C. Jang, E. J. Choi, Y. S. Gho and J. Park. "Microfluidic filtration system to isolate extracellular vesicles from blood." *Lab on a Chip* 12 (2012): 5202-10. 10.1039/c2lc41006k. <Go to ISI>://WOS:000311964700012.
69. Wang, Z. X., H. J. Wu, D. Fine, J. Schmulen, Y. Hu, B. Godin, J. X. J. Zhang and X. W. Liu. "Ciliated micropillars for the microfluidic-based isolation of nanoscale lipid vesicles." *Lab on a Chip* 13 (2013): 2879-82. 10.1039/c3lc41343h. <Go to ISI>://WOS:000321220000003.
70. Liga, A., A. D. B. Vliegenthart, W. Oosthuyzen, J. W. Dear and M. Kersaudy-Kerhoas. "Exosome isolation: A microfluidic road-map." *Lab on a Chip* 15 (2015): 2388-94. 10.1039/c5lc00240k. <Go to ISI>://WOS:000354963400005.
71. Lee, K., H. L. Shao, R. Weissleder and H. Lee. "Acoustic purification of extracellular microvesicles." *Acs Nano* 9 (2015): 2321-27. 10.1021/nn506538f. <Go to ISI>://WOS:000351791800010.
72. Rufino-Ramos, D., P. R. Albuquerque, V. Carmona, R. Perfeito, R. J. Nobre and L. P. de Almeida. "Extracellular vesicles: Novel promising delivery systems for therapy of brain diseases." *Journal of Controlled Release* 262 (2017): 247-58. 10.1016/j.jconrel.2017.07.001. <Go to ISI>://WOS:000411201100025.
73. Ferguson, S. W. and J. Nguyen. "Exosomes as therapeutics: The implications of molecular composition and exosomal heterogeneity." *Journal of Controlled Release* 228 (2016): 179-90. 10.1016/j.jconrel.2016.02.037. <Go to ISI>://WOS:000373429600019.
74. Haraszti, R. A., M.-C. Didiot, E. Sapp, J. Leszyk, S. A. Shaffer, H. E. Rockwell, F. Gao, N. R. Narain, M. DiFiglia and M. A. Kiebish. "High-resolution proteomic and lipidomic analysis of exosomes and microvesicles from different cell sources." *Journal of extracellular vesicles* 5 (2016): 32570.
75. Chiasserini, D., J. R. T. van Weering, S. R. Piersma, T. V. Pham, A. Malelnadeh, C. E. Teunissen, H. de Wit and C. R. Jimenez. "Proteomic analysis of cerebrospinal fluid extracellular vesicles: A comprehensive dataset." *Journal of Proteomics* 106 (2014): 191-204. 10.1016/j.jprot.2014.04.028. <Go to ISI>://WOS:000338621700015.
76. Calderwood, S. K., J. Gong and A. Murshid. "Extracellular hsps: The complicated roles of extracellular hsps in immunity." *Frontiers in immunology* 7 (2016): 159.

77. Willms, E., C. Cabañas, I. Mäger, M. J. Wood and P. Vader. "Extracellular vesicle heterogeneity: Subpopulations, isolation techniques, and diverse functions in cancer progression." *Frontiers in immunology* 9 (2018): 738.
78. Tang, Y. and B. Dawn. *Mesenchymal stem cell derived exosomes: The potential for translational nanomedicine*. Academic Press, 2015,
79. Zhang, Y., Y. Liu, H. Liu and W. H. Tang. "Exosomes: Biogenesis, biologic function and clinical potential." *Cell & bioscience* 9 (2019): 19.
80. Kobayashi, M., G. E. Rice, J. Tapia, M. D. Mitchell and C. Salomon. "Exosomes are fingerprints of originating cells: Potential biomarkers for ovarian cancer." *Research and Reports in Biochemistry* 5 (2015): 101-09.
81. Mathieu, M., L. Martin-Jaular, G. Lavieu and C. Thery. "Specificities of secretion and uptake of exosomes and other extracellular vesicles for cell-to-cell communication." *Nature cell biology* 21 (2019): 9-17.
82. De Toro, J., L. Herschlik, C. Waldner and C. Mongini. "Emerging roles of exosomes in normal and pathological conditions: New insights for diagnosis and therapeutic applications." *Frontiers in immunology* 6 (2015): 203.
83. Oggero, S., S. Austin-Williams and L. V. Norling. "The contrasting role of extracellular vesicles in vascular inflammation and tissue repair." *Frontiers in Pharmacology* 10 (2019):
84. Tadokoro, H., T. Umezu, K. Ohyashiki, T. Hirano and J. H. Ohyashiki. "Exosomes derived from hypoxic leukemia cells enhance tube formation in endothelial cells." *Journal of Biological Chemistry* 288 (2013): 34343-51.
85. Jaiswal, R. and L. M. Sedger. "Intercellular vesicular transfer by exosomes, microparticles and oncosomes-implications for cancer biology and treatments." *Frontiers in oncology* 9 (2019): 125.
86. Skog, J., T. Würdinger, S. Van Rijn, D. H. Meijer, L. Gainche, W. T. Curry, B. S. Carter, A. M. Krichevsky and X. O. Breakefield. "Glioblastoma microvesicles transport rna and proteins that promote tumour growth and provide diagnostic biomarkers." *Nature cell biology* 10 (2008): 1470-76.
87. Mu, W., S. Rana and M. Zöller. "Host matrix modulation by tumor exosomes promotes motility and invasiveness." *Neoplasia* 15 (2013): 875-IN4.
88. Graves, L. E., E. V. Ariztia, J. R. Navari, H. J. Matzel, M. S. Stack and D. A. Fishman. "Proinvasive properties of ovarian cancer ascites-derived membrane vesicles." *Cancer research* 64 (2004): 7045-49.
89. Hallal, S., D. Mallawaaratchy, H. Wei, S. Ebrahimkhani, B. Stringer, B. Day, A. Boyd, G. Guillemin, M. Buckland and K. L. Kaufman. "Extracellular vesicles released by glioblastoma cells stimulate normal astrocytes to acquire a tumor-supportive phenotype via p53 and myc signaling pathways." *Molecular neurobiology* 56 (2019): 4566-81.
90. Kang, X., Z. Zuo, W. Hong, H. Tang and W. Geng. "Progress of research on exosomes in the protection against ischemic brain injury." *Frontiers in Neuroscience* 13 (2019): 1149.
91. Lopatina, T., S. Bruno, C. Tetta, N. Kalinina, M. Porta and G. Camussi. "Platelet-derived growth factor regulates the secretion of extracellular vesicles by adipose mesenchymal stem cells and enhances their angiogenic potential." *Cell Communication and Signaling* 12 (2014): 1-12.
92. Budnik, V., C. Ruiz-Cañada and F. Wendler. "Extracellular vesicles round off communication in the nervous system." *Nature Reviews Neuroscience* 17 (2016): 160-72.
93. Trotta, T., M. A. Panaro, A. Cianciulli, G. Mori, A. Di Benedetto and C. Porro. "Microglia-derived extracellular vesicles in alzheimer's disease: A double-edged sword." *Biochemical pharmacology* 148 (2018): 184-92.
94. Mulcahy, L. A., R. C. Pink and D. R. F. Carter. "Routes and mechanisms of extracellular vesicle uptake." *Journal of extracellular vesicles* 3 (2014): 24641.

95. Toda, Y., K. Takata, Y. Nakagawa, H. Kawakami, S. Fujioka, K. Kobayashi, Y. Hattori, Y. Kitamura, K. Akaji and E. Ashihara. "Effective internalization of u251-mg-secreted exosomes into cancer cells and characterization of their lipid components." *Biochemical and biophysical research communications* 456 (2015): 768-73.
96. Robbins, P. D. and A. E. Morelli. "Regulation of immune responses by extracellular vesicles." *Nature Reviews Immunology* 14 (2014): 195-208.
97. Morelli, A. E., A. T. Larregina, W. J. Shufesky, M. L. Sullivan, D. B. Stolz, G. D. Papworth, A. F. Zahorchak, A. J. Logar, Z. Wang and S. C. Watkins. "Endocytosis, intracellular sorting, and processing of exosomes by dendritic cells." *Blood* 104 (2004): 3257-66.
98. Hromada, C., S. Mühleder, J. Grillari, H. Redl and W. Holnthoner. "Endothelial extracellular vesicles—promises and challenges." *Frontiers in Physiology* 8 (2017): 275.
99. H Rashed, M., E. Bayraktar, G. K Helal, M. F. Abd-Ellah, P. Amero, A. Chavez-Reyes and C. Rodriguez-Aguayo. "Exosomes: From garbage bins to promising therapeutic targets." *International journal of molecular sciences* 18 (2017): 538.
100. Kang, J.-S. "The potential of exosomes as theragnostics in various clinical situations." In *Exosomes*. Elsevier, 2020, 467-86.
101. Willekens, F. L., J. M. Werre, J. K. Kruijt, B. Roerdinkholder-Stoelwinder, Y. A. Groenen-Döpp, A. G. van den Bos, G. J. Bosman and T. J. van Berkel. "Liver kupffer cells rapidly remove red blood cell–derived vesicles from the circulation by scavenger receptors." *Blood* 105 (2005): 2141-45.
102. Takahashi, Y., M. Nishikawa, H. Shinotsuka, Y. Matsui, S. Ohara, T. Imai and Y. Takakura. "Visualization and in vivo tracking of the exosomes of murine melanoma b16-bl6 cells in mice after intravenous injection." *Journal of biotechnology* 165 (2013): 77-84.
103. Charoenviriyakul, C., Y. Takahashi, M. Morishita, A. Matsumoto, M. Nishikawa and Y. Takakura. "Cell type-specific and common characteristics of exosomes derived from mouse cell lines: Yield, physicochemical properties, and pharmacokinetics." *European Journal of Pharmaceutical Sciences* 96 (2017): 316-22.
104. Hood, J. L. "Post isolation modification of exosomes for nanomedicine applications." *Nanomedicine* 11 (2016): 1745-56. 10.2217/nnm-2016-0102. <Go to ISI>://WOS:000379757600009.
105. Smyth, T., K. Petrova, N. M. Payton, I. Persaud, J. S. Redzic, M. W. Graner, P. Smith-Jones and T. J. Anchordoquy. "Surface functionalization of exosomes using click chemistry." *Bioconjugate chemistry* 25 (2014): 1777-84.
106. Kim, R., S. Lee, J. Lee, M. Kim, W. J. Kim, H. W. Lee, M. Y. Lee, J. Kim and W. Chang. "Exosomes derived from microrna-584 transfected mesenchymal stem cells: Novel alternative therapeutic vehicles for cancer therapy." *BMB reports* 51 (2018): 406.
107. Yu, L., S. Gui, Y. Liu, X. Qiu, G. Zhang, X. a. Zhang, J. Pan, J. Fan, S. Qi and B. Qiu. "Exosomes derived from microrna-199a-overexpressing mesenchymal stem cells inhibit glioma progression by down-regulating agap2." *Aging (Albany NY)* 11 (2019): 5300.
108. Bronisz, A., Y. Wang, M. O. Nowicki, P. Peruzzi, K. I. Ansari, D. Ogawa, L. Balaj, G. De Rienzo, M. Mineo and I. Nakano. "Extracellular vesicles modulate the glioblastoma microenvironment via a tumor suppression signaling network directed by mir-1." *Cancer research* 74 (2014): 738-50.
109. Munoz, J. L., S. A. Bliss, S. J. Greco, S. H. Ramkissoon, K. L. Ligon and P. Rameshwar. "Delivery of functional anti-mir-9 by mesenchymal stem cell-derived exosomes to glioblastoma multiforme cells conferred chemosensitivity." *Molecular Therapy-Nucleic Acids* 2 (2013): 10.1038/mtna.2013.60. <Go to ISI>://WOS:000332468600002.
110. Yang, T. Z., P. Martin, B. Fogarty, A. Brown, K. Schurman, R. Phipps, V. P. Yin, P. Lockman and S. H. Bai. "Exosome delivered anticancer drugs across the blood-brain barrier for brain cancer therapy in danio rerio." *Pharmaceutical Research* 32 (2015): 2003-14. 10.1007/s11095-014-1593-y. <Go to ISI>://WOS:000354098600012.

111. Lang, F. M., A. Hossain, J. Gumin, E. N. Momin, Y. Shimizu, D. Ledbetter, T. Shahar, S. Yamashita, B. P. Kerrigan, J. Fueyo*, et al.* "Mesenchymal stem cells as natural biofactories for exosomes carrying mir-124a in the treatment of gliomas." *Neuro-Oncology* 20 (2018): 380-90. 10.1093/neuonc/nox152. <Go to ISI>://WOS:000425492600011.
112. Zhu, L. Y., J. M. Oh, P. Gangadaran, S. Kalimuthu, S. H. Baek, S. Y. Jeong, S. W. Lee, J. Lee and B. C. Ahn. "Targeting and therapy of glioblastoma in a mouse model using exosomes derived from natural killer cells." *Frontiers in Immunology* 9 (2018): 10.3389/fimmu.2018.00824. <Go to ISI>://WOS:000430566600001.
113. Shi, R., P.-Y. Wang, X.-Y. Li, J.-X. Chen, Y. Li, X.-Z. Zhang, C.-G. Zhang, T. Jiang, W.-B. Li and W. Ding. "Exosomal levels of mirna-21 from cerebrospinal fluids associated with poor prognosis and tumor recurrence of glioma patients." *Oncotarget* 6 (2015): 26971.
114. Santangelo, A., P. Imbruce, B. Gardenghi, L. Belli, R. Agushi, A. Tamanini, S. Munari, A. M. Bossi, I. Scambi, D. Benati*, et al.* "A microrna signature from serum exosomes of patients with glioma as complementary diagnostic biomarker." *Journal of Neuro-Oncology* 136 (2018): 51-62. 10.1007/s11060-017-2639-x. <Go to ISI>://WOS:000419472500006.
115. Akers, J. C., V. Ramakrishnan, R. Kim, S. Phillips, V. Kaimal, Y. Mao, W. Hua, I. Yang, C.-C. Fu and J. Nolan. "Mirna contents of cerebrospinal fluid extracellular vesicles in glioblastoma patients." *Journal of neuro-oncology* 123 (2015): 205-16.
116. Manterola, L., E. Guruceaga, J. G. Perez-Larraya, M. Gonzalez-Huarriz, P. Jauregui, S. Tejada, R. Diez-Valle, V. Segura, N. Sampron, C. Barrena*, et al.* "A small noncoding rna signature found in exosomes of gbm patient serum as a diagnostic tool." *Neuro-Oncology* 16 (2014): 520-27. 10.1093/neuonc/not218. <Go to ISI>://WOS:000333286400007.
117. Lan, F., Q. Qing, Q. Pan, M. Hu, H. Yu and X. Yue. "Serum exosomal mir-301a as a potential diagnostic and prognostic biomarker for human glioma." *Cellular Oncology* 41 (2018): 25-33.
118. Pace, K. R., R. Dutt and D. S. Galileo. "Exosomal l1cam stimulates glioblastoma cell motility, proliferation, and invasiveness." *International Journal of Molecular Sciences* 20 (2019): 3982.
119. Kucharzewska, P., H. C. Christianson, J. E. Welch, K. J. Svensson, E. Fredlund, M. Ringnér, M. Mörgelin, E. Bourseau-Guilmain, J. Bengzon and M. Belting. "Exosomes reflect the hypoxic status of glioma cells and mediate hypoxia-dependent activation of vascular cells during tumor development." *Proceedings of the National Academy of Sciences* 110 (2013): 7312-17.
120. Shao, H. L., J. Chung, L. Balaj, A. Charest, D. D. Bigner, B. S. Carter, F. H. Hochberg, X. O. Breakefield, R. Weissleder and H. Lee. "Protein typing of circulating microvesicles allows real-time monitoring of glioblastoma therapy." *Nature Medicine* 18 (2012): 1835-+. 10.1038/nm.2994. <Go to ISI>://WOS:000311999800032.
121. Huang, K., C. Fang, K. K. Yi, X. Liu, H. Z. Qi, Y. L. Tan, J. H. Zhou, Y. Li, M. Y. Liu, Y. Q. Zhang*, et al.* "The role of ptrf/cavin1 as a biomarker in both glioma and serum exosomes." *Theranostics* 8 (2018): 1540-57. 10.7150/thno.22952. <Go to ISI>://WOS:000424662800007.
122. Shtam, T. A., R. A. Kovalev, E. Y. Varfolomeeva, E. M. Makarov, Y. V. Kil and M. V. Filatov. "Exosomes are natural carriers of exogenous sirna to human cells in vitro." *Cell Communication and Signaling* 11 (2013): 10.1186/1478-811x-11-88. <Go to ISI>://WOS:000329171700001.
123. Pascucci, L., V. Cocce, A. Bonomi, D. Ami, P. Ceccarelli, E. Ciusani, L. Vigano, A. Locatelli, F. Sisto, S. M. Doglia*, et al.* "Paclitaxel is incorporated by mesenchymal stromal cells and released in exosomes that inhibit in vitro tumor growth: A new approach for drug delivery." *Journal of Controlled Release* 192 (2014): 262-70. 10.1016/j.jconrel.2014.07.042. <Go to ISI>://WOS:000342460400029.

124. Yang, T., P. Martin, B. Fogarty, A. Brown, K. Schurman, R. Phipps, V. P. Yin, P. Lockman and S. Bai. "Exosome delivered anticancer drugs across the blood-brain barrier for brain cancer therapy in danio rerio." *Pharmaceutical Research* 32 (2015): 2003-14. 10.1007/s11095-014-1593-y. <Go to ISI>://WOS:000354098600012.
125. Waldenstrom, A., N. Genneback, U. Hellman and G. Ronquist. "Cardiomyocyte microvesicles contain dna/rna and convey biological messages to target cells." *Plos One* 7 (2012): 10.1371/journal.pone.0034653. <Go to ISI>://WOS:000305297500049.
126. Sun, D. M., X. Y. Zhuang, X. Y. Xiang, Y. L. Liu, S. Y. Zhang, C. R. Liu, S. Barnes, W. Grizzle, D. Miller and H. G. Zhang. "A novel nanoparticle drug delivery system: The anti-inflammatory activity of curcumin is enhanced when encapsulated in exosomes." *Molecular Therapy* 18 (2010): 1606-14. 10.1038/mt.2010.105. <Go to ISI>://WOS:000281502300006.
127. Zhuang, X. Y., X. Y. Xiang, W. Grizzle, D. M. Sun, S. Q. Zhang, R. C. Axtell, S. W. Ju, J. Y. Mu, L. F. Zhang, L. Steinman*, et al.* "Treatment of brain inflammatory diseases by delivering exosome encapsulated anti-inflammatory drugs from the nasal region to the brain." *Molecular Therapy* 19 (2011): 1769-79. 10.1038/mt.2011.164. <Go to ISI>://WOS:000295828900005.
128. Alvarez-Erviti, L., Y. Seow, H. Yin, C. Betts, S. Lakhal and M. J. A. Wood. "Delivery of sirna to the mouse brain by systemic injection of targeted exosomes." *Nature Biotechnology* 29 (2011): 341-U179. 10.1038/nbt.1807. <Go to ISI>://WOS:000289284900019.
129. Kooijmans, S. A. A., S. Stremersch, K. Braeckmans, S. C. de Smedt, A. Hendrix, M. J. A. Wood, R. M. Schiffelers, K. Raemdonck and P. Vader. "Electroporation-induced sirna precipitation obscures the efficiency of sirna loading into extracellular vesicles." *Journal of Controlled Release* 172 (2013): 229-38. 10.1016/j.jconrel.2013.08.014. <Go to ISI>://WOS:000327601200026.
130. Haney, M. J., N. L. Klyachko, Y. Zhaoa, R. Gupta, E. G. Plotnikova, Z. He, T. Patel, A. Piroyan, M. Sokolsky, A. V. Kabanov*, et al.* "Exosomes as drug delivery vehicles for parkinson's disease therapy." *Journal of Controlled Release* 207 (2015): 18-30. 10.1016/j.jconrel.2015.03.033. <Go to ISI>://WOS:000354060000003.
131. Fuhrmann, G., A. Serio, M. Mazo, R. Nair and M. M. Stevens. "Active loading into extracellular vesicles significantly improves the cellular uptake and photodynamic effect of porphyrins." *Journal of Controlled Release* 205 (2015): 35-44. 10.1016/j.jconrel.2014.11.029. <Go to ISI>://WOS:000352966200006.
132. Goñi, F. M. "The basic structure and dynamics of cell membranes: An update of the singer–nicolson model." *Biochimica et Biophysica Acta (BBA)-Biomembranes* 1838 (2014): 1467-76.
133. Nicolson, G. L. "The fluid—mosaic model of membrane structure: Still relevant to understanding the structure, function and dynamics of biological membranes after more than 40 years." *Biochimica et Biophysica Acta (BBA)-Biomembranes* 1838 (2014): 1451-66.
134. Vereb, G., J. Szöllősi, J. Matko, P. Nagy, T. Farkas, L. Vigh, L. Matyus, T. Waldmann and S. Damjanovich. "Dynamic, yet structured: The cell membrane three decades after the singer–nicolson model." *Proceedings of the national academy of sciences* 100 (2003): 8053-58.
135. Lipowsky, R. "The conformation of membranes." *Nature* 349 (1991): 475-81.
136. Janmey, P. and P. Kinnunen. "Biophysical properties of lipids and dynamic membranes." *Trends in cell biology* 16 (2006): 538-46.
137. Antonny, B. "Mechanisms of membrane curvature sensing." *Annual review of biochemistry* 80 (2011): 101-23.
138. Callan-Jones, A., B. Sorre and P. Bassereau. "Curvature-driven lipid sorting in biomembranes." *Cold Spring Harbor perspectives in biology* 3 (2011): a004648.
139. Das, S. and R. Rand. "Modification by diacylglycerol of the structure and interaction of various phospholipid bilayer membranes." *Biochemistry* 25 (1986): 2882-89.

140. Killian, J. A. and B. de Kruijff. "Nonbilayer lipids affect peripheral and integral membrane proteins via changes in the lateral pressure profile." *Biochimica et Biophysica Acta (BBA)-Biomembranes* 1666 (2004): 275-88.
141. Zhao, H. and E. Shaqfeh. "The dynamics of a vesicle in shear flow." *Annual Research Briefs...* (2009): 445.
142. Van Meer, G., D. R. Voelker and G. W. Feigenson. "Membrane lipids: Where they are and how they behave." *Nature reviews Molecular cell biology* 9 (2008): 112-24.
143. Weiner, M. D. "Coupling and clustering in molecular dynamics simulation studies of lipid membrane biophysics." (2018):
144. Ding, W., M. Palaiokostas, G. Shahane, W. Wang and M. Orsi. "Effects of high pressure on phospholipid bilayers." *The Journal of Physical Chemistry B* 121 (2017): 9597-606.
145. Peters, J., J. Marion, F. Becher, M. Trapp, T. Gutberlet, D. Bicout and T. Heimburg. "Thermodynamics of lipid multi-lamellar vesicles in presence of sterols at high hydrostatic pressure." *Scientific reports* 7 (2017): 1-15.

Chapter 1

High-Pressure Homogenization in microfluidics for large-scale generation of Exosomes from cell lines

Introduction

In the last decades, EVs like Exos have emerged as a promising carrier for therapeutics [1, 2]. Exos are lipidic bilayer enclosed nanovesicles, measure 30–150 nm in diameter, naturally released by a variety of cells [3-5]. They are biocompatible, low immunogenic and intrinsically express many signal molecules as genetic materials, lipids, transmembrane and membrane-anchored proteins [6]. The presence of these natural compound prolongs their blood circulation, promotes the crossing of biological barriers and allows cellular uptake and release of inner exosomal contents [7]. Despite EVs hold immense promise for therapeutic drug delivery, the clinical application is still complex because of their heterogeneity and low productivity [8, 9].
Indeed, the production of sufficient quantities of Exos for in vivo use is still a rate-limiting step. A dose of 10^9–10^{11} Exos administered per mouse is typically used to achieve biological outcomes [10-12] but living cells in nature secrete only few Exos and the final recovery of a suitable amount requires large numbers of cell cultures incubated for several days to just one treatment. Furthermore, up to date, the current processes have not addressed a scalable methodology for purification and loading of therapeutics before their final recovery. So, also after natural release in the biological fluids, the procedures to isolate and collect them are still laborious and time-consuming.

Nonetheless, molecular engineering has offered recent improvements on such complex issues to make Exos versatile beyond their native functions [13]. Generally, engineering of Exos is adapted from well-established cell manipulation technologies considering that Exos are nanosized structure with a higher degree of membrane curvature and a less surface area.
An example, electroporation, sonication, extrusion and freeze-thawing are just some of the most traditional methods used for the manipulation and lysis of the cell membrane, recently adapted for the encapsulation of Exos with exogenous molecules [14]. Interestingly, among all these techniques, extrusion combine the ex-novo production of nanovesicles from cellular membrane, the so-called vesicles-like" or "exosomes-mimetic" structures [15, 16], and the entrapment in the inner space of a specific compound. Indeed, extrusion is a physical manipulation during which cells are squeezed through 100–400 nm pore size membrane filters. These repeated steps allow the cell break up and recombination into small vesicles-like structures [17].
For instance, this technique was used for the first time by Krishnamurthy, Sangeetha, et al. [18] to produce Core–shell type 'nanoghosts'. These vesicles were synthesized with a drug-loaded biodegradable PLGA core and a monocyte cell membrane-derived shell. To obtain a vesicles-like structures, cell membranes from monocytes were purified by hypotonic lysis of the cells, homogenization, and subsequent isolation of the membrane fraction by serial UC. The purified cell membranes were coated onto Doxorubicin-loaded PLGA NPs by serial extrusion through polycarbonate membranes to form nanoghosts.
Interestingly, also Toledano Furman, Naama E., et al. [19] reported nanoghosts reconstructed from the whole cell membrane of mesenchymal stem cells (MSCs). MSC-NGs are manufactured in a reproducible process by isolating intact MSC cell membranes (ghost cells) and homogenizing them into nanosized vesicles while entrapping a therapeutic of choice. Conversely, Jo et al. [20] reported extrusion thought a microfluidic approach. They developed constriction microchannels with small dimensions that allow the application of elongational and shear force on the surface of the membrane leading to a mechanical breakdown of cells into Exos mimetics with shapes and contents like those of Exos secreted by cells.

Vesicles-like structures were also produced by slicing living cell membrane with micro-fabricated silicon nitride blades [21]. Living cells entered the flow were fragmented by the sharp edge of the silicon blade. Then, the cell fragments can reassemble into Exos mimetics due to the minimization of the free energy of lipid bilayers.

Nonetheless, some reports demonstrated that an improvement in membrane vesicles production could be performed not only through engineering of artificial Exos-like structures but also by applying different stimuli on Exos-producing cells.

For example, Watson et al. [22] used a hollow-fiber bioreactor for the efficient production of bioactive EV. Interestingly they find out a yield reactor ~40- fold higher of EV per mL conditioned medium, as compared to conventional cell culture. However, the obtained sample showed a more heterogeneous population with an increased size range (200–800 nm). Haraszti, Reka Agnes, et al. [23] combined the 3D cultures in bioreactors with tangential flow filtration to produce and concentrate Exos showing a cumulative extent yield of 140-fold compared to 2D culture and dUC.

Conversely, Wang et al. [24] examined the secretion of Exos from PDL cells thought application of mechanical force (cyclic stretch). Interestingly they detected ~4,000 ng/mL of Exos for cyclic stretch-exposed PDL cells within 36 hrs compared to 120 ng/mL in a normal culture of PDL cells at 24 hrs.

Other methods such as low pH [25], hypoxia [26], thermal, oxidative [27], photodynamic [28] stress, have therefore been proposed with promising evidence. An example, Parolini et al. [25] investigate the role of low pH in favoring Exos release from melanoma cells. Interestingly they found out that acid condition enhanced Exos yield by 7.5-fold in 4 days without affecting viability and structural stability of cell.

Despite the potential advantages related to all these methods, few of these, if any, are also able to avoid Exos contamination with apoptotic bodies and cellular debris, size heterogeneity and proteomic alteration.

In our work we show that it is possible to increase Exos production in mammalian cells by exposing them to Pressure stimuli. The rationale behind this study is to favor the natural release of EVs, which generally occurs in specific physio-pathological condition, thought the control of physical parameter as Pressure applied on cell surface.

In the past years several studies were conducted on the cellular structure characterization, cellular deformation and response behavior to mechanical stimuli. However, few studies focused on the effect of high pressures system on cell membrane, giving us only information about cell lysis procedures.

Here we use an industrial opposed stream homogenizer to evaluate the effect of hydrostatic pressure on cell suspension without disrupting them. Our final goal is to provide a scaled-up system for Exos production.

Materials and Methods

Human glioblastoma cell line U87 (passages 15-28) was purchased from ATCC. The cell line was cultured in DMEM supplemented with 10% foetal bovine serum (FBS), 0,1% penicillin–streptomycin and 0,1% L-glutamine (growth medium). All media and reagents for cell culture were purchased by Sigma Aldrich (St. Louis, Missouri, USA) and all cells were incubated at 37°C in 5% CO2/ 95% air.

Standard Exos Isolation

4×10^6 cells per 150T culture Flask have been seeded and let grow until 70-80% confluency. At this stage, adherent cells were washed in PBS (1x) twice, the culture media (CM) was removed and replaced with complete culture media containing Exosome-Depleted Foetal Bovine Serum growth (ThermoFisher Scientific Waltham, Massachusetts, USA). After 48 hrs incubation, 50 mL CM was collected under sterile conditions and transferred to 50 mL polypropylene centrifuge tubes for Exos isolation.
Exos were isolated by dUC. Cell culture supernatants were harvested and centrifuged for 10 min at 300 × g (F15-6x 100y ROTOR) using a SL 16R Centrifuge to get rid of dead cells, then at 2000 x g for 10 min and other 30 min at 10000 x g to eliminate cell debris. Exos were pelleted by dUC of supernatant in 8 mL polycarbonate tubes (Beckman Coulter, Brea, CA, USA) at ~110,000 × g (70,000 RPM – MLA-80 ROTOR) for 70 min using an Optima™ MAX-XP Ultracentrifuge (Beckman Coulter, Brea, CA, USA) and the supernatant was discarded. Finally, pellet resuspended in PBS was washed twice. All procedures were carried out at 4° C. The purified Exos were resuspended in 200 µL of PBS and stored at -20° C prior to use.

Generation of EVs thought High-Pressure-Homogenizer stimuli on cell membrane

Exos were extracted from the cytoplasmatic membranes of U87 cell line. Cell source (7×10^6 cells) was harvested, washed with PBS and re-suspended in cold PBS buffer, pH 7.4, (Sigma-AldrichTM). Cells were homogenized using a bench-top microfluidizer (Model M-110P MicrofluidizerTM Materials Processor, Microfluidics, USA) (94 × 71 × 56 mm, w × d × h). To evaluate the effects of the Pressures and Cycles on cell membrane, three different points at 500-1000-1500 bar, 10 Cycles were tested. The Microfluidic device divides the suspension feed into two opposing microchannels in a Y fixed-geometry interaction chamber (diamond F20 Y-75 µm chamber). Then the two jets of liquid suspension are forced to collide with each other at high Pressure, creating extreme shears, along with cavitation and impact.
A thermocouple was placed in the reservoir close to the discharge port to monitor temperature fluctuations during High Pressure Homogenization.
Isolation of Exos from cell and protein aggregates was performed by dUC. The homogenized cells were centrifuged for 20 min at 300 × g (F15-6x 100y ROTOR) using a SL 16R Centrifuge to get rid of dead cells, then at 2000 x g for 10 min and other 30 min at 10000 x g to eliminate cell debris. Exos were pelleted by dUC of supernatant in 8 mL polycarbonate tubes (Beckman Coulter, Brea, CA, USA) at ~110,000 × g (70,000 RPM – MLA-80 ROTOR) for 70 minutes using an Optima™ MAX-XP Ultracentrifuge (Beckman Coulter, Brea, CA, USA) and the supernatant was discarded. Finally, pellet resuspended in PBS was washed twice. All procedures were carried out at 4° C. The purified Exos were resuspended in 200 µL of PBS and stored at -20° C prior to use.

Exos Characterization

Size, morphology and purity of Standard Exos and Exos produced after HPH cells treatment was assessed to validate their stability.
For Scanning Electron Microscopy (SEM), 100 µL of Exos was poured onto a 0,05 µm Millipore polycarbonate membrane, positioned on a vacuum pump system. Specifically, to retain the Exos, the separation of the solid-liquid mixture was performed by means of a Localized Vacuum/Suction Filtration. Subsequently, the samples were dry at room temperature for 24 hrs. Then, sample was metallized by depositing 7 nm of gold

powder through a 208HR High Resolution Sputter Coater (Cressington Scientific; Watford, UK). Exos morphology was analyzed by an Ultraplus Field Emission SEM, Carl Zeiss; Oberkochen, Germany) with an accelerating voltage of 5 kV, using an InLens detector.

For Transmission Electron Microscopy (TEM) analysis briefly, 5 µL aliquots of isolated Exos (pellet resuspended in 200 µL of water) has been adsorbed till a final amount of 10 or 20 µL onto Formvar/Carbon 200 mesh Cu Agar® grids and fixed in 5% glutaraldehyde for 1 hr. Then, the grids have been washed four times with deionized water drops. Exos have been incubated with Osmium tetroxide (OsO_4), a widely used staining agent used in transmission electron microscopy to provide contrast to the image, for 10 minutes at 4 °C. In the staining of the membrane, OsO_4 binds phospholipid head regions, thus creating contrast with the neighboring protoplasm (cytoplasm), as well, in the case of Exos membranes. Following three washes with water of 5 minutes each, the samples have been contrasted for 10 minutes in 1% uranyl acetate (wt/vol) and eventually dehydrated with an ascending sequence of ethanol (30%, 70%, 90%).

Samples were observed in a Tecnai FEI® transmission electron Microscope operated at 120 kV accelerating voltage.

For Cryo-TEM analysis 3 µL of sample were directly dropped onto Formvar/Carbon 200 mesh Cu Agar® grids. Samples were observed in a Tecnai FEI® TEM operated at 80 kV accelerating voltage.

The concentration and mean size of Exos were determined by recording and analyzing the Brownian motion of particles using a NanoSight NS300 system and NPs Tracking Analysis (NTA) 3.3 - Sample Assistant Dev Build 3.3.203- Analytical Software (Malvern, Worcestershire, United Kingdom) according to the 'manufacturer's protocol. The recorded videos were analyzed using a NPs Tracking Analysis software. The samples are injected in the sample chamber with a sterile syringe until the liquid reached the tip of the nozzle. All measurements are performed at room temperature. Purified Exos were diluted 1:100 in 1 mL PBS at RT and monitored for 260 seconds with manual shutter and gain adjustments. Three measurements of the same sample are performed for all samples.

Mean size of Exos diluted in water (0,8% wt/vol) was analyzed at 25 °C, using a Zetasizer Nano ZS (Model ZEN3600, Malvern Instruments Ltd., UK) equipped with a solid-state laser ($\lambda = 633$ nm) at a scattering angle of 173°. The cuvettes used are the 12 mm square glass cuvettes with square aperture for 90° sizing (Malvern; # PCS1115).

Proteomic Analysis

The recovery of Exos was first estimated by measuring the surface protein quantitation using the BCA assay. The Total protein amount was quantified with QuantiPro™ BCA Assay Kit (Sigma Aldrich; St. Louis, Missouri, USA) in each vesicle preparation.

Exosomal Protein Lysis and Digestion

Briefly, Exos from two sample groups PEV-10 and Standard Exos at a final protein concentration of 30 µg/mL were first mixed with SDS and DTT, boiled, cooled to room temperature, and then alkylated with iodoacetamide in the dark for 30 min. Afterward, to the samples was added a final concentration of 1.2% phosphoric acid and six volumes of binding buffer. After gentle mixing, the protein solution was loaded to an S-Trap filter, spun at 2000 rpm, and the flow-through collected and reloaded onto a filter. This step was

repeated three times, and then the filter was washed with binding buffer 3 times. Finally, digestion buffer containing trypsine at 1:10 wt:wt were added into the filter and digested. The peptides solution ware pooled, lyophilized, and resuspend in Formic acid 0.2%.

Peptide Fractionation

After loading, the peptide mixture was first concentrated and desalted on the pre-column (C18 Easy Column L02 cm, ID=100MM). Each peptide sample was fractioned on a C18 reverse phase capillary column (C18 Easy Column L020cm, ID= 7,5Mm,3µm) working at a flow rate of 250 nL/min.
The gradient used for peptide elution ranged from 5% to 95% of buffer B (ACN LC-MS Grade and HCOOH) in 287 minutes.

Liquid Chromatography Coupled to Tandem Mass Spectrometry (LC-MS/MS)

Peptide mixtures were analyzed by an LTQ Orbitrap XL (ThermoScientific, Waltham, MA) coupled to a nanoLC system (nanoEasy II). Samples were fractionated onto a C18 capillary reverse-phase column (100 mm, 75 µm, 5 µm) working at a flow rate of 250 nl/min, using a linear gradient of eluent B (0.2% formic acid in 95% acetonitrile) in A (0.2% formic acid and 2% acetonitrile in LC-MS/MS grade water, Merck) from 5% to 50% in 285 minutes was run.
The mass spectrometer was operated in positive polarity mode with capillary temperature of 275°C. MS/MS analyses were performed using Data-Dependent Acquisition (DDA) mode: one MS scan (mass range from 400 to 1800 m/z) was followed by MS/MS scans of the 10 most abundant ions in each MS scan, applying a dynamic exclusion window of 40 seconds.

Data Processing

Raw data obtained from nanoLC-MS/MS were analyzed with MaxQuant (1.5.2.8) integrated with the Andromeda search engine. The selected parameters for protein identification were the following. Fixed Modification was Carbamidomhetyl ©, the Trypsin/P was specified as the cleavage enzyme, and up to two missed cleavages were allowed. The FDR was set to <1%.

Bioinformatics Analysis

LFQ is an Extracted Ion Chromatogram method that has been developed for use within MaxQuant software and it is one of the most used approaches in label-free quantification.
The algorithm on which it founds allows almost all the operations needed in a label-free workflow, (feature detection, peptides and proteins identification, data normalization), and results in a quantitative value known as "LFQ Intensity" for each sample, whose ratios are used for relative fold change calculations of the proteins through different samples.

Statistical Analysis

Statistical significant proteins were evaluated by MeV software using an unpaired t-test with a p-value threshold of 0.05. Fold Changes (FCs) of statistical significant proteins were calculated by LFQ intensity ratio between Standard Exos average and PEV-10 average.

Results

Isolation and Characterization of U87-MG Exos

To optimize Exos production, U87-MG cells were cultured according to literature with some modifications. The following parameters were tested:

- the cellular confluence, working in a range between $8*10^6$ and $16*10^6$ cells,
- the incubation time once reached the cell confluence, varying between 24 and 48 hours (hrs),
- the absence or presence in the culture medium of the Exos depleted FBS during the 24-48 hrs of incubation.

This study was done to verify if in a nutrient-free environment, the greater cellular stress could affect the release of vesicles.

It turned out that a good compromise between the quality of the cell culture and the quantity of released Exos resulted by incubating 4×10^6 cells for 24 hrs with complete culture media containing Exos depleted FBS growth supplement.

Once vesicles were isolated by dUC, electron microscopy and NTA were performed to validate the presence and purity of intact Exos and if they are more suitable for onward development. Imaging with SEM, Cryo-TEM and TEM (Figure 1 a-c) shows intact Exos with a very heterogeneous morphology and size, ranging between 30 and 150 nm. NTA is a powerful characterization technique, particularly valuable for analyzing polydisperse nanosized particles. The mean size and SD values obtained by the NTA software correspond to the arithmetic values calculated with the size of the nanoparticles analyzed by the software. NTA showed that the Exos had a narrow size distribution, with a mean particle diameter of 123.5 nm.

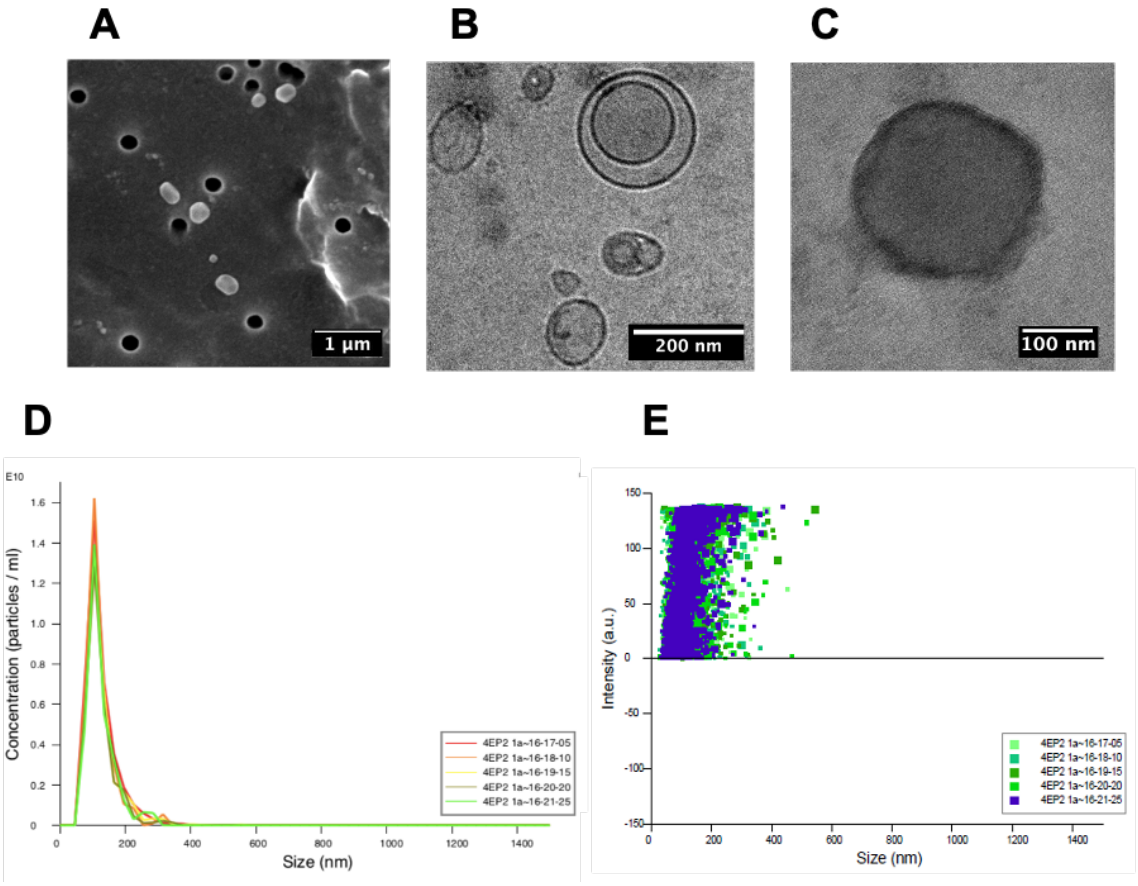

Figure 1. Exos characterization. (a-c) SEM, Cryo-TEM and TEM images of U87 Exos respectively show ovoidal-shaped vesicles with sizes mostly ranging between 30 and 150 nm. (d) particles/mL concentration and (e) distribution by NTA.

Standard Exos vs EVs generated by Pressure cell stimuli: Characterization and Quantification

Here we investigate for the first time the effects of Pressure on cell suspensions to stimulate production and release of Exos from mammalian tumoral cell line.

High-pressure Homogenization is a simple and scalable technique applied for a highly efficient recovery of intercellular materials such as DNA, RNA, proteins or organelles after cell disruption [29-33]. This practice is mostly applied for dense microbial cultures as bacteria, fungi and algae with successful results. However, it often requires pH, chemical, thermal and hypotonic pretreatment along with homogenization. Furthermore, depending on the cell types, Pressure values between 500–2500 bar up to 30 Cycles are applied [34-36].

Such hard conditions are principally due to the recalcitrant prokaryotic cell wall structure and organization. Indeed, Bacteria are multiple layers enclosing cells and the number of layers varies by cell types. An example, gram-positive bacteria have a plasma membrane surrounded by the peptidoglycan layer, whereas gram-negative bacteria, such as *E. coli*, consist of a cytoplasmic membrane, cell wall and an outer membrane. Conversely, mammalian cells as U87-MG tumoral cells, have just a single boundary, the cytoplasmic membrane that encloses the inner contents.

So, with our approach we decided to investigate the effects of relatively mild Pressure condition, between 500 and 1500 bar up to 10 Cycles, applied on U87-MG cell suspension in a physiologic buffer without any kind of pretreatment.
A fixed concentration of $7x10^6$ cell suspension is forced to flow through the Y chamber at three different Pressure values for 10 Cycles. After treatment we performed serial centrifugation ad dUC steps for the final recovery of our Pressured-Cell EVs (PEVs).

Morphology and Size

In Figure 2 are reported results of PEVs stability in terms of morphology (a-d) and average size (e) after Pressure stimuli on cell membrane compared to standard Exos.
Cryo-TEM images show that nanovesicles obtained by treating the cells at 500 (PEV-5) and 1000 bar (PEV-10) are comparable to the standard ones. Indeed, both have a spherical shape and were delimited by a contrasted lipidic bilayer while Exos obtained by treatment at 1500 bar (PEV-15) are elliptical in shape.
Figure 2e shows the effect of Pressure on Exos' average size at 10 Cycles. The Z-Average size by DLS of Standard Exos was 179 nm, EV-5 has a mean size of 160 nm with a polydispersity index (PDI) of 0,382, PEVs-10 has dimension of 95 nm and a PDI of 0,315 while PEVs-15 has dimension of 150 nm and higher PDI (0,500).

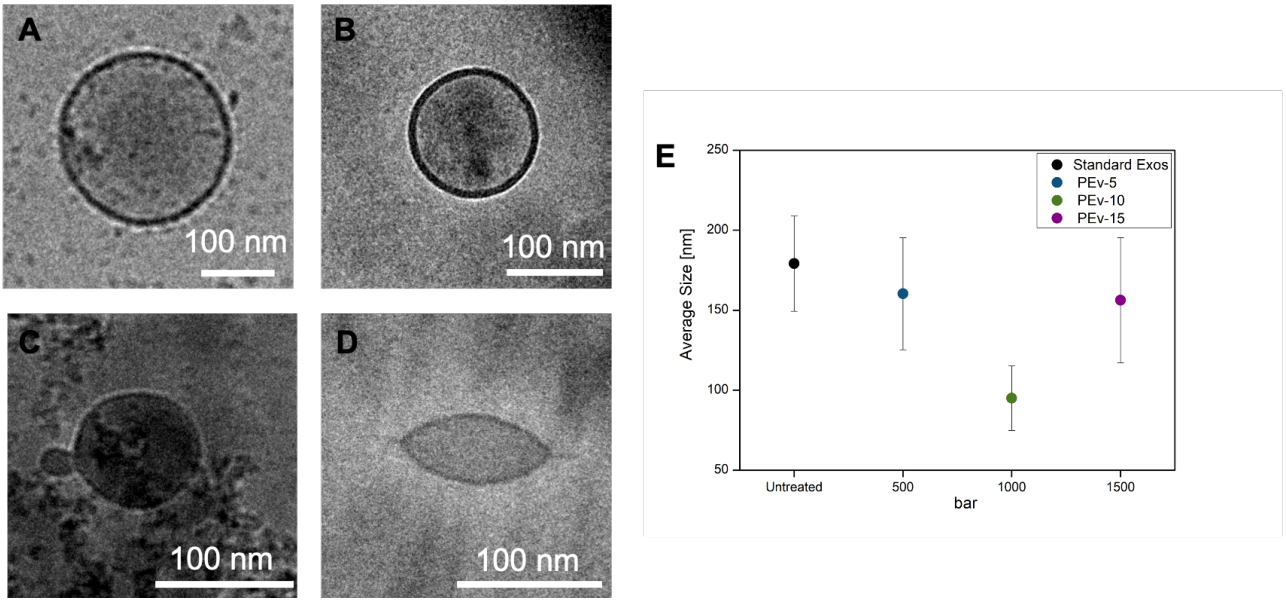

Figure 2. (a-d) Cryo-TEM observation of Exos released by cell in standard condition and under 500-1000-1500 Pressure stimuli after dUC isolation; (a) Standard Exos, (b) PEV-5, (c) PEV-10 and (d) PEV-15; (e) Comparison of Z-Average size by DLS of Standard Exos and PEV.

Among all samples, PEV-10 has a smaller size and higher homogeneity, instead PEV-5 and PEV-15 have a slightly higher dimension but still comparable with standard Exos.
Despite the almost complete overlap of average size between PEV-5 and 15 we can hypothesize two different phenomena during cellular production. The higher PEV-5 polydispersity maybe is due to the coexistence of

smaller sized vesicles and other enclosed structures. Conversely, PEVs-15 Cryo-TEM images show elliptical nanovesicles, so we can hypothesize that stimulation at higher Pressures affects the production of vesicles determining a permanent deformation of their lipidic bilayer.

Nanovesicles Quantification and Biological Stability

Thus, to assess the surface properties and biological stability of PEV-5, PEV-10 and PEV-15, we furthermore analyzed Protein, RNA Content and Zeta Potential (ZP) comparing them with Standard vesicles. Results are reported in Figure 3 (a-c). Figure 3a shows that protein content is almost comparable for Standard Exos and PEV-10. Interestingly, PEV-5 showed a surface protein amount 55% higher than standard Exos while PEV-15 showed 44% less proteins than control vesicles. Figure 3b shows an RNA amount 5 and 3-fold higher in PEV-5 and PEV-10 respectively than Standard Exos while PEV-15 had quite the same concentration.
We can suggest a direct correlation between the biological content of nanovesicles and the applied Pressure: the higher concentration the lower Pressure. Thus, we can speculate that increased Pressure value allows higher instability of biological content and morphology of produced vesicles. Indeed, this hypothesis confirmed by morphological deformation of PEV-15 observed by CRYO-TEM, is in line with ZP data that shows a decreased value in PEV-15 while PEV-5 and 10 have a stable surface charge if compared to control vesicles (Figure 3c). Finally, to confirm our hypothesis we compared NTA particles concentration of PEV-15 with Standard Exos and found out a drastically decrease in PEV-15 particles concentration (Figure 3d).

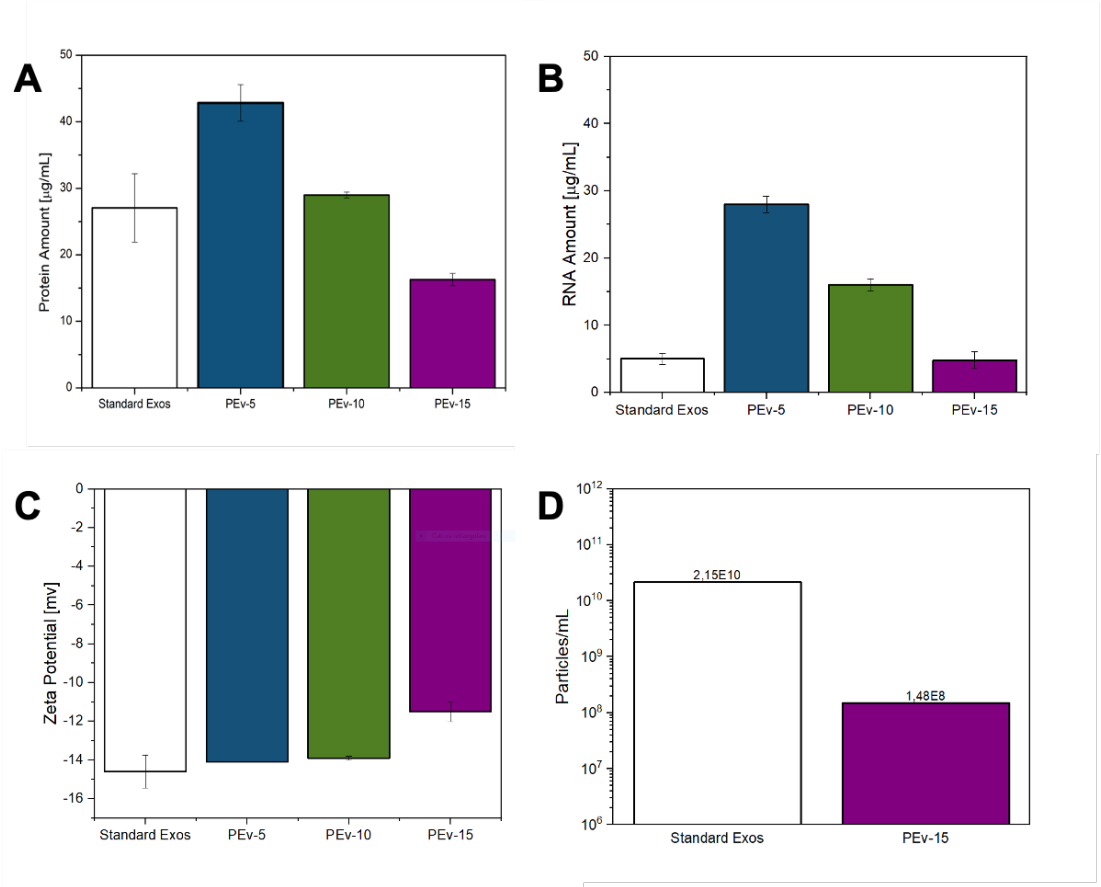

Figure 3. (a) Surface protein, (b) RNA amount after Exos lysis, (c) ZP of Standard Exos and PEV; comparison of NTA analysis of Standard Exos and PEV-15.

Comprehensive Proteomic Analysis of Exos

To further investigate the proteomic stability of our engineered vesicles we compare the proteomic profile of PEV-10, taken as our gold standard, and Standard Exos.

A total of 804 unique proteins were identified in our EVs generated by Pressure cell stimuli. All the proteins identified in our study were compared to those known vesicular proteins in the Exocarta and Vesiclepedia databases. Among the identified proteins, 783 (97%) proteins were common, including some exosomal markers as CD-44 and TGS101 (Appendix). In addition, 21 probable exosomal proteins were also newly identified, which are not present in the Exocarta and Vesiclepedia database (Figure 4a). These data suggested that Pressure stimuli could promote a protein enrichment during Exos biogenesis.

Finally, we compare EV protein contents of PEV-10 and standard Exos. We found a total of 13 statistically significant proteins, among them, 13 were Up-regulated and 0 Down-regulated (Appendix). Volcano plot shows the global proteome changes in PEVs-10 samples vs. control samples (Figure 4b).

Interestingly, many of these 13 Over-expressed proteins are involved in some relevant mechanisms that could favor intercellular communication and fusion of our engineered vesicles with cellular membrane. An example SCAMP3 is a secretory membrane protein that acts as a carrier to the cell surface in post-Golgi recycling pathways during vesicular transport [37]. Another over-expressed protein is VAMP3. This is a vesicle-associated membrane protein and acts as one of the main components of a protein complex involved in the docking and/or fusion of synaptic vesicles with the presynaptic membrane [38].

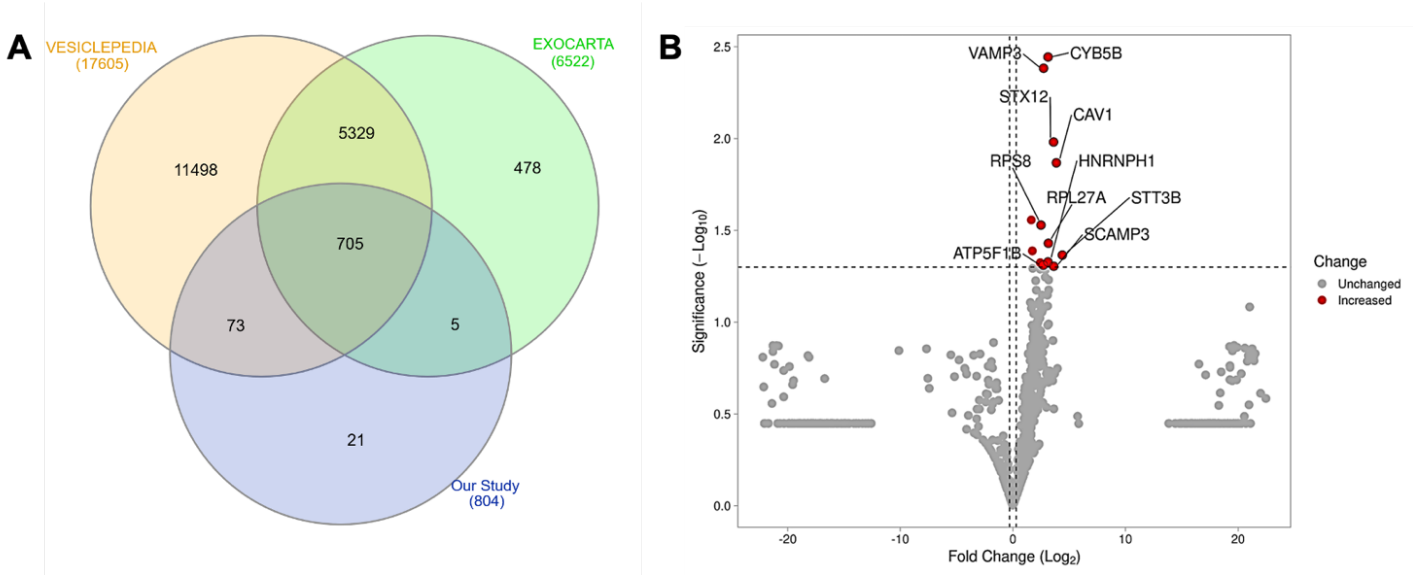

Figure 4. Proteomic analysis of Exos. (a) The Venn diagram displays the overlap of proteins identified in the present study with those in the Exocarta and Vesiclepedia databases (ExoCarta Version 5, Release date: 29 July 2015; Vesiclepedia Version 4.1, Release date: 15 August 2018). (b) Volcano plot showing the global proteome changes in PEVs samples vs. control samples. Individual proteins are represented by red points. The proteins with non-significant differences between the PEVs-10 and control samples are shown in grey.

Discussion

Exos have recently emerged as a promising delivery system to treat malignant tumours. However, the ability to produce large quantities of Exos containing an abundance of endogenous biological material remains a major challenge.

At date a wide range of techniques have been applied to control and increase the biological release of EVs from cells source [22-27].

However, most of these techniques require a long-time incubation in complex bioreactor structures while others stress inducing strategies involve structural damages on cell source membrane. Furthermore, in any case it seems impossible to avoid contamination with cellular debris, and purification methods at date do not allow a complete discrimination between the heterogeneous subpopulation of EVs.

In the present work we proposed the application of Pressure stimuli on cellular membrane as a background method to increase the biological release of EVs from mammalian cell source. The rationale of our work is a controlled manipulation of cell curvature through generation of transient membrane pores to stimulate cellular release of Exos. To achieve a scale-up production of EVs we exploit the application of High-Hydrostatic-Pressure through a High-Pressure-Homogenizer system (HPH). HPH is a wide used technique for cell lysis and isolation of specific cellular components [39]. Indeed, in HPH the liquid stream of suspended cells is forced at high pressure down a narrow channel or across the small gap of a valve. This accelerates its speed, thereby shearing the cells by liquid flow and exploding them by pressure differences between inside and outside of cell. Here we decided to apply mild Pressure condition over 200 bar [40] to induce a nanosecond transient pore formation on cellular membrane without rupture.

Although the precise molecular and cellular mechanisms involved in heightened exosomal production is still a topic of investigation, our results suggest a mechanism by which cellular intrinsic processes can promote Exos generation and subsequent secretion in response to external Pressure stress. Indeed, at three different Pressure condition we obtained EVs different in size, shape, and biological content. Interestingly between 500 and 1000 bar we found out an enrichment in protein and RNA content while at 1500 bar, Pressure seems to have negative effect on EVs release in term of protein assessment and number of particles. Furthermore, it seems also evident that such a high Pressure condition induces a permanent deformation on the lipidic bilayer of released vesicles, elliptic in shape. Once we identified our gold standard procedure for EVs production at 1000 bar 10 Cycles, we further investigated the proteomic expression of PEVs-10. Interestingly proteomic profiling reveled an enrichment with some proteins strongly involved in intercellular communication mechanisms. So further studies are needed to better understand the mechanism related to Exos release under Pressure stimuli and moreover if our engineered nanovehicles could enhance the intercellular communication with targeted cell.

References

1. Yim, N. and C. Choi. "Extracellular vesicles as novel carriers for therapeutic molecules." *BMB reports* 49 (2016): 585.
2. Rufino-Ramos, D., P. R. Albuquerque, V. Carmona, R. Perfeito, R. J. Nobre and L. P. de Almeida. "Extracellular vesicles: Novel promising delivery systems for therapy of brain diseases." *Journal of Controlled Release* 262 (2017): 247-58. 10.1016/j.jconrel.2017.07.001. <Go to ISI>://WOS:000411201100025.
3. Kalra, H., G. P. C. Drummen and S. Mathivanan. "Focus on extracellular vesicles: Introducing the next small big thing." *International Journal of Molecular Sciences* 17 (2016): 10.3390/ijms17020170. <Go to ISI>://WOS:000371830800123.
4. Ferguson, S. W. and J. Nguyen. "Exosomes as therapeutics: The implications of molecular composition and exosomal heterogeneity." *Journal of Controlled Release* 228 (2016): 179-90. 10.1016/j.jconrel.2016.02.037. <Go to ISI>://WOS:000373429600019.
5. Keller, S., J. Ridinger, A. K. Rupp, J. W. G. Janssen and P. Altevogt. "Body fluid derived exosomes as a novel template for clinical diagnostics." *Journal of Translational Medicine* 9 (2011): 10.1186/1479-5876-9-86. <Go to ISI>://WOS:000291822700001.
6. Mentkowski, K. I., J. D. Snitzer, S. Rusnak and J. K. Lang. "Therapeutic potential of engineered extracellular vesicles." *Aaps Journal* 20 (2018): 10.1208/s12248-018-0211-z. <Go to ISI>://WOS:000431135700010.
7. Matsumoto, A., Y. Takahashi, H.-Y. Chang, Y.-W. Wu, A. Yamamoto, Y. Ishihama and Y. Takakura. "Blood concentrations of small extracellular vesicles are determined by a balance between abundant secretion and rapid clearance." *Journal of extracellular vesicles* 9 (2020): 1696517.
8. Bernard, V., J. Ling and A. Maitra. "Heterogeneity of tumor exosomes–role in precision medicine." In *Diagnostic and therapeutic applications of exosomes in cancer*. Elsevier, 2018, 59-67.
9. Jafari, D., S. Malih, M. Eini, R. Jafari, M. Gholipourmalekabadi, M. Sadeghizadeh and A. Samadikuchaksaraei. "Improvement, scaling-up, and downstream analysis of exosome production." *Critical Reviews in Biotechnology* 40 (2020): 1098-112.
10. Kamerkar, S., V. S. LeBleu, H. Sugimoto, S. Yang, C. F. Ruivo, S. A. Melo, J. J. Lee and R. Kalluri. "Exosomes facilitate therapeutic targeting of oncogenic kras in pancreatic cancer." *Nature* 546 (2017): 498-503.
11. Wen, S., M. Dooner, Y. Cheng, E. Papa, M. Del Tatto, M. Pereira, Y. Deng, L. Goldberg, J. Aliotta and D. Chatterjee. "Mesenchymal stromal cell-derived extracellular vesicles rescue radiation damage to murine marrow hematopoietic cells." *Leukemia* 30 (2016): 2221-31.
12. Yi, Y. W., J. H. Lee, S.-Y. Kim, C.-G. Pack, D. H. Ha, S. R. Park, J. Youn and B. S. Cho. "Advances in analysis of biodistribution of exosomes by molecular imaging." *International journal of molecular sciences* 21 (2020): 665.
13. Luan, X., K. Sansanaphongpricha, I. Myers, H. Chen, H. Yuan and D. Sun. "Engineering exosomes as refined biological nanoplatforms for drug delivery." *Acta Pharmacologica Sinica* 38 (2017): 754-63.
14. Xu, M., Q. Yang, X. Sun and Y. Wang. "Recent advancements in the loading and modification of therapeutic exosomes." *Frontiers in bioengineering and biotechnology* 8 (2020):
15. Jang, S. C., O. Y. Kim, C. M. Yoon, D.-S. Choi, T.-Y. Roh, J. Park, J. Nilsson, J. Lotvall, Y.-K. Kim and Y. S. Gho. "Bioinspired exosome-mimetic nanovesicles for targeted delivery of chemotherapeutics to malignant tumors." *ACS nano* 7 (2013): 7698-710.
16. Wu, J.-Y., A.-L. Ji, Z.-x. Wang, G.-H. Qiang, Z. Qu, J.-H. Wu and C.-P. Jiang. "Exosome-mimetic nanovesicles from hepatocytes promote hepatocyte proliferation in vitro and liver regeneration in vivo." *Scientific reports* 8 (2018): 1-11.

17. Lu, M. and Y. Huang. "Bioinspired exosome-like therapeutics and delivery nanoplatforms." *Biomaterials* 242 (2020): 119925.
18. Krishnamurthy, S., M. Gnanasammandhan, C. Xie, K. Huang, M. Cui and J. Chan. "Monocyte cell membrane-derived nanoghosts for targeted cancer therapy." *Nanoscale* 8 (2016): 6981-85.
19. Toledano Furman, N. E., Y. Lupu-Haber, T. Bronshtein, L. Kaneti, N. Letko, E. Weinstein, L. Baruch and M. Machluf. "Reconstructed stem cell nanoghosts: A natural tumor targeting platform." *Nano letters* 13 (2013): 3248-55.
20. Jo, W., D. Jeong, J. Kim, S. Cho, S. C. Jang, C. Han, J. Y. Kang, Y. S. Gho and J. Park. "Microfluidic fabrication of cell-derived nanovesicles as endogenous rna carriers." *Lab on a Chip* 14 (2014): 1261-69.
21. Yoon, J., W. Jo, D. Jeong, J. Kim, H. Jeong and J. Park. "Generation of nanovesicles with sliced cellular membrane fragments for exogenous material delivery." *Biomaterials* 59 (2015): 12-20.
22. Watson, D. C., D. Bayik, A. Srivatsan, C. Bergamaschi, A. Valentin, G. Niu, J. Bear, M. Monninger, M. Sun and A. Morales-Kastresana. "Efficient production and enhanced tumor delivery of engineered extracellular vesicles." *Biomaterials* 105 (2016): 195-205.
23. Haraszti, R. A., R. Miller, M. Stoppato, Y. Y. Sere, A. Coles, M.-C. Didiot, R. Wollacott, E. Sapp, M. L. Dubuke and X. Li. "Exosomes produced from 3d cultures of mscs by tangential flow filtration show higher yield and improved activity." *Molecular Therapy* 26 (2018): 2838-47.
24. Wang, Z., K. Maruyama, Y. Sakisaka, S. Suzuki, H. Tada, M. Suto, M. Saito, S. Yamada and E. Nemoto. "Cyclic stretch force induces periodontal ligament cells to secrete exosomes that suppress il-1β production through the inhibition of the nf-κb signaling pathway in macrophages." *Frontiers in immunology* 10 (2019): 1310.
25. Parolini, I., C. Federici, C. Raggi, L. Lugini, S. Palleschi, A. De Milito, C. Coscia, E. Iessi, M. Logozzi, A. Molinari*, et al.* "Microenvironmental ph is a key factor for exosome traffic in tumor cells." *Journal of Biological Chemistry* 284 (2009): 34211-22. 10.1074/jbc.M109.041152. <Go to ISI>://WOS:000272165200053.
26. King, H. W., M. Z. Michael and J. M. Gleadle. "Hypoxic enhancement of exosome release by breast cancer cells." *BMC cancer* 12 (2012): 1-10.
27. Hedlund, M., O. Nagaeva, D. Kargl, V. Baranov and L. Mincheva-Nilsson. "Thermal-and oxidative stress causes enhanced release of nkg2d ligand-bearing immunosuppressive exosomes in leukemia/lymphoma t and b cells." *PloS one* 6 (2011): e16899.
28. Aubertin, K., A. K. Silva, N. Luciani, A. Espinosa, A. Djemat, D. Charue, F. Gallet, O. Blanc-Brude and C. Wilhelm. "Massive release of extracellular vesicles from cancer cells after photodynamic treatment or chemotherapy." *Scientific reports* 6 (2016): 1-11.
29. Joshi, H. and V. Jain. "Novel method to rapidly and efficiently lyse escherichia coli for the isolation of recombinant protein." *Analytical Biochemistry* 528 (2017): 1-6. 10.1016/j.ab.2017.04.009. <Go to ISI>://WOS:000401685200001.
30. Koschorreck, K., F. Wahrendorff, S. Biemann, A. Jesse and V. B. Urlacher. "Cell thermolysis–a simple and fast approach for isolation of bacterial laccases with potential to decolorize industrial dyes." *Process Biochemistry* 56 (2017): 171-76.
31. Lee, S. Y., J. M. Cho, Y. K. Chang and Y.-K. Oh. "Cell disruption and lipid extraction for microalgal biorefineries: A review." *Bioresource technology* 244 (2017): 1317-28.
32. Zhang, R., J. Chen and X. Zhang. "Extraction of intracellular protein from chlorella pyrenoidosa using a combination of ethanol soaking, enzyme digest, ultrasonication and homogenization techniques." *Bioresource technology* 247 (2018): 267-72.
33. Safi, C., A. V. Ursu, C. Laroche, B. Zebib, O. Merah, P.-Y. Pontalier and C. Vaca-Garcia. "Aqueous extraction of proteins from microalgae: Effect of different cell disruption methods." *Algal Research* 3 (2014): 61-65.

34. Stupak, R., N. Makauskas, K. Radzevičius and Z. Valančius. "Optimization of intracellular product release from neisseria denitrificans using microfluidizer." *Preparative Biochemistry and Biotechnology* 45 (2015): 667-83.
35. Sierra, L. S., C. K. Dixon and L. R. Wilken. "Enzymatic cell disruption of the microalgae chlamydomonas reinhardtii for lipid and protein extraction." *Algal research* 25 (2017): 149-59.
36. Ekpeni, L. E., K. Benyounis, F. F. Nkem-Ekpeni, J. Stokes and A.-G. Olabi. "Underlying factors to consider in improving energy yield from biomass source through yeast use on high-pressure homogenizer (hph)." *Energy* 81 (2015): 74-83.
37. Han, C., T. Chen, M. Yang, N. Li, H. Liu and X. Cao. "Human scamp5, a novel secretory carrier membrane protein, facilitates calcium-triggered cytokine secretion by interaction with snare machinery." *The Journal of Immunology* 182 (2009): 2986-96.
38. Hu, C., D. Hardee and F. Minnear. "Membrane fusion by vamp3 and plasma membrane t-snares." *Experimental cell research* 313 (2007): 3198-209.
39. Shehadul Islam, M., A. Aryasomayajula and P. R. Selvaganapathy. "A review on macroscale and microscale cell lysis methods." *Micromachines* 8 (2017): 83.
40. Tieleman, D. P., H. Leontiadou, A. E. Mark and S.-J. Marrink. "Simulation of pore formation in lipid bilayers by mechanical stress and electric fields." *Journal of the American Chemical Society* 125 (2003): 6382-83.

Chapter 2

Study of Exosomes stability and application of temporary deformability through High Pressure Homogenizer to improve therapeutic application

Introduction

Exos are cell-derived membrane particles that present various advantages over traditional delivery vehicles [1-3]. Their intrinsic cell targeting properties regulates endogenous mechanism for intercellular communication [4, 5]. However, Exos therapeutic applications as drug delivery systems have been limited due to a lack of efficient drug loading methods [6]. At date several approaches are involved but anyway they can be summarized in two different processes, pre and post isolation loading [7].

Generally, loading of small molecules into Exos in a pre-formation approach can be accomplished by transfection of the producer cell with the respective cargo by lipofection [8]. For hydrophobic drugs, Exos loading may be achieved through co-incubation and direct mixing, a practice applicable both before isolation, generally at 37°C combined with an apoptotic UV treatment, and after isolation. For example, Pascucci et al. [9] found that MSCs can acquire strong anti-tumor activity after incubation with a high dosage of Paclitaxel (PTX). Wei et al. [10] recently explored the effect of mesenchymal Exos combined with doxorubicin (DOX) on osteosarcoma in vitro. Loading was achieved by mixing Exos and DOX with a final encapsulation efficiency (EE) of about 12%. Despite these methods do not affect Exos integrity, there is a very low EE due to the lipid bilayer membrane, which restricts passive loading [11]. Moreover, hydrophilic drugs or vectors as nucleic acids cannot incorporate spontaneously into Exos since the drugs have to cross lipophilic Exos bilayer to reach the aqueous core. Generally post-isolation methods are preferred [12].

These processes could involve electroporation, saponin treatment, sonication, extrusion or freeze-thaw cycles [13]. Overall, saponin treatment and electroporation are the most useful methods to load Exos internally with hydrophilic cargo such as siRNA. As example, purified Exos were loaded with approximately 25% of exogenous GAPDH siRNA by electroporation [14]. Momen-Heravi et al. [15] showed that B cell-derived Exos can function as vehicles to deliver exogenous miRNA-155 mimic or inhibitor to primary mouse hepatocytes and RAW 264.7 macrophages, respectively. They optimized electroporation conditions in terms of voltage, capacitance, EVs concentration, and re-isolation method for effective miRNA-155 loading and recovery of B cell Exos. Using optimal settings, 55% of miRNA-155 mimic were loaded successfully into the Exos.

So, electroporation could lead to encapsulation of small molecules in EVs with quite high EE without affecting their integrity and function. Nevertheless, it is a long procedure that can also induce strong aggregation of siRNA even in the absence of Exos leading to possible overestimation of the EE [16]. In addition, it might cause aggregation or fusion of Exos themselves [1].

Surfactants can also be applied to generate pores on exosomal surface, thus increasing membrane permeabilization. For example, saponin and triton have been used to dissolve membrane molecules (e.g. cholesterol) of cell membranes. [17]. Saponin significantly enhances the loading capacity of various types of molecules into Exos, like natural antioxidant [18] or chemotherapeutics [19]. In a recent study DOX and PTX were successfully loaded into SF7761 stem cell-like GMs-derived Exos by microfluidic device in the presence of saponin and shear stress in microfluidic channels [20]. Loading efficiency of DOX and PTX was around 16% and 17.7% respectively. However, there are issues regarding the in vivo hemolytic activity of saponin. Therefore, the concentration of saponin used for drug loading should be limited, and the Exos should be washed and purified immediately after co-incubation.

A valid alternative is represented by sonication. This physical strategy applies an extra mechanical shear force by using a homogenizer probe [21]. The mechanical shear force compromises permanently and temporarily the membrane integrity of the Exos and allows the diffusion of drugs, proteins or other nanomaterials inside

the vesicles during this membrane deformation. Sonication is a spread use loading method especially for hydrophobic drugs. For example, a loading capacity of 11.68 ± 3.68% was demonstrated for Gemcitabine-loaded Exos treated with sonication compared to the incubated sample (2.79 ± 0.72%) [22]. Similarly, Salarpour et al. [23] investigated the effects of 37 °C co-incubation and sonication on EE of PTX and found that the loading of sonication (9.21 ± 0.41 $ng_{PTX}/\mu g_{Exos}$) was higher than that of co-incubation (7.40 ± 0.37 ng/μg). However, in some cases, drugs are not only encapsulated inside the Exos but also attached to the outer layer. Furthermore, this method may lead to aggregation of nanovesicles and damage of their plasma membrane. Nevertheless, Kim et al. [24] demonstrated that this membrane deformation process does not significantly affect the membrane-bound proteins or the lipid contents of the Exos. Indeed, the membrane integrity at some conditions has been found to be restored within an hour after incubation at 37 °C.

During Extrusion, Exos and cargo mixture are forced into a lipid-based syringe with 100–400 nm porous membranes under a controlled temperature. Repeated passages induce the vesicles membrane bilayer collapse and recombination with the drug [3]. Through this method a very high loading efficiency (22.2 ± 3.1%) was achieved for catalase-loaded Exos [25]. Conversely Fuhrmann et al. [26] reported that the loading efficiency of porphyrin into MDA-EVs was dramatically increased by co-incubation with 0.01% (w/v) saponin or by hypotonic dialysis but not by extrusion. Furthermore, they found out that the extrusion method alters the Zeta Potential of the original Exos and causes cytotoxicity. So, whether the harsh mechanical force used in this method changes the membrane properties need further investigations.

However, this strategy offers alluring prospect for the engineering of the so called “vesicles-like” or “exosomes-mimetic” structures [27]. Cells could directly be treated with chemotherapeutic trough a serial extrusion filters with diminishing pore sizes, thus allowing the production of Exos-Mimetic Nanovesicles (EMNVs) [28]. EMNVs showed the same Exos characteristics but a 100-fold higher production yield. Similarly, Naama et al. [29] reported a novel targeted delivery platform based on mesenchymal stem cells nanoghosts (MSC-NGs). These nanosized vesicles. are manufactured in a reproducible process by combination of a homogenizer pretreatment of intact MSC cell membranes (ghost cells) and extrusion of them through 0.4 μm polycarbonate membranes into MSC-NGs.

So together, all these reports demonstrate considerable advanced and improvements for the delicate loading procedure. Nonetheless there is no consensus on which technique results more advantageous and there are still relevant obstacles to overcome before deployment of EVs in large clinical trials. Indeed, the purification of Exos remains laborious, the integrity and biological activity is often compromised, and low EE is still a critical issue. Furthermore, up to date, the current processes have not addressed an industrial application of the Exos Loading and provided a methodology that can guarantee a high and reliable EE in a cost effective and scalable methodology avoiding a time-consuming approach.

In our study we propose High-Pressure Homogenization as the methodology to improve the cargo loading of Exos. This High-Pressure Homogenization works in a turbulent flow situation, thus inducing very high shear forces on the fluid sample in the interaction chamber. It delivers a repeatable process that is guaranteed to scale up to pilot and/or production volumes. At date, biological applications of High-Pressure Homogenizer (HPH) are only aimed at cell lysis for the extraction of proteins or lipids of interest [30-32].

Here, we analyze the dynamic of vesicles in turbulent flow that promotes mixing by a High-Pressure system and take advantage by this system to improve the loading of drug molecules within the Exos. Indeed, Exos, as all vesicle types, are a viscous droplet enclosed by a lipid bilayer. A classical lipid bilayer can be considered as a two-dimensional liquid with its own membrane fluidity and mechanical properties [33].

So, the rationale behind this whole new encapsulation approach is to exploit pressure gradients along with both high shear and elongational stresses acting on vesicles to induce the formation of transient pores or permeabilization of Exos without disrupting them, thus allowing inward diffusion of cargos from the surrounding media.
The goal will be the achievement of the desired stability and reproducibility for loaded Exos treated by HPH and the application of this methodology to obtain a high EE comparable to that of the other drug delivery systems.
To validate our approach, we tested the EE of U87-Exos with different compounds focusing on neurodegenerative and cardiovascular application.

Recently, Exos earned interest in the cardiovascular field due to the fact that, in a multicellular system, such as the heart, communication between different and not always close cells plays a fundamental role in the maintenance of physiological cardiac homeostasis and in the adaptive response to stress [34]. It was demonstrated that EVs are involved in a wide range of cardiovascular processes, both physiological and pathological: Exos are released practically from all cells in the cardiovascular system, and it was shown that stress conditions such as hypoxia or inflammation modulated their cargos and their release in conjunction with the target cells, contributing to improving or to impairing heart function [34].
In particular, atherosclerosis (AS) is the leading cause of coronary atherosclerotic heart disease (CAD), cerebral infarction, and peripheral vascular disease. Currently, treatment in the field of AS is mainly focused on drugs that control blood lipids (such as statins), which do not significantly reduce the prevalence of the disease [35]. Anti-inflammatory strategies have not been confirmed, however Exos application in the field seems an ideal option.
Indeed, emerging evidence suggests that Exos released from endothelial cells, smooth muscle cells, adipose cells, platelets, cardiomyocytes, and stem cells play crucial roles in the development and progression of coronary artery disease [36]. Exos can participate in intercellular communication in a paracrine manner or an endocrine manner, in order to maintain the homeostasis and respond to stress adaptively [37].
Lai et al. [38] first showed that human mesenchymal stem cells (MSCs) secreted 50- to 100 nm membrane vesicles. Using an ex-vivo Langendorff model of ischemia/reperfusion injury, they observed that these purified Exos were able to reduce infarct size in mouse hearts. Arslan et al. [39] further demonstrated that a single intravenous bolus of Exos 5 min prior to reperfusion reduced infarct size by 45% in mice. Importantly, they found that Exos treatment restored energy depletion and redox state in mouse hearts within 30 min after I/R, evidenced by elevation of ATP and NADH levels, and reduction of oxidative stress.
Exos released by cardiac progenitors have been shown to prevent ischemic myocardium against acute ischemia/reperfusion injury through miR-451 [40]. Cardiac progenitor cell-derived Exos could also protect cardiomyocytes against oxidative stress-related apoptosis via exosomal miR-21 by targeting programmed cell death 4 (PDCD4) [41]. Moreover, the exosomal transfer of miR-126 and miR-210 from host cells to transplanted cells could improve the survival of transplanted cardiac progenitor cells into the ischemic myocardium [42].
Bouchareychas et al. [43] in a recent study show that Exos produced by naïve bone marrow-derived macrophages (BMDM-exo) contain anti-inflammatory microRNA-99a/146b/378a that are further increased in Exos produced by BMDM polarized with IL-4 (BMDM-IL-4-exo). Repeated infusions of BMDM-IL-4-exo into Apoe/ mice fed a Western diet reduce excessive hematopoiesis in the bone marrow and thereby the number

of myeloid cells in the circulation and macrophages in aortic root lesions. This also leads to a reduction in necrotic lesion areas that collectively stabilize atheroma.

Also in the neurodegenerative field, with a particular focus on glioma treatment and diagnosis, promising experiments showed Exos application as an ideal delivery system.
Exos ability as signaling in local and remote intercellular crosstalk enables them to deliver more efficiently macromolecular drugs, lipids, proteins, and genetic material such as miRNA siRNA to the brain [44].
Further benefits can be achieved through exogenous or endogenous modification strategies.
Exogenous modification occurs after cell culture production through the surface conjugation of specific receptors or encapsulation with hydrophilic/hydrophobic compounds. Exos might be modified endogenously through manipulation at the cellular level. In this case, the modification of progenitor cells can occur by the incubation of drug molecules or by transfection or transduction with expression vectors that lead to the secretion of EVs containing drug molecules, viral proteins, nucleic acids, RNA, and proteins [12].
At date, Exos derived from MSCs transfected with anti-tumor miRNAs have been found to be promising therapeutic tools for glioma therapy [45].
An example, Kim et al. [46] used Exos derived from MSCs transfected with miRNA-584. miRNA-584 acts as a tumor suppressor in some cancers and inhibits specifically glioma cells activity by binding to the 3′-UTR of CYP2J2. Interestingly, they demonstrated that MSCs exosomal miRNA-584 affects invasive ability of U-87 MG cells in vitro and decrease tumor mass weights in U87 MG xenograft nude mouse model.
The glioma development could also be prevented by down-regulation of Arf GTPase- activating protein-2 (AGAP2), a target gene of microRNA-199a (miR-199a). In lines with this finding, Yu et al. [47] showed that miR-199a when delivered via MSCs-derived Exos inhibiting in vitro U251 glioma cell proliferation, migration and invasion. Additionally, Katakowski et al. [48] tested MSC Exos as a miRNA delivery vehicle in malignant glioma. Over-expressed miR-146b in MSC Exos (M146-exo) were tested both in vitro and in vivo. Initially, they conducted an in vitro study on 9L cells and found out that, after 7 days, in vitro growth of M146-exotreated 9L cells was significantly less than normal MSC Exos-treated control. Finally, to determine if M146-Exo had an anti-tumor effect in vivo, they administered M146-exo or M67-exo to Fischer rats bearing 9L gliosarcoma. One intra-tumor injection of M146-exo, 5 days after intracranial tumor xenograft implantation, led to a significant reduction in tumor volume at 10 days post-implant compared to control.
Although MSC Exos are the most used therapeutic tool for miRNA transfection in glioma treatment, also tumoral Exos could be applied. Indeed, it can not be excluded that the overexpression of specific tumoral biomolecules may further favor cellular Exos communication with receiving cell and selectivity to the tumoral microenvironment. In this regard, Bronisz et al. [49] identified miR-1 deficiency as a contributor to glioma invasiveness and neovascularization and demonstrated that reintroduction of miR-1 into GBM Exos through transfection of U-87 MG and X12 cells reverted paracrine-stimulated malignancy and microenvironmental remodeling by tumor. These findings support the hypothesis that miRNA replacement approaches have strong therapeutic potential and can be mediated by EVs. In addition, they raise the possibility that modified tumor Exos might be employed as biological Trojan horses to suppress tumor cells and their effect upon the brain microenvironment.
Reinforcing this point, it seems clear that miRNAs are often involved in the inhibition of tumor developmental processes. On the other hand, miRNA can behave not exclusively as tumor suppressors but also as oncogenes.

Indeed, deregulation of microRNA expression has been observed in several cancers' progression mechanisms, including GBM.

Among these, Munoz et al. [50] focused on miR-9 molecules that have been shown to suppress the mesenchymal differentiation of GBM cells. They identified an increase of miR-9 concentration in TMZ-resistant GBM cells, involved in the expression of the drug efflux transporter P-glycoprotein. On this basis, they showed that reversed chemoresistance of GBM cells to TMZ occurred by targeting of anti-miR through MSCs. To block miR-9, they tested anti-miR-9-Exos obtained from transfection with MSC cells. Cell viability assay showed that the anti-miR-9-Exos treatment enhances TMZ-induced cell death in U87 MG and T98G.

Furthermore, transwell studies indicated that MSCs could communicate with cancer cells through gap junctional intercellular communication (GJIC) and through secreted Exos. Although further investigations have to be performed, this finding is relevant in the comprehension of Exos and in vivo studies could confirm that the release of Exos can affect GBM at a considerable distance from the MSCs.

Finally, several studies exploited drug-loaded Exos as a novel drug delivery systems. Although cellular packaging during EV biogenesis is a common and simple strategy, it involves the use of large amount of material and often has inefficient loading outcomes. The loading of EVs with therapeutic products after their isolation could represent a valid alternative. The simplest method is the passive incubation of isolated EVs with the therapeutic molecule, as reported by Yang et al. [51].

First of all, they highlighted the effect of the molecular characteristics of Exos derived from the human brain neuronal glioblastoma-astrocytoma U-87 MG and the brain endothelial bEND.3 on their ability of interaction and the crossing of biological barriers. Their results demonstrated that bEND.3-derived Exos allowed a higher internalization of the fluorescent marker in bEND.3 cells via an energy-dependent internalization process (cell uptake studies were performed both at 37 °C and 4 °C). Moreover, this active process was assumed to be receptor-mediated endocytosis by CD63 tetraspanins transmembrane proteins that are overexpressed in brain endothelial cells. Reinforcing this point, they reported the use of both U-87 MG and bEND.3 Exos to deliver paclitaxel (PTX) or doxorubicin (DXR) across the BBB in a zebrafish model of brain tumor employing U-87 MG glioma. Freely administered DXR and PTX are not able to cross the BBB while the vesicles-packaged tool facilitated drug delivery across the BBB, reducing tumor progression.

Promising experiments showed the possibility of simultaneous Exos engineering through surface modification and drug loading for imaging and therapy in vitro and in vivo. Jia et al. [52] firstly loaded superparamagnetic iron oxide nanoparticles (SPIONs) and curcumin (Cur) into Exos and then conjugated the Exos membrane with neuropilin-1-targeted peptide (RGERPPR, RGE) by click chemistry to obtain glioma-targeting Exos with imaging and therapeutic functions.

Furthermore, the engineering of Exos by both drug loading and surface functionalization was also recently performed by Ye et al. [53]. They reported a double functionalization of methotrexate (MTX)-loaded EVs with both the targeting pro-apoptotic peptide, KLA, and the targeted low-density lipoprotein, LDL, for selective binding to the LDL receptor (LDLR) overexpressed on the BBB and GBM cell lines. Indeed, the role of KLA was highlighted by observation under confocal microscopy. EVs decorated with KLA and LDL (EVs-KLA-LDL) were incubated with U-87 MG glioma spheroids for 12 h to assess their penetrating ability. EVs modified with the targeting peptide had an increased uptake by U-87 MG cells as well as an augmented permeation capacity into tumor cells. Furthermore, ex vivo fluorescence studies of the brain performed after intravenous injections of DiR-labeled EVs or EVs-KLA-LDL confirmed that EVs-KLA-LDL crosses the BBB and

penetrates the brain more efficiently than blank-EVs, which might be attributed to the interaction between the LDL peptide and the LDLR over-expressed at the BBB.
Thus, the engineering of the EV surface prompts the process of membrane receptor-mediated internalization both in vitro and in vivo and provides a unique opportunity to deliver KLA and MTX to the U-87 MG glioma.
To improve the BBB permeation, studies have focused not only on chemical modifications and genetic engineering. The application of a focused ultrasound system (FUS) produce a reversible and local disruption of BBB; Bai et al. [54] designed a drug delivery system that combines doxorubicin (Dox)-loaded Exos derived from macrophages (R-Exos) and blood serum (B-Exos) for glioma diagnostics and therapy with two FUS treatments. Importantly, through this combination, they demonstrated a visible regression of tumor growth in orthotopic gliomas and an extended survival time, leading to a significant improvement over free Dox and Exos-Dox treatments.

Aim of our work is the creation of a new theranostic platform for the Atherosclerosis Plaque (AP) and glioma treatments. To validate the feasibility of our system we will exploit Exos interaction with different active substance, small hydrophilic molecules, lipophilic drug, and more complex structures.
In detail we choose:

- prodrug Irinotecan (IRI) a chemotherapy agent used in the treatment of a variety of solid tumors, such as colorectal, pancreatic, ovarian, and lung cancers with promising activity against a wide spectrum of malignancies, including GBM [55]. It causes S-phase-specific cell killing by poisoning topoisomerase I in the cell and, as a prodrug, it needs to be converted in the active SN-38 a competitive analogue of topoisomerase-I inhibitor [56]. To the best of our knowledge, at date no study on interaction between IRI and Exos has yet been conducted for the treatment of glioblastoma (GBM).
- Gd-diethylenetriamine penta-acetic acid (Gd-DTPA) a positive contrast agent for MRI, currently adopted in clinical practice [57].
- Cerium oxide nanoparticles (CeO_2NPs) novel synthetic antioxidant agents proposed for treating oxidative stress-related diseases. Owing to their antiradical activity, different studies have shown that CeO_2NPs help reducing symptoms of many oxidative stress-related diseases, including neurodegenerations, retinitis, chronic inflammation, diabetes, and cancer and significantly improves endothelial-dependent vasodilation in cardiovascular system [58-61].

So first, we applied our novel procedure to encapsulate U87-MG Exos with two small molecules as Gd-DTPA and IRI. After the optimization of Exos loading, we validate their nanobiointeraction, uptake mechanisms and cytotoxic effect in a 2D model of glioma tumoral microenvironment.
Then, we conducted preliminary analysis in a more complex environment such as the human AP removed by surgical endarterectomy. First, we optimized synthesis of CeO_2NPs to improve their structural stability, then we observed their cytotoxicity and uptake in vitro and ex vivo.
Furthermore, to confirm the pathophysiological production of Exos within the AP we evaluated their localization in such a complex environment.

Next step will be the Co-encapsulation of small active compounds and more complex structures as Ce_2ONPs for the creation of a complete theranostic platform.

Materials and Methods

Cerium (III) nitrate hexahydrate ($Ce((NO_3)_36H_2O)$), ethylene glycol (EG), were purchased from Sigma-Aldrich, USA. Ammonium hydroxide (NH_4OH) (29.44%) was purchased from Fisher Scientific, USA. Millipore water was used for all experiments.

Glutaraldehyde (25% aqueous solution; EM Grade, molecular formula $OCHCH_2CH_2CH_2CHO$, CAS no. 111-30-8) paraformaldehyde (16% aqueous solution, EM Grade, methanol-free solution, specific gravity: 1.09, molecular formula: HCHO), sodium cacodylate buffer (prepared from sodium cacodylate trihydrate, F.W. 214.02), potassium ferrocyanide (ACS reagent, molecular formula K3Fe(CN)6, F.W. 329.25), osmium tetroxide (4% aqueous solution, molecular formula OsO_4, F.W. 254.20), uranyl acetate (4% aqueous solution ACS reagent, molecular formula $UO_2(OCOCH_3)_2 \cdot 2H_2O$, F.W. 424.14), Spurr epoxy resin (low-viscosity kit: Nonenyl Succinic Anhydride (NSA), EM grade, DER 736, specific gravity: 1.14, ERL 4221 Cycloaliphatic Epoxide Resin specific gravity ($H_2O = 1$), DMAE 2-dimethylaminoethanol $C_4H_{11}NO$, F.W. 89.14, specific gravity: 0.883–0.888) were purchased from Electron Microscopy Sciences. The Milli-Q Water (Milli-Q Plus) was used for synthesis and characterization.

Human glioblastoma cell line U87 (passages 15-28) was purchased from ATCC. The cell line was cultured in DMEM supplemented with 10% foetal bovine serum (FBS), 0,1% penicillin–streptomycin and 0,1% L-glutamine (growth medium). All media and reagents for cell culture were purchased by Sigma Aldrich (St. Louis, Missouri, USA) and all cells were incubated at 37°C in 5% CO_2/ 95% air.

Cell viability was assessed by Trypan Blue stain 0.4% (Invitrogen™, ThermoFisher Scientific; Waltham, Massachusetts, USA) and determined using a Countess II FL Automated Cell Counter (ThermoFisher Scientific; Waltham, Massachusetts, USA).

Irinotecan HCl Trihydrate-CPT 11 (molecular formula $C_{33}H_{39}ClN_4O_6$, Mw = 677.18 g/mol) was purchased from Selleckchem (Houston, USA).

The selected cell line for the NPs in vitro study was the Panc-1, human epithelioid carcinoma of pancreatic tissue. The A549 cells, human epithelial carcinoma of lung tissue, were used as a control cell line. Panc-1 and A549 cells were cultured in (DMEM), supplemented with 2mM Glutamine and 10% Fetal Bovine Serum (FBS) and 1% penicillin/ streptomycin (Gibco, Invitrogen, Belgium). A549 cells were passaged every 48 h and split 1/5, while Panc-1 cells were passaged every 48 h and split 1/3. Cells were passaged when reaching near 80% confluency by lifting the cells with 0.05% trypsin and were plated (1/5 or 1/3) onto flasks.

Exos production and Isolation

4×10^6 cells per 150T culture Flask have been seeded and let grow until 70-80% confluency. At this stage, adherent cells were washed in PBS (1x) twice, the CM was removed and replaced with complete CM containing Exosome-Depleted Foetal Bovine Serum growth (ThermoFisher Scientific Waltham, Massachusetts, USA). After 48 hrs incubation, 50 mL CM was collected under sterile conditions and transferred to 50 mL polypropylene centrifuge tubes for Exos isolation.

Exos were isolated by dUC. Cell culture supernatants were harvested and centrifuged for 10 min at 300 xg (F15-6x 100y ROTOR) using a SL 16R Centrifuge to get rid of dead cells, then at 2000 xg for 10 min and other 30 min at 10000 xg to eliminate cell debris. Exos were pelleted by dUC of supernatant in 8 mL polycarbonate tubes (Beckman Coulter, Brea, CA, USA) at ~110,000 × g (70,000 RPM – MLA-80 ROTOR) for 70 minutes using an Optima™ MAX-XP Ultracentrifuge (Beckman Coulter, Brea, CA, USA) and the supernatant was discarded. Finally, pellet resuspended in PBS was washed twice. All procedures were carried out at 4° C. The purified Exos were resuspended in 200 µL of PBS and stored at -20° C prior to use.

Exos Characterization

Size, morphology and purity of Exos were observed before and after HPH treatment to validate the stability of vesicles.

For Cryo-TEM analysis 3 µL of sample were directly dropped onto Formvar/Carbon 200 mesh Cu Agar® grids. Samples were observed in a Tecnai FEI® TEM operated at 80 kV accelerating voltage.
The concentration and mean size of Exos were determined by recording and analyzing the Brownian motion of particles using a NanoSight NS300 system and NPs Tracking Analysis (NTA) 3.3 - Sample Assistant Dev Build 3.3.203- Analytical Software (Malvern, Worcestershire, United Kingdom) according to the manufacturer's protocol. Purified Exos were diluted 1:100 in 1 mL PBS at RT and monitored for 260 seconds with manual shutter and gain adjustments. The recorded videos were analyzed using a NPs Tracking Analysis software. Mean size of Exos diluted in water (0,8% wt/vol) was analyzed at 25 °C, using a Zetasizer Nano ZS (Model ZEN3600, Malvern Instruments Ltd., UK) equipped with a solid-state laser ($\lambda = 633$ nm) at a scattering angle of 173°. The cuvettes used are the 12 mm square glass cuvettes with square aperture for 90° sizing (Malvern; # PCS1115). The recovery of Exos was indirectly estimated by measuring the surface protein quantitation using the BCA assay. Total protein amount was quantified with QuantiPro™ BCA Assay Kit (Sigma Aldrich; St. Louis, Missouri, USA) in each vesicle preparation.

Exos stability to HPH Treatment

To assess the stability of Exos subjected to HPH, samples were processed using a bench-top microfluidizer (Model M-110P Microfluidizer™ Materials Processor, Microfluidics, USA) (94 × 71 × 56 mm, w × d × h). To evaluate the effects of the Pressures and Cycles, three different points at 500-1000-1500 bar and from 1 up to 10 Cycles were tested. The Microfluidic device divides the suspension feed into two opposing microchannels in a Y fixed-geometry interaction chamber (diamond F20 Y-75 µm chamber). Then the two jets of liquid suspension are forced to collide with each other at high Pressure, creating extreme shears, along with cavitation and impact.
A thermocouple was placed in the reservoir close to the discharge port to monitor temperature fluctuations during HPH. An ice bath to cool the cooling external coil was used to keep the temperature in a range from 4-10 °C.

HPH treatment as a novel encapsulation method

IRI was incorporated into Exos through HPH. For high drug-loading efficiency, a series of ratios were assessed. Three different Molar concentrations (50-75-100 μM) were pre-mixed with naive Exos at a fixed concentration of 3.24×10^{23} particles/mL in PBS and fed to the system through a stainless-steel feed reservoir. HPH was carried out at fixed Pressures and Cycles (500 bar-9 Cycles, 1000 bar-5 Cycles, 1500 bar-2 Cycles). Then, the collected sample was purified through Spin-X corning Centrifugation 3KDa Cut-off performed at 3000 xg 60 minutes 4° C.

Finally, EE was determined. The Exos bilayer was disrupted with 0,075 % v/v Triton X-100 to release the encapsulated drug. The concentration of drug in the solution was determined using a UV−vis spectrophotometer at a wavelength of 364 nm.

The loading capability of Gd-DTPA is calculated by Inductively Coupled Plasma (ICP-MS) NexION 350 measurements. All data are collected and processed using the Syngistix Nano Application Module. Gd-DTPA is measured at m/z 157 using a 100 μs dwell time with no settling time.

In vitro MR of loaded Exos were compared to control water solutions at a known concentration of Gd-DTPA. After vigorous stirring, 300 μl of the sample are put in glass tubes and changes in relaxation time (T1) were evaluated at 1.5 Tesla by Minispec Bench Top Relaxometer (Bruker Corporation). The relaxation time distribution is obtained by a CONTIN Algorithm and the relaxation spectrum is normalized by its processing parameters. The integral of a peak corresponds to the contribution of the species exhibiting this peculiar relaxation to the relaxation time spectrum. Experiments were repeated at least ten times.

In vitro preliminary study

Release profile and cytotoxicity in vitro

In order to measure the in-vitro drug release profile, 5 mL of IRI-Exos-15 were transferred into dialysis tubes with 3 KDa cut-off immersed in PBS at pH 7.4 or pH 4.2. The drug release study was performed at 37°C and at different time intervals, up to 48 hrs.

The antitumor effect of engineered Exos loaded with IRI was evaluated by the standard MTT assay on U87-MG cells. Briefly, tumor cells (15×10^3 cells/well) were seeded in 200 μL of media in a 96-well plate overnight. Tumor cells were treated with concentrations of Free-IRI and IRI-Exos-15 ranging between 0.25 and 10 μM for 24 and 48 hrs at 37°C and 5% CO_2. After incubation, CM was removed, and cells were incubated with MTT reagent for 3–4 hrs. Subsequently, 100 μL of DMSO was added to solubilize purple formazan crystals. Cytotoxic activity of Free-IRI and IRI-Exo-15 was then evaluated by standard MTT assay. Absorbance was measured by spectrophotometer at 545–630 nm. Survival rates were assessed compared to the negative control (wells containing only Untreated Exos). All experiments were repeated 3 times.

Exos uptake flow cytometry study

$1x10^5$ U87 MG cells/well were seeded in 48-well plates (Falcon®) and incubated for 24 hrs. Afterwards, cells were incubated with CM supplemented with IRI-Exos-15 or Free-IRI for 30 min, 2 hrs, 4 hrs, 6 hrs, 8 hrs, 24 hrs and 48 hrs at a final concentration of 10 μM. Negative control consisted in the complete medium condition (medium, FBS, L-glutamine and penicillin/streptomycin) with an equal amount of PBS.

After different time points contacts, CM was removed, and the samples were washed three times with PBS (1x) to ensure particle removal from the outer cell membrane. Cells were then trypsinized for 5 minutes at 37° C. After cell detachment confirmation at optical microscope, CM was added to neutralize the trypsin and all the content transferred to polystyrene round-bottomed tubes (Falcon®), before samples were immediately analyzed by flow cytometry.
Every flow cytometry study has been conducted in triplicate, and the average of the three samples is considered for Forward Scattering (FSC), Side Scattering (SSC) and Fluorescence Intensity Mean in order to obtain reliable results in terms of viability and internalization information. All the analyses have been conducted on BD FACSMelodyTM.
Results are reported as the mean of the distribution of cell fluorescence intensity obtained by measuring 10000 events averaged between 3 independent replicas. Error bars correspond to the standard deviation between the triplicates.

Exos Confocal microscopy analysis

$8x10^4$ U87 MG cells were seeded in 8-well µ-slide (inverted for high-end microscopy) (Ibidi®) and incubated at 37°C for 24 hrs. Afterwards, cells were incubated 24 hrs with IRI-Exos-15 previously stained with PKH67 according to the manufacturer's protocol.
At different timepoints, CM was removed, samples were washed three time with PBS (1x) and fixed with 4% paraformaldehyde (PFA) for 15 minutes. Cells were stored at 4°C until confocal microscopy was performed. After fixation cellular nucleus was stained with Hoechst dye 1:1000.
The sample was then observed using an TCS SP5 Confocal Laser Microscope (Leica Microsystems©).
Two lasers with different wavelengths were used for excitation of PKH67 and Hoechst dyes, respectively at 488 nm and 543 nm excitation and 500-530 nm and 560-610 nm emission wavelengths. HCX PL APO CS 63x1.40 Oil objective was used; laser intensities were between 5 and 20%.

CeO_2 NPs synthesis and characterization

7,8 mL of EG was slowly dissolved in 92,2 mL of Milli-Q water in a round-bottom flask. After the complete dissolution, 5,16 g of cerium nitrate (0.012 mol) (1:10 ethylene glycol) was added to the mix. Solution was then stirred 5 minutes and 4,5 ml of NH_4OH was added to reach pH 9.6.
The round-bottom flask containing the sample was put into the oil bath and the reaction was conducted for 50 minutes at 50° C. After heating, 0,001% of Tween 80 was added to the solution under mild stirring. Samples was than washed three times by centrifugation and the pellet obtained was freeze-dried to obtain a powder.
For TEM analysis 0,1 mg of powder were suspended in 1 mL of water. 5 µL of sample was also analyzed with a Tecnai FEI® transmission electron Microscope with a Formvar/Carbon 200 mesh Cu Agar® filter.
SEM observation was performed after 100 µL were deposited on a polycarbonate Isopore Membrane Filter (0.05 µm) by ultrafiltration vacuum system. The deposited particles were gold palladium coated, and an ULTRA PLUS field emission scanning electron microscope (FE-SEM Carl Zeiss, Oberkochen, Germany) was used to observe particles morphology. The samples for FT-IR analysis were pelletized using KB at 0.25% w/w.

CeO_2 NPs Cell viability, Oxidative stress and mitochondrial health

Panc-1 were seeded in a concentration of 2000 cells/ well in the 96 well Plate. The cells were incubated with NPs at a maximum concentration of 100 μg/mL for 24 hrs.

After cell labeling, cells were washed twice with 100 μL PBS/well to remove any remaining NPs. It was added to each well (100 μL/well) the medium with 200nM of MitoTracker and 100 nM of Image- iT DEAD Green and the cells were incubated for 30 min at 37°C in a 5% CO_2 atmosphere. Cells were then washed twice with PBS and fixed with 4% paraformaldehyde for 15 min at RT in dark conditions.

The fixative was then washed with 100 μL PBS/well and treated with 4′,6- diamidino-2-phenylindole (DAPI) at 300 nM in PBS for 10 min in the dark. Each well was aliquoted with 100 μL of PBS and plates were analyzed on the InCell 2000 analyzer (GE Healthcare Life Sciences, Belgium) where phase contrast and fluorescence-based images for the red, green and blue channel were collected at minimum 2000 cells/well.

The level of cell viability was calculated as follows:

First, cells were segmented based on the phase contrast images and cell cytoplasm was then segmented based on the green channel using the segmented phase contrast images as seed images. Then, the total number of cells minus the number of dead cells (red channel; dead cells are defined as clear red dots, with intensity levels minimally 3-fold above noise level and size of minimally 2 μm within the cytoplasmic area of a single cell, where multiple red dots can be colocalized with a single cytoplasmic area). These values are then normalized to the control values (= 1) to indicate the degree of cell viability.

The level of oxidative stress was calculated as follows:

First, cells were segmented based on the phase contrast images and cell nuclei was segmented based on the green channel (upon oxidation, the CellROX probe will localize to the nucleus). The intensity of every nucleus was then calculated and normalized to the intensity level of untreated control cells (100%). Mitochondrial health was evaluated similarly, where the intensity of the MitoTracker Red CMXRos probe depends on the mitochondrial membrane potential and thus is lost in nonfunctional mitochondria. All red spots localized within a single cytoplasm (based on phase contrast images using the green channel as seed images for the nucleus) were counted and the average intensity of all mitochondria per cell was then measured. This value was then normalized to the intensity level of untreated control cells (100%).

Morphological Characterization of AP by Electron Microscopy

APs are harvested by carotid endarterectomy from subjects with severe atherosclerotic disease (>70% stenosis or 50% to 70% stenosis with clinical symptoms—according to the American Heart Association guidelines) and donated for research with the written consent by 6 male patients recruited by the Department of Public Health (Vascular Surgery Unit) of the University of Naples Federico II (Ethical Committee of the University of Naples Federico II-Number 157/13, September 9, 2013). APs are collected and transported in saline solution at 4°C, within 2 hrs of explantation. If not used right after the removal, APs are stored in liquid nitrogen and progressively defrosted in 24 h prior to use.

The morphology of APs is investigated by both SEM and TEM. After macroscopic analysis and classification, atherosclerotic plaques containing some adherent intima and media are dissected and subsequently treated for electron microscopy imaging. For the TEM observation, samples are cut into

pieces less than 1 mm^3 and fixed with 0.5% glutaraldehyde plus 4% PFAin 0.1 M sodium cacodylate overnight at 4°C then washed three times with 0.1 M sodium cacodylate buffer. APs are then postfixed with 1% osmium tetroxide /1% potassium ferrocyanide mixing in 0.1 M sodium cacodylate, for 1 hour in ice, in the dark, and washed in a chilled buffer. The en-bloc staining is performed with 4% uranyl acetate aqueous solution overnight at 4°C followed by washing in chilled water. The dissected pieces are dehydrated with an ascendant series of ethanol (30%-50%-70%-95%-absolute) on ice. Dehydrated samples for TEM imaging are embedded in Spurr epoxy resin and after polymerization at 60°C for 72 h were sectioned by Ultramicrotome (FC7-UC7, Leica). The 70 nm slices obtained are seeded on 200 mesh copper grids, and imaging is carried out by using a Tecnai G2-20 (FEI, USA) at a 120 kV, in a range of magnification between 2 μm and 500 nm. Dehydrated samples intended for SEM imaging are subjected to Critical Point Drying (CPD) process before the imaging. A layer of 20 nm of gold is sputtered (HR 208, Cressington) before imaging with a Field emission SEM (Ultraplus, Zeiss, Germany). The secondary electron detector is used, and the images were acquired at 10 kV in a range of magnification between 2 μm and 200 μm.

Results

High Pressure effect on Exos stability

Exos isolated by U87 cell line were treated by HPH to evaluate their stability at different Pressures and Cycles. The process parameters that were intended to be fine-tuned are the Pressure and Cycles, to ensure the structural stability of Exos, Temperature, to avoid protein denaturation, Dilution ratio, by implementing the protocol, to prevent excessive material losses.

In Figure 1 are reported results in terms of average size (a) and morphology (b) obtained at three Pressure values, 500, 1000 and 1500 bar, by increasing the number Cycles up to 10.
Hydrodynamic radius (Rh) of Exos was calculated by DLS measurements. DLS data of Untreated Exos (No HPH treatment) as control are also reported in Figure 1 (a-c). The Z-average size by DLS of the control was 170 nm with a polydispersity index (PDI) of 0.22. In particular, PDI indicated a relative variability in particle size distribution for all the controls (Figure 1).
In details, Figure 1 (a-c) analyzes the effect of the number of Cycles on Exos' average size at constant Pressure. In the samples treated at 500 bar (Exos-5), Figure 1a, three different regions/phases were identified. In the first one, a constant average size was observed up to 3 Cycles (phase 1), then, a decrease in the range 3-5 Cycles (phase 2) and, finally size remains constant up to 9 Cycles (phase 3). After Cycle 9, size was not changing, but the instability and permanent changes in the morphology of the samples were observed (phase 4).
A similar phenomenon was also observed for Exos treated at 1000 bar (Exos-10) as showed in Figure 1b. However, at this condition, the region/phase 1 at constant size was reduced to only 1 Cycle while the average size of Exos promptly decreases between 2-4 Cycles (phase 2) and remains constant up to 6 Cycles (phase 3). After 6 Cycles, however, instability and changes in morphologies were again detected (phase 4). Finally, for Exos treated at 1500 bar (Exos-15) a shortening/overlapping of the phases was reported (Figure 1c). Indeed, a similar prompt reduction was observed up to 2 Cycles (phase 2) but also direct transition to phase 4 was

detected. DLS results obtained at numbers of Cycles beyond phase 4 for all the samples are not reported due to the measurement's instability.
In Figure 1 (d-f), CRYO-TEM images of the Exos corresponding to the identified phases are reported at the different conditions. The images were used to evaluate relation between size, at different Pressure and Cycles, and coalescence, breaking and deformation phenomena affecting the Exos membrane and stability. A further explanation of these phenomena will be reported in the Discussion section.

As shown in figure 1d, even though DLS reported a decrease in size, Exos-5'morphology remains spherical up to 9 Cycles while, after 9 Cycles, elongated Exos-5 are detected. Starting with these observations, we can hypothesize the overlapping of several phenomena in the regions/phases. As previously reported on liposomes and oil-in-water emulsions treated by HPH [62-67], we may suppose that in the first phase/region, shear forces cut the bilayer membrane only of larger vesicles reducing the polydispersity and, therefore, the principal peak value of PSD. Moreover, we have to consider that a small amount of amphiphiles in aqueous solution could re-assembly to reduce their thermodynamic energy forming smaller bilayer structures without compromising the role of naive Exos. However, in the second phase, the nanovesicles seems to be subjected to temporary deformations that become permanent only at 10 Cycles.

The same phenomena of break up and size reduction seemed visible also at 1000 bar, Exos-10, where smallest particles and reassembled vesicles in turbulent flow are probably subjected to a dynamic deformation of lipidic bilayer that become permanent only at 6 Cycles (Figure 2 b-left).
Moreover, it was possible to notice in both Exos-10 and Exos-15 an almost complete overlap of average size behavior up to 3 Cycles. Nevertheless, Figure 2-f-left demonstrated a combination of size decrease and permanent elongation of the particle membrane. So, for Exos-15, we may hypothesize that overlapping of breaking and permanent deformation phenomena is occurring. In such High-Pressure conditions they directly become non-convex, thus maintaining the characteristic minimum energy shape in a quiescent flow. In this situation, the vesicle membrane serves as a geometrical constraint maintaining the conservation of surface area and the enclosed volume.
Finally, the conducted experiments highlighted that morphology of Exos drastically changed while approaching phase 4, where a permanent deformation induced by the combination of Pressure and the number of Cycles is observed for all the treatments.
Moreover, it has been possible to identify for each Pressure a specific Cycle leading to breaking, coalescence or permanent deformation of lipidic bilayers.

To assess the surface properties and biological stability of Exos-5, Exos-10 and Exos-15 just before and after the transition between phase 3 and 4, we analyzed Protein Content and ZP comparing Untreated vesicles. Results are reported in Figure 1 (g-h) for the Protein Content and surface charge, respectively.

BCA assay was performed to confirm the total Protein Content and the absence of protein denaturation and degradation phenomena, possibly due to shear and elongational forces and high temperatures encountered in HPH valve (Figure 1f). Protein denaturation can be defined as an alteration in the biological, chemical, and physical properties of the protein by mild disruption of its structure [68]. It consists in the irreversible loss of the three dimensional structure due to the breakage of non-covalent bonds brought by using various chemical

denaturants or by changing temperature or pH [68]. Most bio-functional proteins, such as enzymes with specific bioactivities, are very sensitive to denaturation; even slight changes may cause inactivation and result in the loss of their biological function [69]. In our case, for all the treatments, a reduction from 10 to 30% of total Protein Content is observed only for the achieving of the permanent deformation region, phase 4, while a stable amount of surface proteins with respect to the control is reported for the other phases. We believe that the stability of protein at high Pressure and Cycle is supported by the operative choice to perform the process under mild Pressure conditions keeping the Temperature in a range of 5-10 °C. Indeed, several studies reported the use of microfluidization for bio-funtional protein recovery, due to its ability to rupture cells under mild temperature and without solvents [30, 70]. Besides that, it is also scalable with the possibility of treating large amounts of biomass. Interestingly, it was reported that to secure the solubility and functionality of water-soluble proteins, temperatures above 35 °C should be avoided, as proved in treatment of green microalgae Chlorella vulgaris [71]. Furthermore, another study demonstrated that the effects of Pressure below 5000 bar on an aqueous solvent do not contribute significantly to the phenomenon of protein compressibility and unfolding [72].

A similar behavior is also reported by ZP analysis in Figure 1g for all the samples. Indeed, it has already been proved that Exos spontaneously acquire surface electrical charge when brought into contact with a polar medium, such as a PBS buffer, and, like the plasma membrane of cells, their surface is generally negatively charged [73]. So, also our Untreated Exos showed usually a surface charge of about -15eV while a reduction up to 30% of the negative values was only detected in phase 4. Indeed, for all the treated Exos approaching to phase 4, this change can be attributed to the partial denaturation of protein, aggregation and breaking of the Exos but also to the deformation altering the charge distribution and detection on the surface, thus interfering with the stability of the colloidal system of Exos and reflected in a less negative ZP value [73].

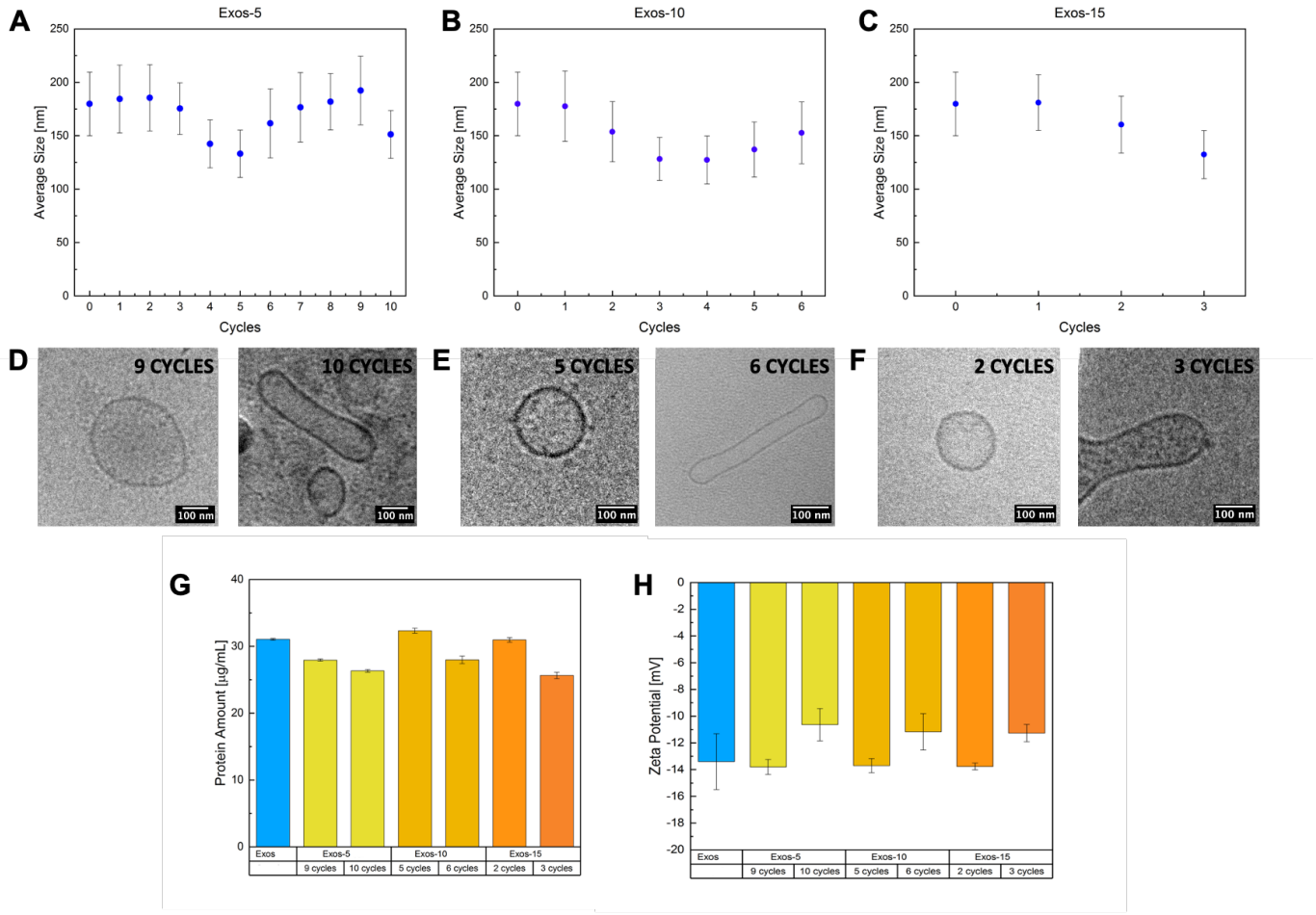

Figure 1. (a-c) Z-average size by DLS of (a) Exos-5 at Cycles ranging from 0 to 10, (b) Exos-10 at Cycles ranging from 1 to 6; and (c) Exos-15 at different Cycles ranging from 0 to 3; (d-f) Cryo-TEM observations before and after the achievement of permanent deformation for relevant Pressure value: (d) Exos 5 at Cycles 9 and 10, (d) Exos 10 at Cycles 5 and 6, (d) Exos 15 at Cycles 2 and 3; (g) Protein Concentration and (h) and ZP of Untreated and Treated Exos before and after the achievement of permanent deformation for relevant Pressure values and Cycles.

Exos Encapsulation

Here, we present how our studies on the effect of High-Pressure Homogenization on the Exos'morphology can be utilized to control the drug-loading capacity of bilayer/natural vesicles (Figure 2). In the previous paragraph, we reported that Exos treated by HPH undergoes to a temporary or permanent deformation of the membrane and that the temporary deformation happens without destabilizing their proteo-lipidic architecture, surface charge and total protein cargo. For all the next experiments, therefore, conditions at which we hypothesize Exos are subjected to temporary deformation will be used. In detail, in the next experiments, we will always refer at Exos-5 at 9 Cycles, as Exos-5, Exos-10 at 5 Cycles as Exos-10 and Exos-15 at 2 Cycles as Exos-15 and will refer to them as gold standard conditions. In Figure 2a, we report EE% of the HPH approach for Exos treated at standard conditions Exos-5, 10 and 15 starting at three different theoretical concentrations of IRI. In detail, the same amount of Exos was put in contact with each solution containing 50, 75 and 100 µM of IRI (IRI-Exos). The obtained suspensions were treated at the standard conditions Exos-5, Exos-10 and Exos-

15. Results showed that the entrapment of chemotherapeutic agent was promoted through a Pressure-dependent manner: the higher Pressure value, the higher EE%, increasing from about 15 to 40% at different Pressure by keeping the IRI concentration constant (Figure 2b). In particular, for the condition of IRI-Exos-15 a stable and average EE of 40% was reported at all the IRI concentrations. The EE results of co-incubated Exos obtained at different IRI concentration and treated at 37 °C for 2 hrs are reported in Figure 2a and showed a constant EE of about 8%.

As already stated, therapeutic agents have been encapsulated into Exos using various passive and active methods, including incubation at RT with or without saponin permeabilization, electroporation, freeze–thaw cycles, sonication, extrusion and dialysis [26, 74]. Usually, as previously described, these methodologies for the encapsulation of drug in Exos are time-consuming, resulting in poor stabilities of the drugs in Exos and a variable and very low loading efficiencies up to 10%.

Up to date, no similar EE has never been achieved with other encapsulation methods and, moreover, obtained in a fast, highly effective, easy to make and reproducible process that could really change the application of Exos in the treatment of diseases. Indeed, the proposed approach can allow the stable encapsulation also of low soluble drugs, such as IRI, used also for GBM [75], and pave the way to their repositioning on other diseases, such as brain tumors, where their pharmacodynamics can be effective, but they are rejected due to their poor delivery properties.

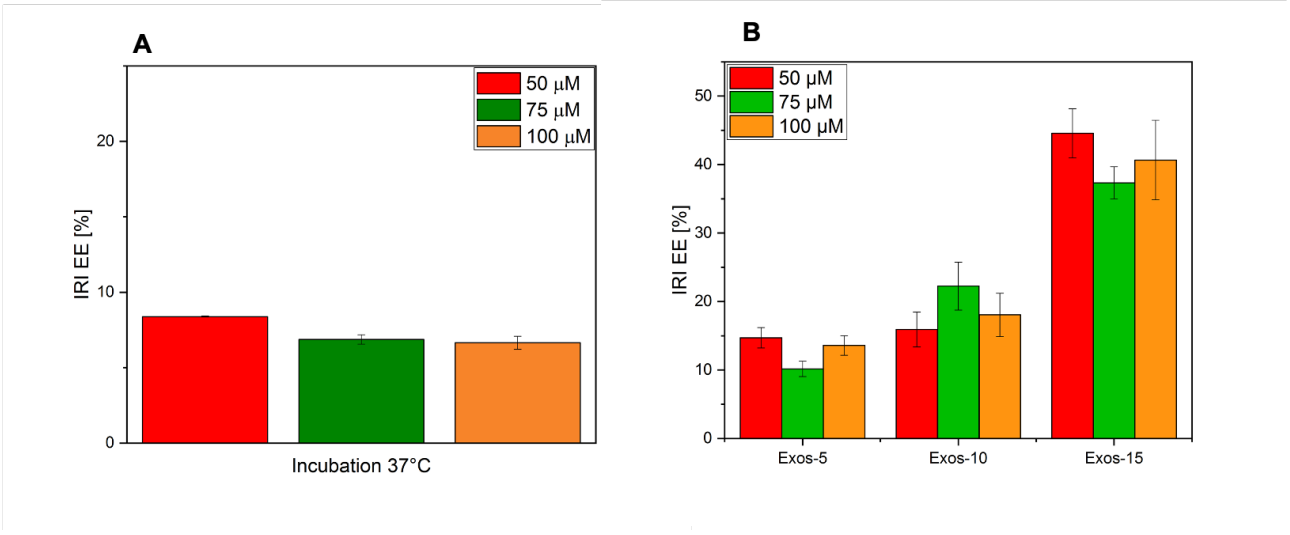

Figure 2. EE% of Co-incubated and HPH-treated Exos with IRI at three different concentrations of 50, 75 and 100 µM; (a) Co-incubation 2 hrs at 37°C (b) IRI-Exos treated at gold standard conditions Exos-5, Exos-10, Exos-15.

To validate the reproducibility of our system we used the gold standard of Exos-15 for the encapsulation of a small molecule with a molecular weight as low as the IRI one but with a high hydrophilicity, the contrast agent Gd-DTPA.

As shown in Figure 3 we performed in vitro MRI and ICP-MS analysis of Gd-DTPA EE at three different concentrations. Interestingly as for IRI also Gd-DTPA show a maximum EE% of 40%.

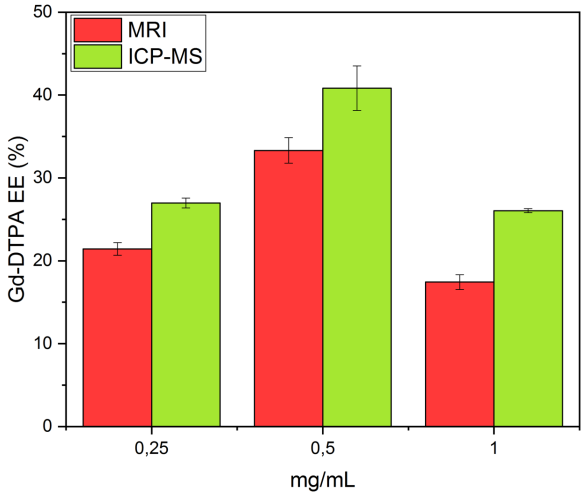

Figure 3. EE% of Exos at three different concentration Exos-15 encapsulated with 0,25, 0,5 and 1 mg/mL of Gd-DTPA.

Drug Delivery Behavior and Biological interactions of Exos-15

The exploitation of stability, release behavior of Exos-15 with Irinotecan (IRI Exos-15)

To evaluate the cargo ability, release behavior and biological interactions of IRI-Exos-15 obtained with HPH with respect to the traditional encapsulation by co-incubation, we investigated their release profile, surface charge and biological specificity by DLS, ZP, Surface Protein and RNA amount. (Figure 4 a-d).

Since the EE of IRI was higher for the Exos-15 condition, and the therapeutic dosage of IRI reported clinically is between 1 and 100 µM [76] we investigated the nano-bio interactions and drug delivery ability for IRI-Exos-15. In particular, DLS and ZP results in Figure 3a and 3b showed a regular particles size distribution and also stable surface charge, respectively, compared to Untreated Exos. Also, the surface protein analysis and RNA extraction after vesicles lysis (Figure 4c) further demonstrated that the encapsulation did not affect the transport of their naive biological content in the outer and inner side of lipidic layer.
Finally, to investigate the in-vitro drug release profile of IRI-Exos-15, we mimicked the physiological environment and endolysosomal compartment respectively at pH of 7.4 or 4.2, 37°C up to 48 hrs (Figure 4d). In PBS dialysate at pH 7.4, the release of Exo-IRI was about 25% after 24 hrs, while in PBS dialysate at pH 4.2 the release rate achieved was about 40%. This result suggested that acidic environment, such as late endosomes and lysosomes of cancer cells, accelerates its activation and release. The observed behavior can be considered relevant in the ability of Exos to escape the intracellular barriers allowing the release, activation and pharmacodynamics of the drug, in our case allowing the esterification of IRI prodrug in its metabolite SN-38.

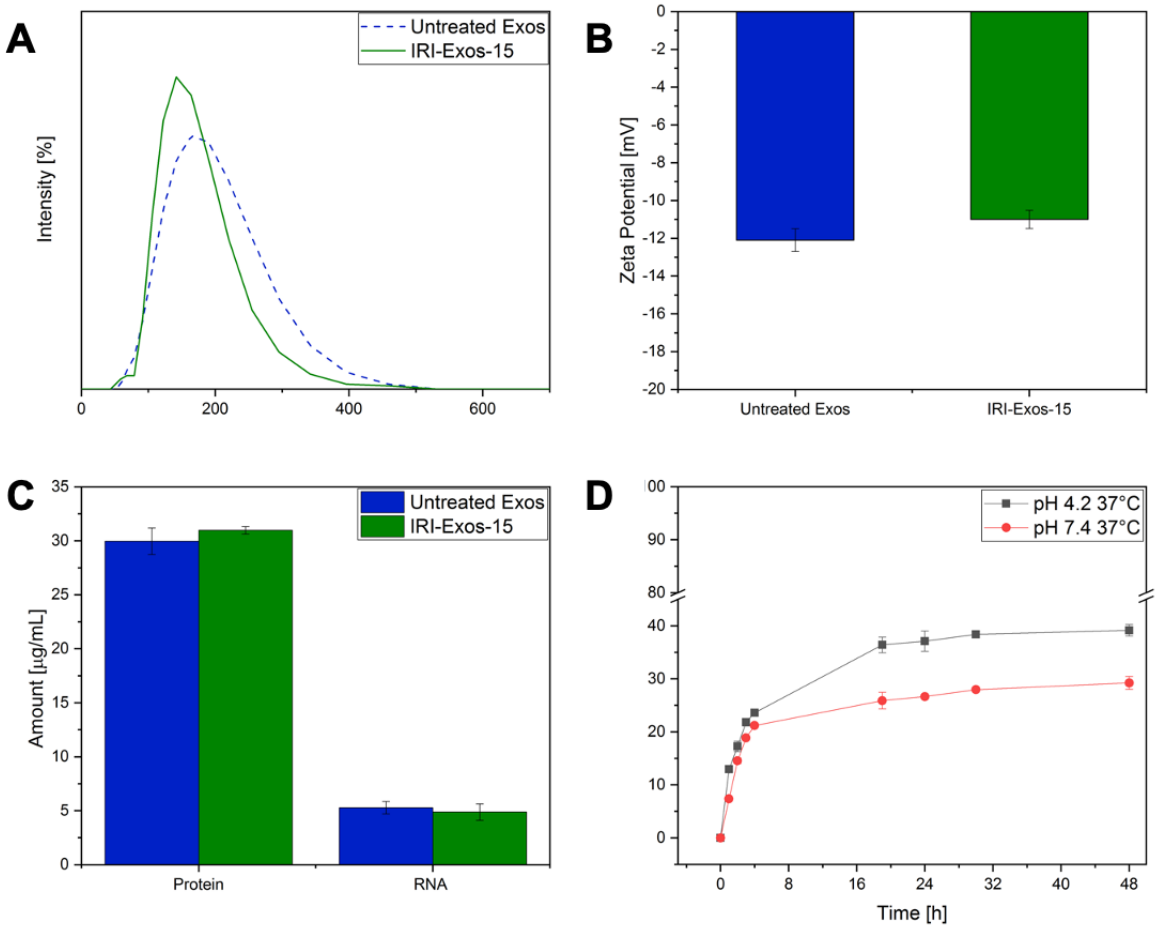

Figure 4. (a) PSD, (b) ZP (c) Surface protein and RNA amount of Untreated Exos and IRI-Exos-15; (d) Drug release profile of IRI-Exos-15 up to 48 hrs in PBS at 37° C and pH 4.2 and pH 7.4.

Cytotoxicity, Cytofluorimetry study and Uptake behavior of Exos 15 with u87 cells.

According to literature, Free-IRI shows benefits in attaining a lower cell viability or equivalently, higher cytotoxicity at very high concentration of 100 µM [77, 78]. As IRI inhibited cell proliferation mainly by arresting cells in the G2-S phases of the cell cycle, in the present study, IRI-Exos-15 in vitro behavior on U87 cells was recorded up to 48 hrs to allow complete cells proliferation. Cytotoxicity analysis (Figure 5 a-b) was performed ranging the IRI concentration from 0.25 to 10 µM. Cell viability decreased for both Free-IRI and IRI-Exos-15 after 24 and 48 hrs, reaching the minimum viability of 70% and 20% respectively, in 48 hrs. Results confirmed the enhanced cargo ability of IRI Exos-15 in terms of faster uptake and improved cytotoxicity at lower concentration with respect to the Free-IRI, holding the great promise to look at Exos as a safe and efficient means of advanced delivery system.

Furthermore, to evaluate the interaction between cells and IRI-Exos-15, quantitative measurement of nanoparticle uptake by flow cytometry was performed (Figure 5 c-e). FSC is a parameter representative of cell size. Changes in FSC intensity reflect the swelling or shrinking of cells [79] and provide an indirect indication of cell viability [80]. IRI Exos-15 and Free-IRI were tested at 10 µM up to 48 hrs. Figure 4c showed a slight reduction of cell viability after 24 hrs for both IRI samples compared to negative control. However, as

expected, IRI-Exos-15 at 48 hrs had higher cytotoxicity if compared to Free-IRI. This data was also confirmed by SSC intensity (Figure 5d). Indeed, SSC is related to the number and type of organelles present in the cell [81]. This inner granularity value has been often used to show differences in the physical state of the cell, including mitosis and particle uptake [60, 79]. Interestingly in our case SSC increase just at 24 hrs up to 48 hrs. As a confirm, also the Mean Fluorescence Intensity, reported as internalization value in Figure 4e, showed an increasing trend with a maximum value up to 24 hrs of cell coincubation. However, the signal remains high also up to 48 hrs highlighting a competition between the number of cells replicating and the amount of treated Exos available in the system that could hide the cytotoxic and internalization phenomena.

Taking together all these considerations, we can speculate that at 24 hrs we reached the maximum peak of internalization of vesicles inside cells. This contextually allows an increase in granulometry and decrease in size of tumoral cells leading to the cytotoxic activity of IRI.

Furthermore, the ability of cells to internalize Exos was assessed with confocal microscopy (Figure 5 f-h). Nanovesicles were distributed throughout the cytoplasm, especially in the perinuclear region. Moreover, the brightest signals were observed after 24 hrs of incubation, confirming cytofluorimetric analysis.

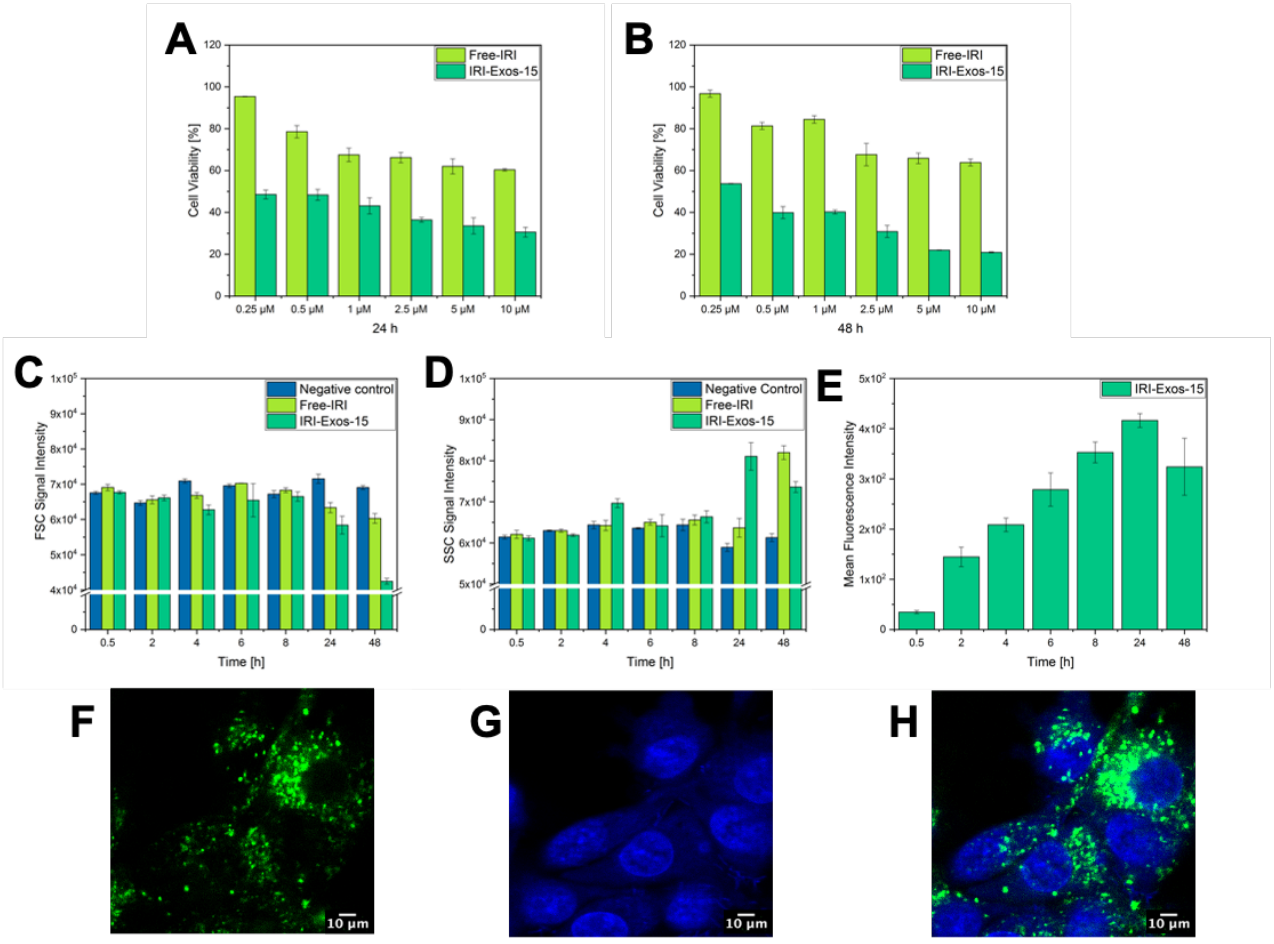

Figure 5 (a) Cytotoxicity of IRI-Exos-15 and Free-IRI cultured on U87-MG cells at 24 hr and 48 hrs; (b) Flowcytometry of IRI-Exos-15 up to 48 hrs of incubation with U87-MG cells: (c) FSC signal, (d) SSC analysis and (e)Mean Fluorescence Intensity. All data are presented as mean±s.d (n=3). Images of Exos internalization at 24 hrs of incubation with U87-MG cells (f) IRI-Exos-15 stained with PKH67; (g) U87-MG cells nuclei stained with Hoechst and (h) merged channels.

CeO_2 NPs size and morphology

CeO_2 NPs were prepared using an ammonia-induced EG-assisted precipitation method, which was carried out in two distinct steps of a single synthetic procedure. TEM images of CeO_2 NPs (Figure 6a) revealed the production of square-shaped nanoparticles in a range of 20-30 nm in size.

SEM images of CeO_2 NPs were shown in Figure 5b. It has been emphasized in the literature that, the average size of the CeO_2 NPs should be less than 30 nm, to have maximum oxidase like activity [58]. Thus, the particle size of the CeO_2 NPs used in this study is appropriate.

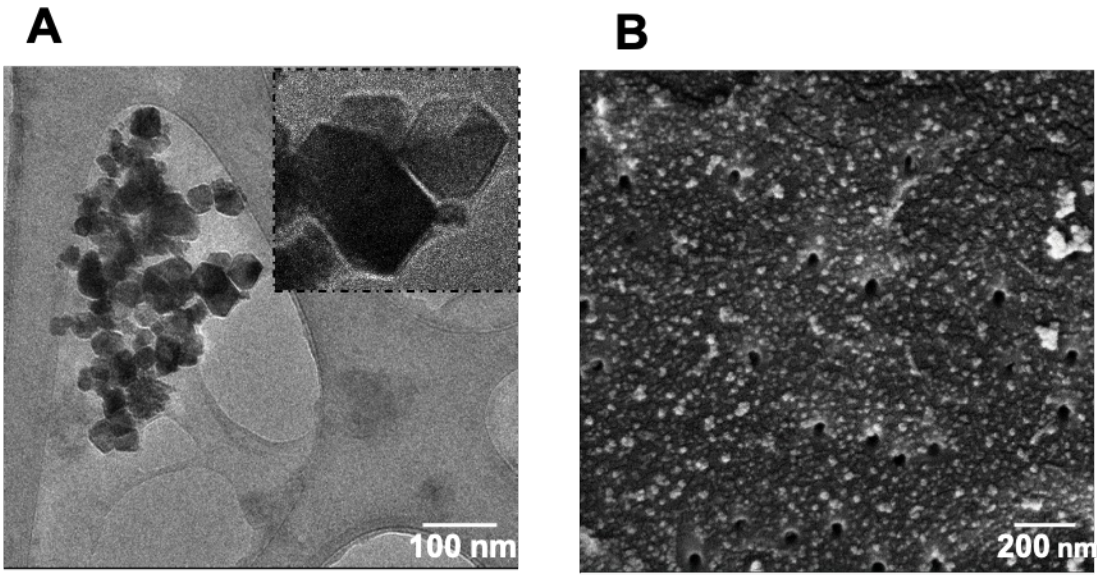

Figure 6. Characterization of CeO_2NPs. (a) Representative TEM and (b) SEM images of NPs with Crystalline Structure and dimension mostly ranging between 30 and 50 nm.

The FTIR spectrum (Figure 7) was recorder in the wave number range of 500-4000 cm^{-1}. The prominent peaks at the region 1600 cm^{-1} represents the amine (N–H) bending due to the reagents (ammonium hydroxide) used for the preparation of the NPs. The bands at 3375 cm^{-1} the hydroxyl stretches. The absorption band starting at wavenumber of 500 cm -1 confirm the presence of Ce-O stretch.

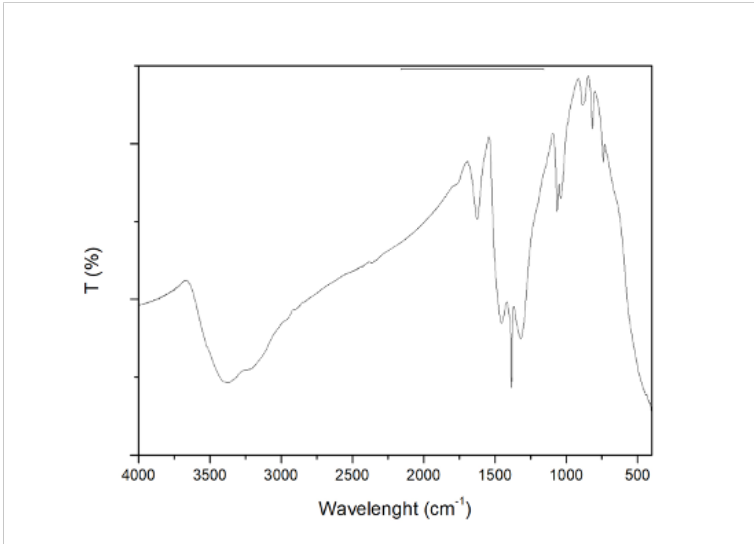

Figure 7. CeO_2 NPs FTIR spectrum.

In vitro CeO_2 NPs analysis

The effect of CeO_2 NPs on cell proliferation and viability was analyzed with Panc-1 cells at concentrations of 10-25-50-75-100 µg/mL over 24 hrs (Figure 8). NPs at the highest concentration were found to not reduce cell proliferation within the first 24 hrs if compared to the negative control (Figure 8a) as also confirmed by optical microscopy observation (Figure 8b).

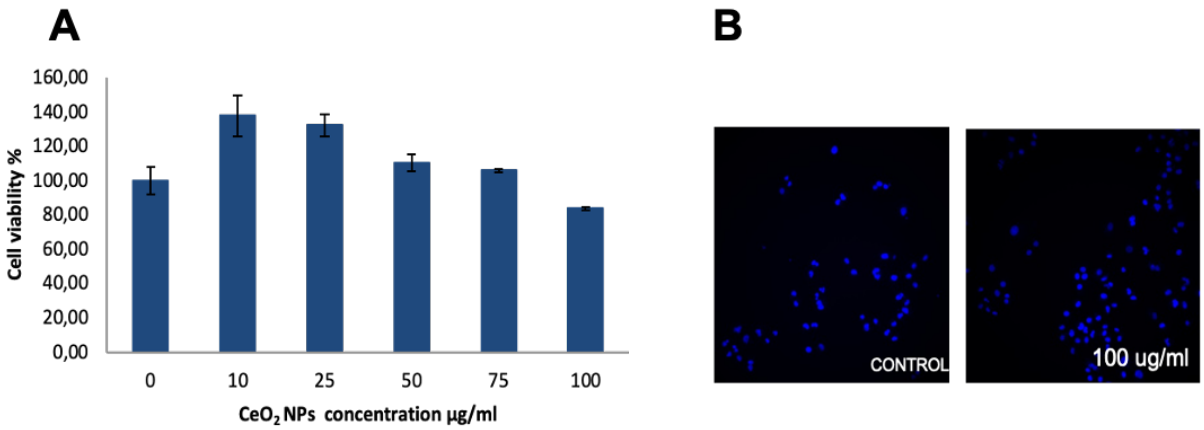

Figure 8. 24 hrs Cell viability of CeO_2NPs; (a) cell viability assay performed at different NPs concentration, (b) optical microscopy observation of stained-cell viability.

The antioxidant properties of the CeO_2 NPs were investigated by exposing Panc-1 cells to NPs for 24 hrs (Figure 9) Mitochondrial area and intracellular ROS levels were measured by InCell 2000 analyzer. As shown in Figure 9a NPs, irrespective of concentration, did not affect the physiological mitochondrial structure, indeed as confirmation also intracellular ROS production did not increase (Figure 9b).

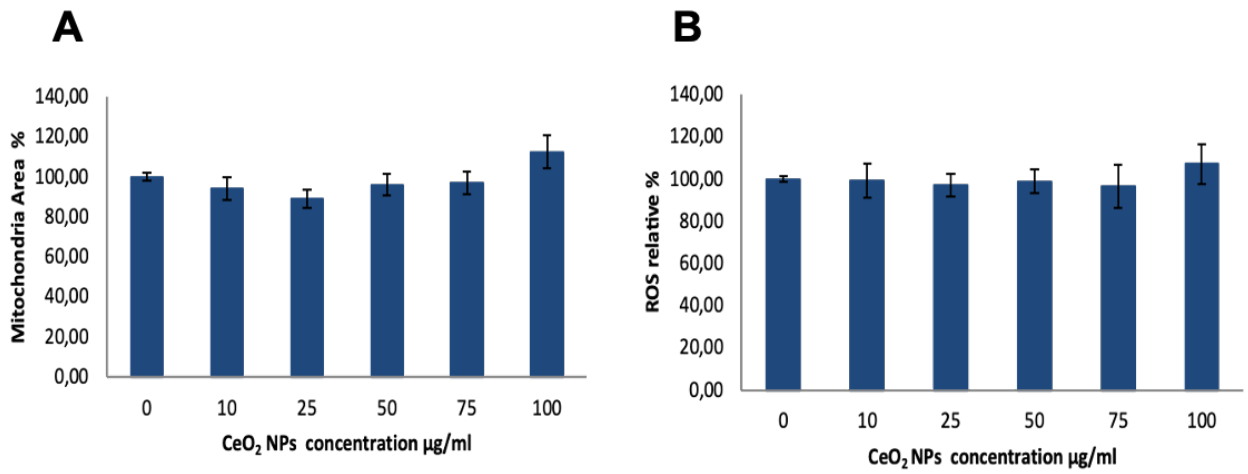

Figure 9. 24 hrs cellular stress analysis of CeO_2NPs; (a) Mitochondria Area and (b) ROS% evaluation at different NPs concentration.

Nevertheless, further studies must be conducted in order to validate not only the cell viability but also the decrease of cellular oxidative stress and consequentially the antioxidant activity that, as reported in the literature, occurs for concentrations of NPs above 200 µg/mL and for a period of cellular exposure not less than 48 hrs.

Electron Microscopy Characterization of Human AP

Atherosclerosis is activated by alterations of the endothelial layer of blood vessels [82]. For this reason, the characterization of endothelium alterations is particularly relevant to understand both the physiopathology of the disease and the composition of the tissue interacting with the imaging probe during the diagnostic investigation when injected into blood circulation. In this work, both scanning and transmission electron microscopy (SEM and TEM) are used to characterize human carotid APs and in particular their luminal wall. Figure 9 shows SEM images of a transversal section of a human AP. Each sample analyzed has disrupted endothelial lining and presents delamination in different layers. Indeed, as shown in Figures 10(a) and 10(b), the endothelium of tunica intima is detached from the basal lamina (red arrow head), and in some areas, the endothelial lining appears to be interrupted and damaged (black arrow head). In some points, the endothelial layer is completely absent showing only the fibrinous reticulum, as presented in Figure 10(c). Also, in the areas covered by the endothelial layer, there are cells showing pseudopodia (white arrow head in Figure 10d) and microvilli. The formation of microvilli may indicate diffuse endo/exocytosis phenomena, confirming that dysfunctional endothelium is characterized by altered permeability.

After ultrastructural analysis of APs we further investigate the interaction of our CeO_2 NPs with such a complex environment applying scanning electron microscopy/energy dispersive X-ray spectroscopy (SEM/EDS).

Briefly we analyzed the energy dispersive spectra of the samples obtained after an over-night adsorption of our CeO_2NPs at a final concentration of 200 µg/mL on the upper endothelial layers of APs.

Notably, we detected a diffusion of CeO_2NPs from the endothelial structure to the fibrinous reticulum. Moreover, NPs tend to aggregate forming some cluster areas.

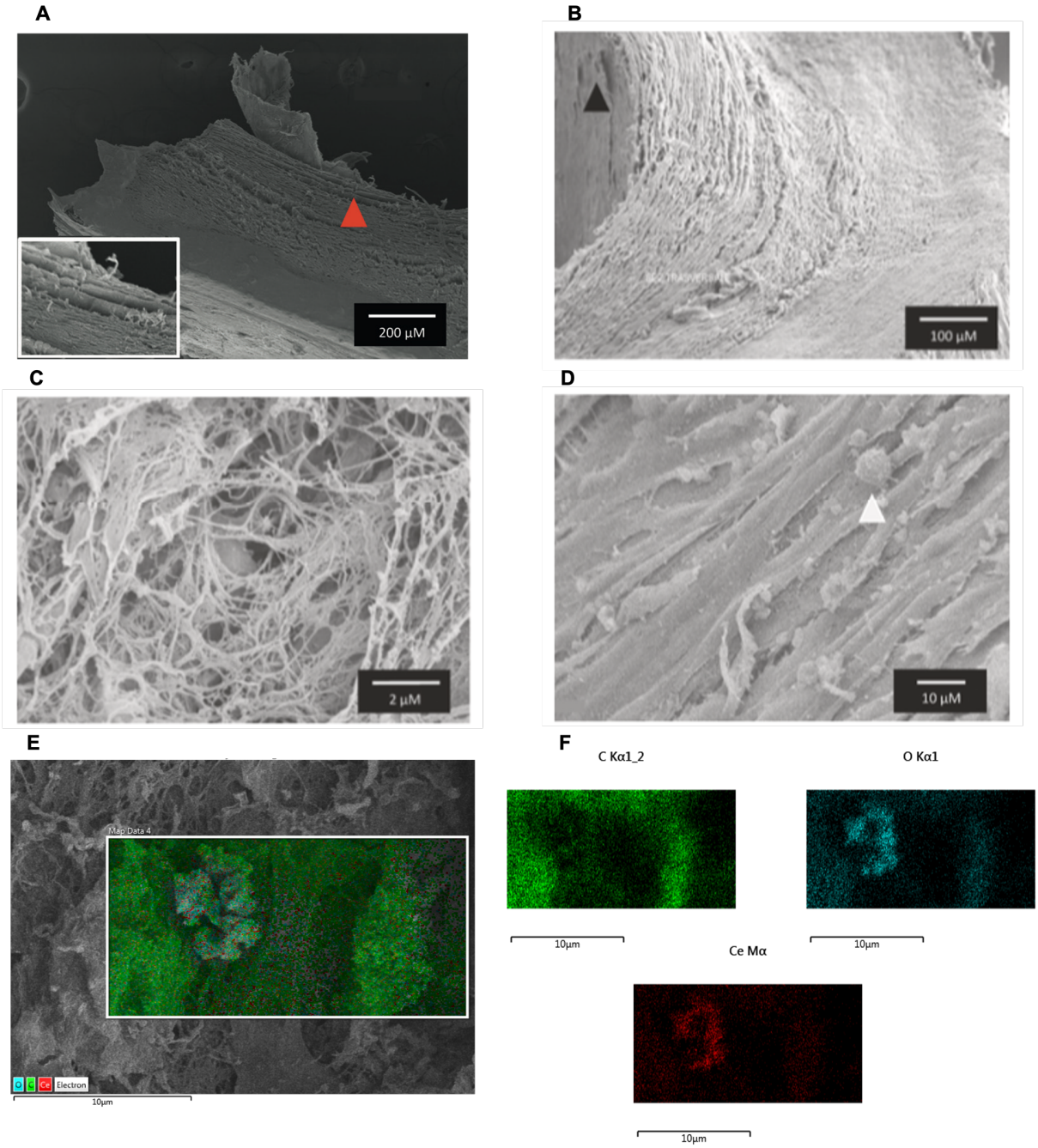

Figure 10. SEM of transversal sections of a human AP and EDS analysis of CeO_2 NPs injected in AP; (a) tunica intima with detached basal lamina (red arrow head), (b) Interrupted or damaged endothelial layer (black arrow head), (c) Fibrinous reticulum in the area with absent endothelial lining, (d) Cells in the endothelial layer showing pseudopodia (white arrow head) and microvilli, (e-f) SEM-EDS analysis of CeO_2 NPs with Carbon, oxygen and Cerium identification and localization.

TEM imaging is showed in Figure 11. Figure 11a shows a cross section of human carotid AP particularly abundant in lipid droplets of different sizes and surrounded by calcium deposits (red arrow) which are mixed in the fibrinous reticulum. In Figure 11b, the matrix reveals also the presence of interspersed cholesterol crystals which Grebe and Latz [83] defined as a hallmark of advanced atherosclerotic plaques. In Figure 11c, the cross section of the tunica intima shows the absence of endothelial cells and thus the complete damage of

the endothelial lining, as observed by SEM imaging. To further understand if in this complex environment cardiovascular cells can release Exos in a pathological condition we further investigate their presence on the endothelial layer of the AP. Interestingly the electron microscopy of the tissue confirmed the biogenesis and release of Exos (Figure 11 d-f). Indeed, we observed the formation of early endosomes in MVB (Figure 11d), their budding through the PM (figure 11e) and a robust release in the extracellular space (Figure 11f). So, before proceeding with the encapsulation of CeO_2 NPs in engineered Exos and their interaction with AP, further analyzes must be carried out in order to discriminate specifically their localization in the extracellular matrix.

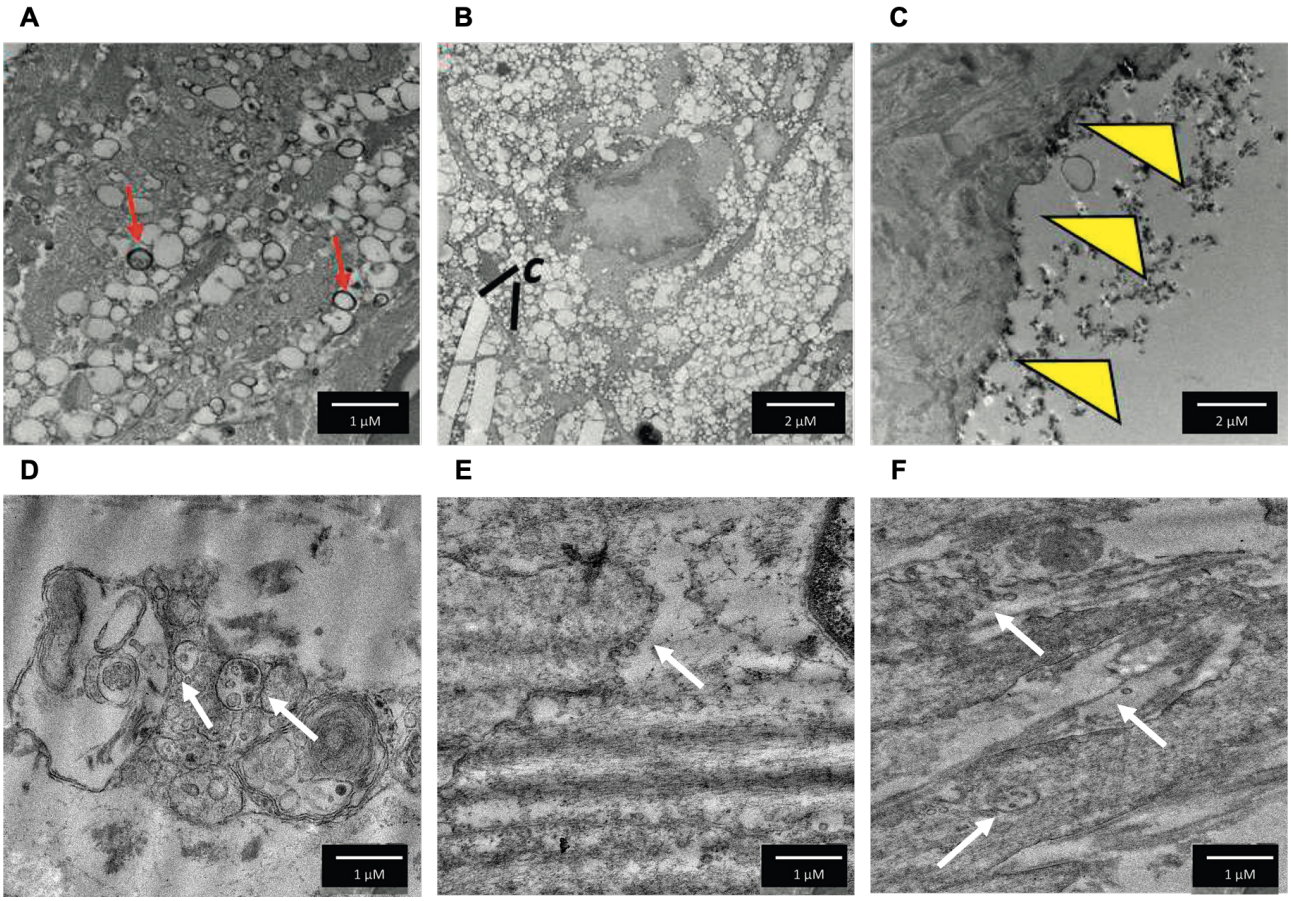

Figure 11. TEM of a cross section of a human AP showing (a) lipid droplets of different sizes, surrounded by calcium deposits (red arrows) and dispersed in the fibrinous reticulum; (b) interspersed cholesterol crystals (C and black lines); (c) Damaged tunica intima (yellow arrow heads) showing the absence of endothelial cells, as observed in SEM imaging; (d) Early endosomes in the MVB (white arrows) (e) Budding of the cellular wall to release the Exos into the lumen (white arrows); (f) Exos in the extracellular space (white arrows).

Discussion

Exos are small endosomal derived membrane nanovesicles that have observed increasing attention over the past decade as a novel model of intercellular communication, impacting many cellular processes, such as signaling, antigen presentation and T cell stimulation, and immune response.

Moreover, only recently, these EVs have been investigated as functional vehicles that carry an endogenous and exogenous cargo of proteins, lipids, and nucleic acids, capable of delivering these cargos to specific target cells.

However, the use of their promising properties in the nanobiotheranostic field to deliver active compounds such as tracers or drugs has been limited by the lack of efficient drug loading methods [7].

In the current study, we propose High-Pressure Homogenization to improve the cargo loading of Exos. At date, HPH has been applied as an efficient means of cellular disruption extracting intracellular products such as DNA, ribosomes and mitochondria; moreover, it has been industrially used in the food engineering field to improve microbial safety and extend the product shelf life of liquid foods, enhance emulsion stability, stabilize proteins in solutions, reduce particle size distributions, and increase the accessibility of health-promoting compounds.

Currently, methodologies used for the encapsulation of Exos obtaining an Encapsulation Efficiency (EE) maximum value of 10% while the use of HPH for the treatment of Exos, that we propose, allows for the first time an increase of the EE up to 45%, reaching the best values of EE obtained for the traditional encapsulation of nanoparticles and making the cargo properties of Exos comparable with polymer and lipid-based vectors and useful in the precision nanomedicine field.

In our procedure, Exos samples are subjected to high Pressures and are forced through a narrow static valve, undergoing to stress forces such as cavitation and shear are generated. In details, the operative parameters such as the valve geometry, Pressure level, inlet Temperature, and the number of homogenization cycles are analyzed to affect the thermodynamic of the lipid bilayer by controlling Turbulence, High Shear, Cavitation, and Temperature increase to enhance the stability of Exos, stabilize the surface protein and increase the loading of active compounds.

It has already been reported [84] for bilayer of living cells that various kinds of environmental stress, such as Temperature stress and osmotic stress, cause alterations in the physical properties of the membrane lipids due to the presence of proteins and cholesterol on their surface.

Here, the above HPH parameters have been investigated to tune the loading capability of the Exos taking advantages by the control of the fluidity of their bilayer membrane.

Indeed, as previously reported [85], cholesterol and proteins are also essential components of exosomal membranes and, among the biomolecules, the responsible of the membrane fluidity and most sensitive to high Pressure. Furthermore, it is well-known that specific lipids are enriched in Exos compared to their parent cells and that lipid class enrichment in EVs depends on vesicle type and source cell type [86]. Our results started from U87, originated by Human glioblastoma astrocytoma, for the isolation of Exos. From literature, it is reported that Glycolipid, free fatty acid and phosphatidylserine enrichment is generally observed in all U87, mainly used in this work, while Lyso derivatives and structural membrane lipid are usually depleted in Exos [84]. Therefore, the role of these lipid components could also interfere with the fluidity of the of the membrane and, therefore the stiffness and flexibility, influencing the thermodynamic state under viscous stresses at high pressure conditions.

Furthermore, the effects induced by the Temperature have to be necessarily taken into account in HPH, where the high velocity of the fluid flow, which is then impinging on the zirconium valve of the homogenizer, leads to the dissipation of a significant fraction of the mechanical energy as heat in the fluid temperature increase. Indeed, during homogenization, a rise of the Temperature (about 2.5°C per 10MPa), related to the fluid employed, is generally observed in the fluid downstream of the valve. We decide not to take advantage by the

high Temperature to protect the stability of the proteins. However, at low temperatures, phospholipids tend to cluster together, but steroids in the phospholipid bilayer fill in between the phospholipids, disrupting their intermolecular interactions and increasing fluidity. Therefore, we took advantage by this temperature-sensitivity behavior of the intracellular components, it has been crucial to control and limit the product exposure to temperature increase by a cooled jacket at 10°C at the inlet of the instrument and through a heat-exchanging cooling coils to extract heat quickly, and nullify the temperature increase, affecting the permeabilization only by the high pressure effect.

So, in the current study, we successfully improved and shortened to less than 1 hr the encapsulation process of the Exos through HPH, preserving their morphological integrity and biological identity, repositioning the Exos in the first line for the exploitation of their use in the nanobiotheranostic field. To validate our approach, we selected the prodrug IRI currently under investigation for the treatment of GBM due to its ability to cytotoxic activity against central nervous system tumor xenografts and against glioblastoma cells with multi-drug resistance [87]. The operative parameters, Pressure and number of Cycles were studied to control the Encapsulation Efficiency (EE) % of the HPH approach for Exos treated at constant Temperature. Three different theoretical concentrations of IRI were testes for all Pressures and at selected number of Cycles that had not preliminary showed instability of Exos or protein denaturation. A constant EE of 45% was reported for the gold standard condition Exos-15 (Exos treated at 1500 bars and 2 cycles), obtained in about 45 minutes, much shorter than the usual methodology several hrs or days longer with an ineffective EE of about 10%. We also investigated the cargo ability, release behavior and biological interactions of the IRI- Exos-15 comparing them with traditional encapsulation by co-incubation. The synthetic identity of the Exos, such as their release profile, surface charge and biological specificity, were studied by DLS, Zeta Potential, and Surface Protein and RNA amount and results showed a constant release behavior of IRI Exos-15 at 48 hrs. Furthermore, in vitro tests on U87 cells, obtained by flow cytometry and confocal microscopy, proved the effect of their biological identity showing a maximum peak of internalization of vesicles inside cells at 24 hr and higher cytotoxicity at 48 hrs with respect to the free-IRI.

In conclusion, we established a feasible approach based on High-Pressure Homogenization to improve and shorten the loading of Exos at effective therapeutic concentrations. Indeed, as already stated, up to date, the current application and translation of Exos to clinics were limited by a series of key factors, among them the stable and adequate loading methods, that should be over crossed. In this perspective, our results confirm Exos' high sensitivity and specificity that remain ideal candidates for early diagnosis and effective therapy. We proved that an approach based on High-Pressure Homogenization could potentially speed up their translation in the clinical practice, being a repeatable process guaranteed to scale up to pilot and/or production volumes.

Moreover, we optimize the synthesis of inorganic CeO_2NPs and performed preliminary analysis on their cytotoxicity and uptake behavior in the complex biological environment of APs.

However, further work is needed to allow the simultaneous encapsulation through our novel system of these inorganic NPs and other active compounds in EVs. and moreover, to evaluate their stability in body circulation after loading.

References

1. Vader, P., E. A. Mol, G. Pasterkamp and R. M. Schiffelers. "Extracellular vesicles for drug delivery." *Advanced drug delivery reviews* 106 (2016): 148-56.
2. Witwer, K. W. and J. Wolfram. "Extracellular vesicles versus synthetic nanoparticles for drug delivery." *Nature Reviews Materials* (2021): 1-4.
3. Luan, X., K. Sansanaphongpricha, I. Myers, H. Chen, H. Yuan and D. Sun. "Engineering exosomes as refined biological nanoplatforms for drug delivery." *Acta Pharmacologica Sinica* 38 (2017): 754-63.
4. Simons, M. and G. Raposo. "Exosomes–vesicular carriers for intercellular communication." *Current opinion in cell biology* 21 (2009): 575-81.
5. Cicero, A. L., P. D. Stahl and G. Raposo. "Extracellular vesicles shuffling intercellular messages: For good or for bad." *Current opinion in cell biology* 35 (2015): 69-77.
6. Kanchanapally, R., S. K. Deshmukh, S. R. Chavva, N. Tyagi, S. K. Srivastava, G. K. Patel, A. P. Singh and S. Singh. "Drug-loaded exosomal preparations from different cell types exhibit distinctive loading capability, yield, and antitumor efficacies: A comparative analysis." *International Journal of Nanomedicine* 14 (2019): 531-41. 10.2147/ijn.s191313. <Go to ISI>://WOS:000455504200005.
7. Batrakova, E. V. and M. S. Kim. "Using exosomes, naturally-equipped nanocarriers, for drug delivery." *Journal of Controlled Release* 219 (2015): 396-405. 10.1016/j.jconrel.2015.07.030. <Go to ISI>://WOS:000365587800032.
8. Li, S.-p., Z.-x. Lin, X.-y. Jiang and X.-y. Yu. "Exosomal cargo-loading and synthetic exosome-mimics as potential therapeutic tools." *Acta Pharmacologica Sinica* 39 (2018): 542-51.
9. Pascucci, L., V. Coccè, A. Bonomi, D. Ami, P. Ceccarelli, E. Ciusani, L. Viganò, A. Locatelli, F. Sisto and S. M. Doglia. "Paclitaxel is incorporated by mesenchymal stromal cells and released in exosomes that inhibit in vitro tumor growth: A new approach for drug delivery." *Journal of Controlled Release* 192 (2014): 262-70.
10. Wei, H., J. Chen, S. Wang, F. Fu, X. Zhu, C. Wu, Z. Liu, G. Zhong and J. Lin. "A nanodrug consisting of doxorubicin and exosome derived from mesenchymal stem cells for osteosarcoma treatment in vitro." *International journal of nanomedicine* 14 (2019): 8603.
11. Fu, S., Y. Wang, X. Xia and J. C. Zheng. "Exosome engineering: Current progress in cargo loading and targeted delivery." *NanoImpact* (2020): 100261.
12. Hood, J. L. "Post isolation modification of exosomes for nanomedicine applications." *Nanomedicine* 11 (2016): 1745-56.
13. Xu, M., Q. Yang, X. Sun and Y. Wang. "Recent advancements in the loading and modification of therapeutic exosomes." *Frontiers in bioengineering and biotechnology* 8 (2020):

14. Alvarez-Erviti, L., Y. Seow, H. Yin, C. Betts, S. Lakhal and M. J. Wood. "Delivery of sirna to the mouse brain by systemic injection of targeted exosomes." *Nature biotechnology* 29 (2011): 341-45.
15. Momen-Heravi, F., S. Bala, T. Bukong and G. Szabo. "Exosome-mediated delivery of functionally active mirna-155 inhibitor to macrophages." *Nanomedicine: Nanotechnology, Biology and Medicine* 10 (2014): 1517-27.
16. Kooijmans, S. A., S. Stremersch, K. Braeckmans, S. C. de Smedt, A. Hendrix, M. J. Wood, R. M. Schiffelers, K. Raemdonck and P. Vader. "Electroporation-induced sirna precipitation obscures the efficiency of sirna loading into extracellular vesicles." *Journal of Controlled Release* 172 (2013): 229-38.
17. Podolak, I., A. Galanty and D. Sobolewska. "Saponins as cytotoxic agents: A review." *Phytochemistry Reviews* 9 (2010): 425-74.
18. Haney, M. J., N. L. Klyachko, Y. L. Zhaoa, R. Gupta, E. G. Plotnikova, Z. J. He, T. Patel, A. Piroyan, M. Sokolsky, A. V. Kabanov*, et al.* "Exosomes as drug delivery vehicles for parkinson's disease therapy." *Journal of Controlled Release* 207 (2015): 18-30. 10.1016/j.jconrel.2015.03.033. <Go to ISI>://WOS:000354060000003.
19. Goh, W. J., C. K. Lee, S. Zou, E. C. Woon, B. Czarny and G. Pastorin. "Doxorubicin-loaded cell-derived nanovesicles: An alternative targeted approach for anti-tumor therapy." *International journal of nanomedicine* 12 (2017): 2759.
20. Thakur, A., R. K. Sidu, H. Zou, M. K. Alam, M. Yang and Y. Lee. "Inhibition of glioma cells' proliferation by doxorubicin-loaded exosomes via microfluidics." *International journal of nanomedicine* 15 (2020): 8331.
21. Thanu, D. P., M. Zhao, Z. Han and M. Keswani. "Fundamentals and applications of sonic technology." *Developments in Surface Contamination and Cleaning: Applications of Cleaning Techniques* (2019): 1-48.
22. Li, Y.-J., J.-Y. Wu, J.-M. Wang, X.-B. Hu, J.-X. Cai and D.-X. Xiang. "Gemcitabine loaded autologous exosomes for effective and safe chemotherapy of pancreatic cancer." *Acta biomaterialia* 101 (2020): 519-30.
23. Salarpour, S., H. Forootanfar, M. Pournamdari, M. Ahmadi-Zeidabadi, M. Esmaeeli and A. Pardakhty. "Paclitaxel incorporated exosomes derived from glioblastoma cells: Comparative study of two loading techniques." *DARU Journal of Pharmaceutical Sciences* 27 (2019): 533-39.
24. Kim, M. S., M. J. Haney, Y. Zhao, V. Mahajan, I. Deygen, N. L. Klyachko, E. Inskoe, A. Piroyan, M. Sokolsky and O. Okolie. "Development of exosome-encapsulated paclitaxel to overcome mdr in cancer cells." *Nanomedicine: Nanotechnology, Biology and Medicine* 12 (2016): 655-64.
25. Haney, M. J., N. L. Klyachko, Y. Zhao, R. Gupta, E. G. Plotnikova, Z. He, T. Patel, A. Piroyan, M. Sokolsky and A. V. Kabanov. "Exosomes as drug delivery vehicles for parkinson's disease therapy." *Journal of Controlled Release* 207 (2015): 18-30.
26. Fuhrmann, G., A. Serio, M. Mazo, R. Nair and M. M. Stevens. "Active loading into extracellular vesicles significantly improves the cellular uptake and photodynamic effect of porphyrins." *Journal of Controlled Release* 205 (2015): 35-44.

27. Lu, M. and Y. Huang. "Bioinspired exosome-like therapeutics and delivery nanoplatforms." *Biomaterials* 242 (2020): 119925.
28. Jang, S. C., O. Y. Kim, C. M. Yoon, D.-S. Choi, T.-Y. Roh, J. Park, J. Nilsson, J. Lotvall, Y.-K. Kim and Y. S. Gho. "Bioinspired exosome-mimetic nanovesicles for targeted delivery of chemotherapeutics to malignant tumors." *ACS nano* 7 (2013): 7698-710.
29. Toledano Furman, N. E., Y. Lupu-Haber, T. Bronshtein, L. Kaneti, N. Letko, E. Weinstein, L. Baruch and M. Machluf. "Reconstructed stem cell nanoghosts: A natural tumor targeting platform." *Nano letters* 13 (2013): 3248-55.
30. Stupak, R., N. Makauskas, K. Radzevičius and Z. Valančius. "Optimization of intracellular product release from neisseria denitrificans using microfluidizer." *Preparative Biochemistry and Biotechnology* 45 (2015): 667-83.
31. Choi, H., L. Laleye, G. Amantea and R. Simard. "Release of aminopeptidase from lactobacillus casei sp. Casei by cell disruption in a microfluidizer." *Biotechnology techniques* 11 (1997): 451-53.
32. Baldwin, C. and C. W. Robinson. "Disruption of saccharomyces cerevisiae using enzymatic lysis combined with high-pressure homogenization." *Biotechnology techniques* 4 (1990): 329-34.
33. Vitkova, V. and C. Misbah. "Dynamics of lipid vesicles: From thermal fluctuations to rheology." In *Advances in planar lipid bilayers and liposomes*. 14. Elsevier, 2011, 257-92.
34. Bellin, G., C. Gardin, L. Ferroni, J. C. Chachques, M. Rogante, D. Mitrečić, R. Ferrari and B. Zavan. "Exosome in cardiovascular diseases: A complex world full of hope." *Cells* 8 (2019): 166.
35. Zodda, D., R. Giammona and S. Schifilliti. "Treatment strategy for dyslipidemia in cardiovascular disease prevention: Focus on old and new drugs." *Pharmacy* 6 (2018): 10.
36. Zhou, H., B. Wang, Y. Yang, Q. Jia, Z. Qi, A. Zhang, S. Lv and J. Zhang. "Exosomes in ischemic heart disease: Novel carriers for bioinformation." *Biomedicine & Pharmacotherapy* 120 (2019): 109451.
37. Safdar, A., A. Saleem and M. A. Tarnopolsky. "The potential of endurance exercise-derived exosomes to treat metabolic diseases." *Nature Reviews Endocrinology* 12 (2016): 504.
38. Lai, R. C., F. Arslan, M. M. Lee, N. S. K. Sze, A. Choo, T. S. Chen, M. Salto-Tellez, L. Timmers, C. N. Lee and R. M. El Oakley. "Exosome secreted by msc reduces myocardial ischemia/reperfusion injury." *Stem cell research* 4 (2010): 214-22.
39. Arslan, F., R. C. Lai, M. B. Smeets, L. Akeroyd, A. Choo, E. N. Aguor, L. Timmers, H. V. van Rijen, P. A. Doevendans and G. Pasterkamp. "Mesenchymal stem cell-derived exosomes increase atp levels, decrease oxidative stress and activate pi3k/akt pathway to enhance myocardial viability and prevent adverse remodeling after myocardial ischemia/reperfusion injury." *Stem cell research* 10 (2013): 301-12.
40. Chen, L., Y. Wang, Y. Pan, L. Zhang, C. Shen, G. Qin, M. Ashraf, N. Weintraub, G. Ma and Y. Tang. "Cardiac progenitor-derived exosomes protect ischemic myocardium from acute ischemia/reperfusion injury." *Biochemical and biophysical research communications* 431 (2013): 566-71.

41. Xiao, T. T., W. W. Zhang, B. Jiao, C. Z. Pan, X. X. Liu and L. Shen. "The role of exosomes in the pathogenesis of alzheimer' disease." *Translational Neurodegeneration* 6 (2017): 6. 10.1186/s40035-017-0072-x. <Go to ISI>://WOS:000395040800001.
42. Ong, S.-G., W. H. Lee, M. Huang, D. Dey, K. Kodo, V. Sanchez-Freire, J. D. Gold and J. C. Wu. "Cross talk of combined gene and cell therapy in ischemic heart disease: Role of exosomal microrna transfer." *Circulation* 130 (2014): S60-S69.
43. Bouchareychas, L., P. Duong, S. Covarrubias, E. Alsop, T. A. Phu, A. Chung, M. Gomes, D. Wong, B. Meechoovet and A. Capili. "Macrophage exosomes resolve atherosclerosis by regulating hematopoiesis and inflammation via microrna cargo." *Cell Reports* 32 (2020): 107881.
44. Khan, A. R., X. Yang, M. Fu and G. Zhai. "Recent progress of drug nanoformulations targeting to brain." *Journal of controlled release* 291 (2018): 37-64.
45. Schwarzenbach, H. and P. B. Gahan. "Microrna shuttle from cell-to-cell by exosomes and its impact in cancer." *Non-coding RNA* 5 (2019): 28.
46. Kim, R., S. Lee, J. Lee, M. Kim, W. J. Kim, H. W. Lee, M. Y. Lee, J. Kim and W. Chang. "Exosomes derived from microrna-584 transfected mesenchymal stem cells: Novel alternative therapeutic vehicles for cancer therapy." *BMB reports* 51 (2018): 406.
47. Yu, L., S. Gui, Y. Liu, X. Qiu, G. Zhang, X. a. Zhang, J. Pan, J. Fan, S. Qi and B. Qiu. "Exosomes derived from microrna-199a-overexpressing mesenchymal stem cells inhibit glioma progression by down-regulating agap2." *Aging (Albany NY)* 11 (2019): 5300.
48. Katakowski, M., B. Buller, X. G. Zheng, Y. Lu, T. Rogers, O. Osobamiro, W. Shu, F. Jiang and M. Chopp. "Exosomes from marrow stromal cells expressing mir-146b inhibit glioma growth." *Cancer Letters* 335 (2013): 201-04. 10.1016/j.canlet.2013.02.019. <Go to ISI>://WOS:000323853200025.
49. Bronisz, A., Y. Wang, M. O. Nowicki, P. Peruzzi, K. I. Ansari, D. Ogawa, L. Balaj, G. De Rienzo, M. Mineo and I. Nakano. "Extracellular vesicles modulate the glioblastoma microenvironment via a tumor suppression signaling network directed by mir-1." *Cancer research* 74 (2014): 738-50.
50. Munoz, J. L., S. A. Bliss, S. J. Greco, S. H. Ramkissoon, K. L. Ligon and P. Rameshwar. "Delivery of functional anti-mir-9 by mesenchymal stem cell-derived exosomes to glioblastoma multiforme cells conferred chemosensitivity." *Molecular Therapy-Nucleic Acids* 2 (2013): 10.1038/mtna.2013.60. <Go to ISI>://WOS:000332468600002.
51. Yang, T. Z., P. Martin, B. Fogarty, A. Brown, K. Schurman, R. Phipps, V. P. Yin, P. Lockman and S. H. Bai. "Exosome delivered anticancer drugs across the blood-brain barrier for brain cancer therapy in danio rerio." *Pharmaceutical Research* 32 (2015): 2003-14. 10.1007/s11095-014-1593-y. <Go to ISI>://WOS:000354098600012.
52. Jia, G., Y. Han, Y. L. An, Y. A. Ding, C. He, X. H. Wang and Q. S. Tang. "Nrp-1 targeted and cargo-loaded exosomes facilitate simultaneous imaging and therapy of glioma in vitro and in vivo." *Biomaterials* 178 (2018): 302-16. 10.1016/j.biomaterials.2018.06.029. <Go to ISI>://WOS:000440959000021.
53. Ye, Z. L., T. Zhang, W. S. He, H. L. Jin, C. W. Liu, Z. Yang and J. H. Ren. "Methotrexate-loaded extracellular vesicles functionalized with therapeutic and targeted peptides for the

treatment of glioblastoma multiforme." *Acs Applied Materials & Interfaces* 10 (2018): 12341-50. 10.1021/acsami.7b18135. <Go to ISI>://WOS:000430642100024.

54. Bai, L., Y. Liu, K. Guo, K. Zhang, Q. Liu, P. Wang and X. Wang. "Ultrasound facilitates naturally equipped exosomes derived from macrophages and blood serum for orthotopic glioma treatment." *ACS applied materials & interfaces* 11 (2019): 14576-87.
55. Kciuk, M., B. Marciniak and R. Kontek. "Irinotecan—still an important player in cancer chemotherapy: A comprehensive overview." *International Journal of Molecular Sciences* 21 (2020): 4919.
56. Xu, Y. and M. Villalona-Calero. "Irinotecan: Mechanisms of tumor resistance and novel strategies for modulating its activity." *Annals of oncology* 13 (2002): 1841-51.
57. Niendorf, H., J. Haustein, I. Cornelius, A. Alhassan and W. Clauss. "Safety of gadolinium-dtpa: Extended clinical experience." *Magnetic resonance in medicine* 22 (1991): 222-28.
58. Forest, V., L. Leclerc, J.-F. Hochepied, A. Trouvé, G. Sarry and J. Pourchez. "Impact of cerium oxide nanoparticles shape on their in vitro cellular toxicity." *Toxicology in Vitro* 38 (2017): 136-41.
59. De Marzi, L., A. Monaco, J. De Lapuente, D. Ramos, M. Borras, M. Di Gioacchino, S. Santucci and A. Poma. "Cytotoxicity and genotoxicity of ceria nanoparticles on different cell lines in vitro." *International journal of molecular sciences* 14 (2013): 3065-77.
60. Lord, M. S., M. Jung, W. Y. Teoh, C. Gunawan, J. A. Vassie, R. Amal and J. M. Whitelock. "Cellular uptake and reactive oxygen species modulation of cerium oxide nanoparticles in human monocyte cell line u937." *Biomaterials* 33 (2012): 7915-24.
61. Eriksson, P., A. A. Tal, A. Skallberg, C. Brommesson, Z. Hu, R. D. Boyd, W. Olovsson, N. Fairley, I. A. Abrikosov and X. Zhang. "Cerium oxide nanoparticles with antioxidant capabilities and gadolinium integration for mri contrast enhancement." *Scientific reports* 8 (2018): 1-12.
62. Yadav, K. S. and K. Kale. "High pressure homogenizer in pharmaceuticals: Understanding its critical processing parameters and applications." *Journal of Pharmaceutical Innovation* (2019): 1-12.
63. Wang, F. C., N. Acevedo and A. G. Marangoni. "Encapsulation of phytosterols and phytosterol esters in liposomes made with soy phospholipids by high pressure homogenization." *Food & function* 8 (2017): 3964-69.
64. Durán-Lobato, M., A. Enguix-González, M. Fernández-Arévalo and L. Martín-Banderas. "Statistical analysis of solid lipid nanoparticles produced by high-pressure homogenization: A practical prediction approach." *Journal of nanoparticle research* 15 (2013): 1-14.
65. Apostolidis, E. and I. Mandala. "Modification of resistant starch nanoparticles using high-pressure homogenization treatment." *Food Hydrocolloids* 103 (2020): 105677.
66. Floury, J., A. Desrumaux and J. Lardières. "Effect of high-pressure homogenization on droplet size distributions and rheological properties of model oil-in-water emulsions." *Innovative Food Science & Emerging Technologies* 1 (2000): 127-34.
67. Hidajat, M. J., W. Jo, H. Kim and J. Noh. "Effective droplet size reduction and excellent stability of limonene nanoemulsion formed by high-pressure homogenizer." *Colloids and Interfaces* 4 (2020): 5.

68. Eckersall, P. D. "Proteins, proteomics, and the dysproteinemias." *Clinical biochemistry of domestic animals* 6 (2008): 114-55.
69. Phong, W. N., P. L. Show, T. C. Ling, J. C. Juan, E.-P. Ng and J.-S. Chang. "Mild cell disruption methods for bio-functional proteins recovery from microalgae—recent developments and future perspectives." *Algal research* 31 (2018): 506-16.
70. Kelly, W. J. and K. R. Muske. "Optimal operation of high-pressure homogenization for intracellular product recovery." *Bioprocess and biosystems engineering* 27 (2004): 25-37.
71. Postma, P., T. Miron, G. Olivieri, M. Barbosa, R. Wijffels and M. Eppink. "Mild disintegration of the green microalgae chlorella vulgaris using bead milling." *Bioresource technology* 184 (2015): 297-304.
72. Roche, J. and C. A. Royer. "Lessons from pressure denaturation of proteins." *Journal of The Royal Society Interface* 15 (2018): 20180244.
73. Midekessa, G., K. Godakumara, J. Ord, J. Viil, F. Lättekivi, K. Dissanayake, S. Kopanchuk, A. Rinken, A. Andronowska and S. Bhattacharjee. "Zeta potential of extracellular vesicles: Toward understanding the attributes that determine colloidal stability." *ACS omega* 5 (2020): 16701-10.
74. Melzer, C., J. v. d. Ohe and R. Hass. "Anti-tumor effects of exosomes derived from drug-incubated permanently growing human msc." *International Journal of Molecular Sciences* 21 (2020): 7311.
75. Vredenburgh, J. J., A. Desjardins, D. A. Reardon and H. S. Friedman. "Experience with irinotecan for the treatment of malignant glioma." *Neuro-oncology* 11 (2009): 80-91.
76. Mohammady, H., R. Dinarvand, M. Esfandyari Manesh and P. Ebrahimnejad. "Encapsulation of irinotecan in polymeric nanoparticles: Characterization, release kinetic and cytotoxicity evaluation." *Nanomedicine Journal* 3 (2016): 159-68.
77. Li, J., B. Li, L. Sun, B. Duan, S. Huang, Y. Yuan, Y. Ding and A. Hu. "Self-delivery nanoparticles of an amphiphilic irinotecan–enediyne conjugate for cancer combination chemotherapy." *Journal of Materials Chemistry B* 7 (2019): 103-11.
78. Poudel, B. K., B. Gupta, T. Ramasamy, R. K. Thapa, Y. S. Youn, H.-G. Choi, C. S. Yong and J. O. Kim. "Development of polymeric irinotecan nanoparticles using a novel lactone preservation strategy." *International journal of pharmaceutics* 512 (2016): 75-86.
79. Ha, M. K., K. H. Chung and T. H. Yoon. "Heterogeneity in biodistribution and cytotoxicity of silver nanoparticles in pulmonary adenocarcinoma human cells." *Nanomaterials* 10 (2020): 36.
80. Jochums, A., E. Friehs, F. Sambale, A. Lavrentieva, D. Bahnemann and T. Scheper. "Revelation of different nanoparticle-uptake behavior in two standard cell lines nih/3t3 and a549 by flow cytometry and time-lapse imaging." *Toxics* 5 (2017): 15.
81. Zucker, R., E. Massaro, K. Sanders, L. Degn and W. Boyes. "Detection of tio2 nanoparticles in cells by flow cytometry." *Cytometry Part A* 77 (2010): 677-85.
82. Gimbrone Jr, M. A. and G. García-Cardeña. "Endothelial cell dysfunction and the pathobiology of atherosclerosis." *Circulation research* 118 (2016): 620-36.
83. Grebe, A. and E. Latz. "Cholesterol crystals and inflammation." *Current rheumatology reports* 15 (2013): 313.

84. Ballweg, S., E. Sezgin, M. Doktorova, R. Covino, J. Reinhard, D. Wunnicke, I. Hänelt, I. Levental, G. Hummer and R. Ernst. "Regulation of lipid saturation without sensing membrane fluidity." *Nature communications* 11 (2020): 1-13.
85. Peters, J., J. Marion, F. Becher, M. Trapp, T. Gutberlet, D. Bicout and T. Heimburg. "Thermodynamics of lipid multi-lamellar vesicles in presence of sterols at high hydrostatic pressure." *Scientific reports* 7 (2017): 1-15.
86. Haraszti, R. A., M.-C. Didiot, E. Sapp, J. Leszyk, S. A. Shaffer, H. E. Rockwell, F. Gao, N. R. Narain, M. DiFiglia and M. A. Kiebish. "High-resolution proteomic and lipidomic analysis of exosomes and microvesicles from different cell sources." *Journal of extracellular vesicles* 5 (2016): 32570.
87. Vredenburgh, J. J., A. Desjardins, J. E. Herndon, J. Marcello, D. A. Reardon, J. A. Quinn, J. N. Rich, S. Sathornsumetee, S. Gururangan and J. Sampson. "Bevacizumab plus irinotecan in recurrent glioblastoma multiforme." *Journal of clinical oncology* 25 (2007): 4722-29.

Chapter 3

Engineered Mesenchymal Exosomes as a Promising tool for the Treatment of Chondrosarcoma in a Spheroid-Based 3D model

Introduction

Chondrosarcomas (CHS) are malignant bone tumor composed of cartilage-producing cells [1]. This heterogeneous group of tumors is the third most common primary malignancy of bone after myeloma and osteosarcoma, constituting 20–27% of all primary malignant osseous neoplasms [2].

The disease course and prognosis depend on many variables, one of the most important is the tumor grade. Indeed, high-grade tumors (II and III) may progress with the development of lung metastases having a worse prognosis compared to low-grade tumors [3].

Despite during recent decades the survival rate of cancer patients has been improved due to the development of potent anticancer drugs, at date surgery is the main treatment for most types of CHS while conventional chemotherapeutics are not an attractive option. Indeed, CHS are highly chemo and radiotherapy resistant due to their extracellular matrix, low percentage of dividing cells, and poor vascularity [4].

In this scenario, nanovectors, including liposomes, micelles, and polymeric nanoparticles, are emerging treatment options for CHS, given many advantages specialized for targeted drug delivery to cancer [5]. These nanovehicles have the potential to improve the stability, the safety and efficacy of encapsulated cargos, promoting their transport across membranes and prolonging their circulation times.

In a recent study [6], Poly-lactic acid (PLA) nanoparticles were designed for the targeted delivery of palovarotene to CHS lesion. Palovarotene is an anticancer drug currently investigated in phase 3 clinical trials for the treatment of fibrodysplasia ossificans progressiva and multiple osteochondromas [7]. As an agonist of RARγ, a nuclear Retinoic Acid (RA) receptor, it has effects on cartilage biology and has been demonstrated to play a critical role in the inhibition of heterotopic ossification [8]. Notably, the subcutaneous application of PLA nanoparticles reduced the weight of mice CHS tumors by 90% with no cancer growth for 9 weeks [6].

Sahin et al. [9] synthesized N-acetyl-d-glucosamine (GA) carrying hyaluronic acid nanoparticles [GA-PEG@nano(HA)]. These engineered nanoparticles showed not only a controlled release pattern of GA but an improved cellular penetration efficiency reducing the CHS cells proliferation. However, although GA@nanoHA exhibited no significant effect in the generation of ECM and elevation of chondrogenic markers, those nanoparticles promoted the chondrogenic differentiation of bone marrow-derived mesenchymal stem cells (MSC).

Interestingly, pegylated liposomes encapsulating Doxorubicin (Doxil) have also been used in a recent work [10]. Trucco et al. [10] conducted a Phase I/II study on the combination of Doxil with temsirolimus (Torisel), an intravenous mTOR inhibitor that is rapidly converted to sirolimus in vivo, for patients with recurrent and refractory bone and soft tissue sarcomas. Thus, this nanoscale therapeutics combination allows improved localization of drug to tumors and cell sensitization to chemotherapeutics.

Despite the promising results in efficacy and targeting of these nanocarriers, immunogenicity and toxicity are still some of the main issues related to traditional delivery system [5]. Thus, in recent decades, nanoparticles naturally released by cells, have been exploited as a novel biological nanoplatform for diagnosis and therapy [11]. Among all EVs, Exos are the most promising for their small size, ranging between 30-200 nm, and their homing features [12]. Furthermore, those nanosized secreted vesicles contain complex cargo, both in their lumen and the lipid membrane, that regulate the intercellular communication. Their natural composition and unique architecture allow, through the crossing of various natural barriers, a selective interaction with a target cell and protect Exos cargo from degradation in the bloodstream [13]. Many types of cells such as epithelial, hematopoietic, tumor and MSCs are known to secrete Exos [14]. Among these, MSCs are recognized as an

ideal cell candidate for the mass production of Exos because of the large ex vivo expansion capacity, the tropism toward tumor tissue, the high tumor-matrix crosstalk, low immunogenicity and side effect [15]. Indeed, many miRNAs have been found in MSC-derived Exos and are reportedly involved in both physiological and pathological processes such as organism development, epigenetic regulation, immunoregulation (miR-155 and miR-146) [16], tumorigenesis and tumor progression (miR-23b, miR-451, miR-223, miR-24, miR-125b, miR-31, miR-214, and miR-122) [17]. Over 900 species of proteins have been collected from MSC-Exos according to ExoCarta [18]. Several studies have also shown that MSC-Exos harbor cytokines and growth factors, such as TGFβ1, interleukin-6 (IL-6), IL-10, and hepatocyte growth factor (HGF), which have been proven to contribute to immunoregulation [19].

So, MSC-Exos may have the versatility and capacity to interact with multiple cell types within the immediate vicinity and remote areas to elicit appropriate cellular responses. MSCs through their secreted Exos target housekeeping processes to restore tissue homeostasis and enable cells within the tissue to recover, repair and regenerate [20].

This hypothesis provides a rationale for their therapeutic efficacy in a wide spectrum of diseases and rationalizes their additional use as an adjuvant to support and complement other therapeutic modalities.

Promising results demonstrated that MSC-EVs can inhibit angiogenesis and maintain vascular homeostasis in activated endothelial cells [21]. However, most studies focus on the application of EVs as potential therapeutical assets against tumoral cells. Li et al. [22] found that Exos derived from human umbilical cord MSCs (hucMSC) ameliorate liver fibrosis by inhibiting both the epithelial-mesenchymal transition of hepatocytes and collagen production, significantly restore the serum aspartate aminotransferase activity and inactivate the TGF-β1/Smad2 signaling pathway by decreasing collagen type I/III and TGF-β1 and the phosphorylation of Smad2. Tan et al. [23] found that HuES9.E1 MSC-Exos elicit hepatoprotective effects through an increase in hepatocyte proliferation, as demonstrated by high expression of proliferation proteins (proliferating cell nuclear antigen and Cyclin D1), the anti-apoptotic gene Bcl-xL and the signal transducer and activator of transcription 3 (STAT3).

The study of the interaction between the vesicles and the tumoral biological environment can be carried out on both 2D and 3D models. The arrangement of cells in tridimensional conformations often offers a better physiological model of drug therapy. The popularization of 3D culturing has come with the observation that this type of cell cultures often retains heterogeneity. Moreover, 3D cultures offer advantages over conventional monolayered cell cultures including preservation of the topology and cell-to-matrix interactions [24]. This feature allows the study of tumor evolution. On the other hand, the application of 3D cultures is also challenging, given the difficulties to stabilize the cultures, and the requirement of specific material to perform the culture [24].

Motivated by this rationale, we explored the feasibility of delivering the chemotherapeutic Doxorubicin (DXR) to tumor tissue using our engineered Exos. In a previous study [25] it was demonstrated that DXR and cisplatin, that are widely employed in CHS, were less effective on 3D-CHS spheroids when compared to standard monolayer models. In our work, using SW1353 cells, we developed a 3D in vitro culture model to mimic in vivo features of CHS microenvironment and evaluated the enhanced cytotoxicity effect both on 2D and 3D-cultures of our engineered DXR-MSC-Exos.

One of the major challenges associated with EVs as a promising drug delivery system is their capability for efficient drug loading. Here we applied our innovative technique of encapsulation through a HPH system to further assess the reproducibility of the entrapping mechanisms of active compounds in Exos originated from

different cell sources. In line with our previous study on tumoral Exos, we find out an EE up to 30% also in MSC-Exos with a hydrophobic small molecule as DXR. Thus, we demonstrate that the phenomena of temporary deformation applied through our HPH system on lipidic bilayer are suitable for many types of EVs, with a different proteo-lipid arrangement.

Materials and Methods

The murine bone marrow MSC and Chondrosarcoma SW1353 cell line were purchased from the American Type Culture Collection (ATCC). All media and reagents for cell culture were purchased by Sigma Aldrich (St. Louis, Missouri, USA). Cell viability was assessed by Trypan Blue stain 0.4% (Invitrogen™, ThermoFisher Scientific; Waltham, Massachusetts, USA) and determined using a Countess II FL Automated Cell Counter (ThermoFisher Scientific; Waltham, Massachusetts, USA). Doxorubicin HCl (molecular formula $C_{22}H_{29}NO_{11}HCl$ Mw = 579.98 g/mol) was purchased from Selleckchem (Houston, USA).

Cell culture

Chondrosarcoma SW1353 cell line was purchased from ATCC. The cell line was cultured in IMDM supplemented with 10% foetal bovine serum (FBS). All media and reagents for cell culture were purchased by Sigma Aldrich (St. Louis, Missouri, USA) and all cells were incubated at 37°C in 5% CO_2/95% air.
To obtain 3D spheroids by the hanging-drop method, 5,000 SW1353 cells were plated in 96-well Round Bottom Ultra-low attachment plate (Costar) in 200 mL of IMDM. Additional 200 mL of filtered IMDM were added to each well and the lid placed over the plate, with specific supports fixed at every corner. Then, the plate was turned and incubated in gentle stirring at 37℃ and 5% CO o/n. The next day, the plate was flipped again, 200 mL of medium were removed, and the formed spheroids were let grow, monitoring them constantly by using a Nikon Eclipse-TE 2000-S microscope (Nikon, Tokyo, Japan).

Exos Isolation by dUC

After growing to 70–80% confluency, murine MSCs cells at passage 4 were cultured in DMEM medium without FBS for 48 hrs. Then, the conditioned medium was collected, and Exos were isolated with dUC method. Briefly, the conditioned medium was centrifuged at 300 xg for 10 min to dislodge cells and debris then at 2000 xg for 10 min and other 30 min at 10000 xg to eliminate cell debris. Exos were pelleted by dUC of supernatant in 8 mL polycarbonate tubes (Beckman Coulter, Brea, CA, USA) at ~110,000 × g (70,000 RPM – MLA-80 ROTOR) for 70 minutes using an OptimaTM MAX-XP Ultracentrifuge (Beckman Coulter, Brea, CA, USA) and the supernatant was discarded. Finally, pellet resuspended in PBS was washed twice. All procedures were carried out at 4° C. The purified Exos were resuspended in 200 μL of PBS and stored at -20° C prior to use.

Efficient Loading of therapeutic cargo in MSC-Exos by High Pressure Homogenization

DXR was incorporated into Exos through HPH treatment. Three different concentrations of DXR (6-12-24 μg/mL) were pre-mixed with naive Exos at a fixed concentration of 11,61* 10^^{8} particles/mL in PBS and fed to the system through a stainless-steel feed reservoir. HPH was carried out at 1500 bar-2 Cycles. Then, the collected samples were purified through Spin-X corning Centrifugation 3KDa Cut-off performed at 3000 xg 60 minutes 4° C.
The amount of DXR loaded into Exos was calculated from a standard curve obtained by detecting the absorbance value at the wavelength of 480 nm.

MSC-Exos Characterization: size, morphology and biological content

After purification of naïve Exos and engineering with DXR (DXR-MSC-Exos) the hydrodynamic size, particles concentration, protein content, surface charge of samples and morphology were analyzed. Purified Exos were diluted 1:5 in 1 mL PBS, the concentration was determined by recording and analyzing the Brownian motion of particles using a qNano System. Mean size of Exos diluted in water (0,8% wt/vol) was analyzed at 25 °C, using a Zetasizer Nano ZS (Model ZEN3600, Malvern Instruments Ltd., UK) equipped with a solid-state laser (λ = 633 nm) at a scattering angle of 173°. The cuvettes used are the 12 mm square glass cuvettes with square aperture for 90° sizing (Malvern; # PCS1115). For Cryo-TEM analysis 3 μL of sample were directly dropped onto Formvar/Carbon 200 mesh Cu Agar® grids. Samples were observed in a Tecnai FEI® TEM operated at 80 kV accelerating voltage. Surface protein content was quantified with QuantiPro^{TM} BCA Assay Kit (Sigma Aldrich; St. Louis, Missouri, USA) in each vesicle preparation.

In Vitro Cytotoxicity of DXR-MSC-Exos

The cytotoxicity of DXR-MSC-Exos was determined by the standard MTT assay on SW1353 cells monolayers. Briefly, tumor cells (15×10^3 cells/well) were seeded in 200 μL of media in a 96-well plate overnight. Tumor cells were treated with concentrations of free-DXR and DXR-MSC-Exos ranging between 43 and 0,001 μM up to 72 hrs at 37°C and 5% CO_2. After incubation, CM was removed, and cells were incubated with MTT reagent for 3–4 hrs. Subsequently, 100 μL of DMSO was added to solubilize purple formazan crystals. Cytotoxic activity of Free-DXR and DXR-MSC-Exo was then evaluated by standard MTT assay. Absorbance was measured by spectrophotometer at 545–630 nm. Survival rates were assessed compared to the negative control (wells containing only Untreated Exos). All experiments were repeated 3 times.
The acid phosphatase assay was used to measure cell viability in 3D cultures. After 1 week, cells were treated with DXR at two different concentrations (250–500 nM). After 48 hrs of treatment, the supernatant was discarded, cells were washed with 200 mL/well of PBS, and 100 mL/well of NaAc-buffer (Sodium Acetate, Sigma–Aldrich, Milan, Italy) containing p-Nitrophenyl phosphate disodium hexahydrate were added. After 2 hrs of incubation at 37℃ and 5% CO_2, the reaction was stopped with 10 mL/well of NaOH 1M and the absorbance at 405 nm was recorded by using a microplate-reader (Tecan Infinite F200pro, Tecan, Milan, Italy). Results were expressed as percentage of viable cells with respect to the control.

Results

MSC-Exos stability after DXR entrapment with HPH system

To optimize the loading capability of the MSC-Exos with DXR, samples were treated in HPH system at three different concentrations ranging between 6 and 24 µg/mL according to literature [26-28].
In line with our previous study on tumoral glioblastoma-U87 derived Exos and IRI, we find out a final EE over 30% regardless of the initial amount of Free-drug mixed with naïve vesicles.
Surprisingly, this result confirms that the phenomena of temporary deformation applied on the nanovesicles bilayer are successful for both U87 and MSC cells derived Exos despite the different proteolipid structure.

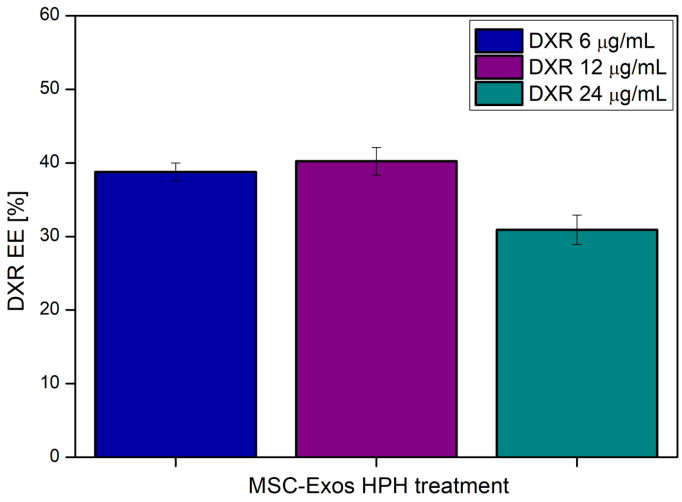

Figure 1. EE% of HPH-treated Exos at different DXR concentration of 6, 12 and 24 µg/mL.

The morphological investigation of Exos after loading with DXR was performed by transmission electron microscope (TEM). As shown in Figure 2a the typical Exos structures can be observed after HPH treatment. DLS (Figure 2b) indicated that the Exos had a relatively narrow size distribution. The peak diameter of MSC-Exos was at 159 nm while after loading with DXR, it shows a slight increasing to 167 nm. ZP and the protein analysis (Figure 2 d-e) showed also a stable surface composition compared to MSC-Exos further demonstrating that the encapsulation did not affect the transport of their naïve biological content on the lipidic bilayer.

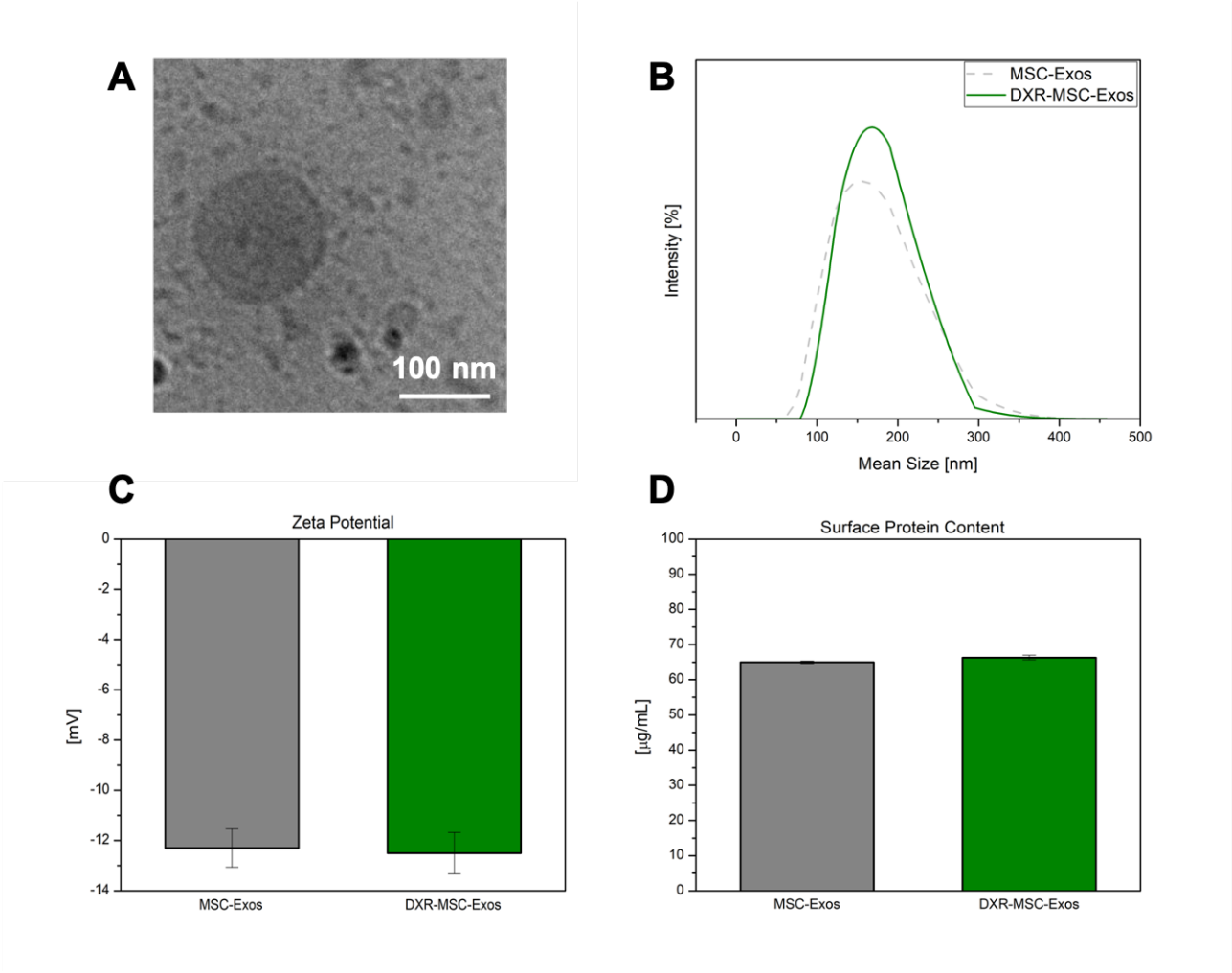

Figure 2. (a) Cryo-TEM observations after HPH loading of DXR; comparison between MSC-Exos and DXR-MSC-Exos (b) PSD, (c) ZP and (d) Surface protein amount.

Preliminary analysis of Cytotoxicity and internalization behavior of DXR-MSC-Exos in CHS 2D-monolayer

To determine the effect of DXR-MSC-Exos on the viability of cancer cells, SW1353 cells were incubated with cell culture medium (control), DXR, or DXR-MSC-Exos in a 96-well plate. The viability was measured with Free-DXR in a wide range, between 1 nM and 43 µM. In line with literature [29], we find out that cell viability decreases below 20% in 48 hrs in the range 0,8-43 µM (Figure 3a). So, we decided to investigate cytotoxic activity in a lower concentration range within 72 hrs and to compare Free-DXR and DXR-MSC-Exo to evaluate whether MSC-Exos use as drug delivery system could favor intercellular communication with targeted area and increase of cytotoxicity even at lower concentrations. Interestingly, we find out that DXR-MSC-Exos treatment was much more effective to inhibit cell proliferation rather than Free-DXR treatment. Indeed Free-DXR allowed a reduction of cell viability of just 75% up to 72 hrs while with DXR-MSC-Exos viability start decreasing 60% in 48 hrs reaching only 20% of viability after 72 hrs (Figure 3 b-c).

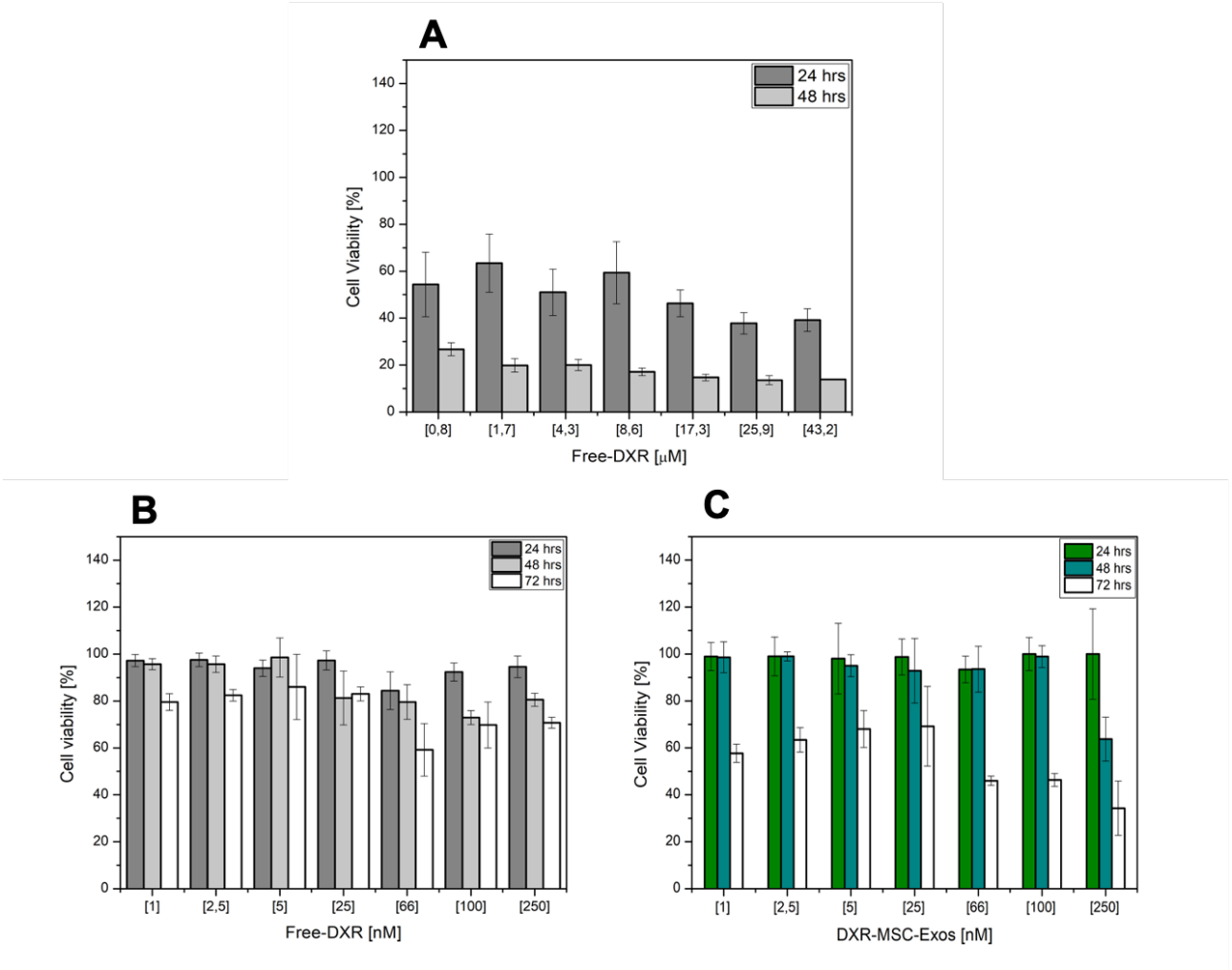

Figure 3. Cell viability of SW1353 cells exposed to different concentrations of Free-DXR and DXR-MSC-Exos, (a) Free-DXR exposure ranging between 0,8 and 43,2 μM up to 48 hrs, (b) Free-DXR and DXR-MSC-Exos (c) exposure between 1 and 250 nM up to 72 hrs.

To further investigate DXR-MSC-Exos interaction and internalization phenomena, quantitative measurement by flow cytometry was performed. As showed in Figure 4 a-c, Free-DXR and DXR-MSC-Exos were tested at two different concentrations (250 and 500 nM) after 72 hrs of contact. Figure 4a shows the Mean Fluorescence Intensity, reported as an internalization parameter and detected at 480 nm.

Mean Fluorescence Intensity demonstrated a higher value for DXR-MSC-Exos at the 500 nM concentration confirming that the interaction with cellular environment is higher for our nanovesicles than for the Free-drug. In line with this founding, SSC intensity is reported as the inner granularity value [30] (Figure 4b). After cellular uptake Exos, similarly to granulocytes in physiological situations, allow a higher increase of the surface granularity of cellular membrane than Free-DXR. Finally, to investigate the therapeutic potential of our DXR-MSC-Exos, Forward Scattering (FSC) is recorded as indication of cell viability (Figure 4c). In line with cytotoxicity analysis the cell viability was lower for DXR-MSC-Exos than Free-DXR in a dose-dependent manner.

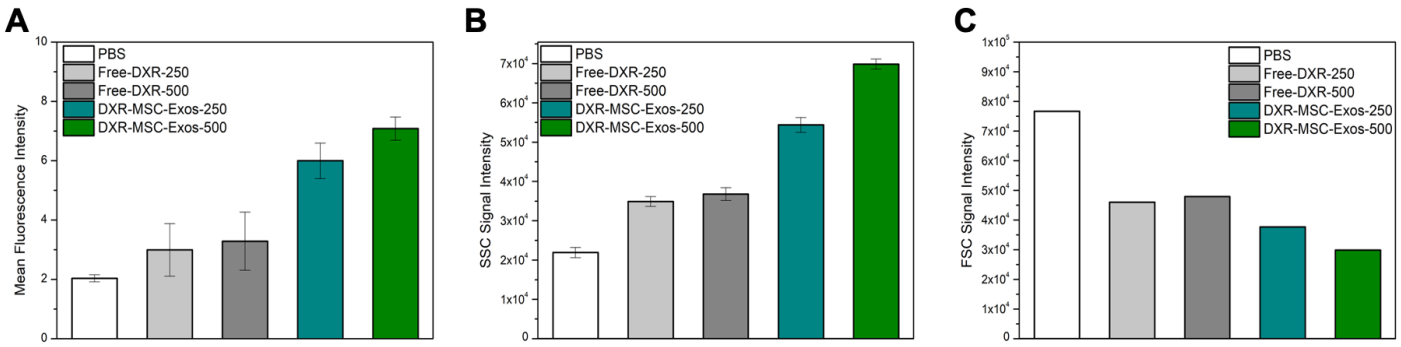

Figure 4 Flow cytometry of DXR-MSC-Exos at 72 hrs of incubation with SW1353 cells: (a) Mean Fluorescence Intensity (b) SSC Signal, (c) FSC Signal. All data are presented as mean±s.d (n=3).

DXR-MSC-Exos as an Effective Drug delivery system to Inhibits the Growth of 3D-Cultures of CHS

SW1353 spheroids generated from $5x10^3$ cells/well reached a diameter of approximately 500 mm after 7 days. After 1 week, the cytotoxicity of DXR was tested up to 48 hrs (Figure 5a). We observed a dose-dependent inhibition of cell growth after 48 hrs of drug treatment with our engineered Exos. In line with previous studies [25], we confirmed the chemoresistance of 3D-structure of CHS spheroids treated with Free-DXR. Notably, DXR carried by MSC-Exos, even at a very low concentration, could increase drug sensitivity with a final reduction of cell viability over 30 % up to 48 hrs (Figure 5b).

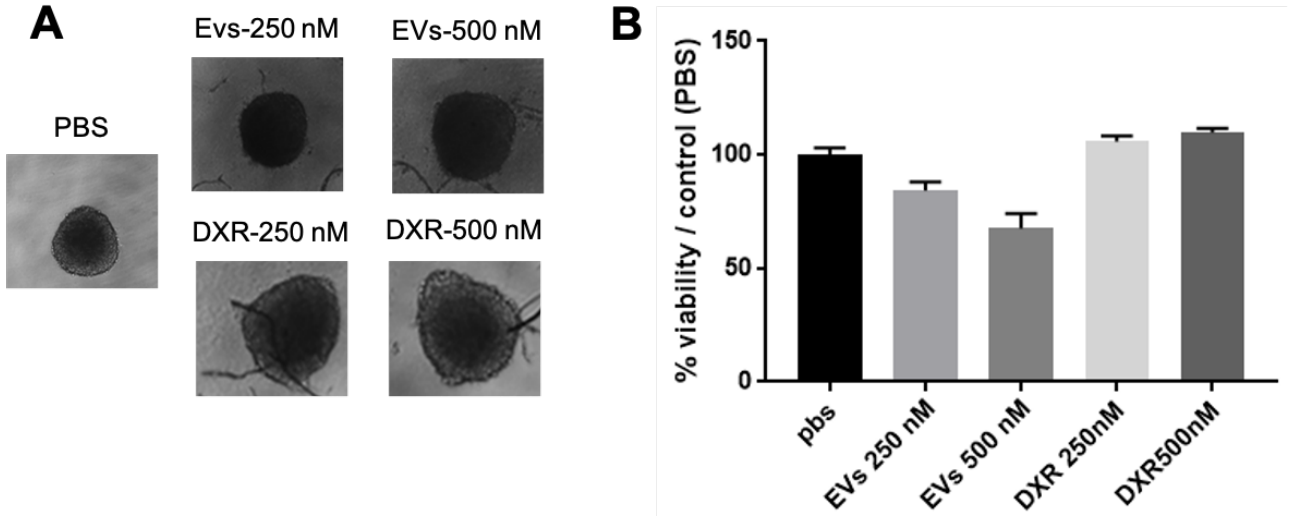

Figure 5. SW 1353 hanging drop spheroid. (a) Optical visualization of SW1353 spheroids at 9 Day, after 48 hrs of contact with drug, (b) Effect of DXR and DXR-MSC-Exos on CHS cells viability, in 3D-CHS cultures. Differences between spheroids groups were analyzed with Mann–Whitney test.

Discussion

The successful treatment of CHS is still a big challenge due to the chemoresistance, and there is and urgent need to develop reliable systems to assess preclinically the efficacy of therapeutic agents. This assessment is particularly true for testing of Drug Delivery Systems. It has already been proved that 3D cell culture models reproduce the physical and metabolic complexity of CHS better than traditional monolayer cultures. So, we studied DXR, a drug that is highly effective in other sarcomas, on SW1353 cells cultured as monolayers and spheroids. In a recent publication [31] it was observed a lower cytotoxic effect on spheroid cultures, confirming the limited efficacy of conventional anticancer drugs in CHS. The reason is that the traditional 2D cultures differ from 3D cultures in their morphological characteristics, proliferation rate , degree of differentiation, level of cell-to-cell interaction and cell-to-matrix, as well as their resistance to drugs [32, 33]. So, the peculiar microenvironmental feature of 3D cell growing structure mimics drug resistance in 3D-CHS cultures. Indeed, 3D organoid-like cultures rely not only on cell autonomy or cell–cell interactions, but also on intrinsic or extrinsic biochemical signals that constitute the tumor microenvironment, including local hypoxia, low access to nutrients, and acidosis. The establishment of low pH and decreased oxygen tension conditions are particularly important for CHS, since CHS are not vascularized and highly hypoxic tumors [34].
The application of complex culture models to unravel the role of EVs in cancer research has not been yet investigated among EVs research especially for the treatment of CHS. In this work,we demonstrated for the first time that MSC-Exos could be used to load chemotherapeutic drug DXR with a very high EE and that our therapeutic nanoplatform is as an effective nanocarrier in both 2D and 3D CHS models. DXR-MSC-Exos could be taken up by SW1315 cells and induce cytotoxicity. The study on 2D model revealed that DXR-MSC-Exos, compared with Free-DXR, can kill CHS cells more effectively in 72 hrs. Furthermore, this cytotoxicity is confirmed also in 3D model after 48 hrs.
As we already state, MSC- Exos, unlike traditional nanocarriers and active compounds, transport key therapeutical molecules. So, we can hypothesize that MSC-Exos function as a communication vehicle to elicit appropriate cellular responses in tumoral microenvironment since MSCs-Exos exhibit enhanced natural tropism toward tumor tissue than free drugs. Furthermore, the presence in the outer and inner parts of the lipidic bilayer of proteins such as sonic hedgehog [34] and platelet derived growth factor (PDGF) [31] or the transfer of mRNA and miRNAs [22] might contribute to their higher bioavability in such a complex system as the 3D tumoral model resulting in a more efficient release of drug in the affected area.

Furthermore, with the present study we pointed out some relevant findings stated in our previous work.
We demonstrate the reliability of our novel encapsulation method for the entrapping of different active compound in EVs extracted from various cell sources.
Indeed, Exos can transport many bioactive proteins, lipids as well as metabolism-related enzymes and, as we have already state, this enrichment is cell-type-specific.
Monounsaturated and polyunsaturated fatty acid as cholesterol, glycolipid, free fatty acid and phosphatidylserine are essential component in all Exos [35]. However, MSC seems to be highly enriched with other form of fatty acid depleted in tumoral EVs as U87-MG Exos [36], including leukotrienes, arachidonic acid (AA), phosphatidic acid, prostaglandins lysophosphatidylcholine (LPC), and docosahexaenoic acid (DHA) [37].

So, with our system, we are able to control the fluidity of lipidic bilayer of several EVs independently from their composition. Through the application of a physical stress, we induced a temporary manipulation only on the lipids present in higher percentages (as cholesterol and phosphatidylserine) common to most EVs preserving their morphological integrity and biological identity. Thus, the contribution of other minor lipid components, that could interfere with the fluidity of the membrane, is minimized.

In conclusion with our work, we demonstrate that HPH treatment could be a useful novel system for an efficient, fast and scaled-up approach to the encapsulation of EVs with various compounds. Furthermore, we demonstrate that the treatment of a 3D model of CHS with our engineered DXR-Exos is highly effective.

References

1. Donati, D. M. and G. Bianchi. "Chondrosarcomas (chs)." In *Diagnosis of musculoskeletal tumors and tumor-like conditions*. Springer, 2020, 157-79.
2. Kim, M.-J., K.-J. Cho, A. G. Ayala and J. Y. Ro. "Chondrosarcoma: With updates on molecular genetics." *Sarcoma* 2011 (2011):
3. Nazeri, E., M. G. Savadkoohi, K. Majidzadeh-A and R. Esmaeili. "Chondrosarcoma: An overview of clinical behavior, molecular mechanisms mediated drug resistance and potential therapeutic targets." *Critical reviews in oncology/hematology* 131 (2018): 102-09.
4. Simard, F. A., I. Richert, A. Vandermoeten, A.-V. Decouvelaere, J.-P. Michot, C. Caux, J.-Y. Blay and A. Dutour. "Description of the immune microenvironment of chondrosarcoma and contribution to progression." *Oncoimmunology* 6 (2017): e1265716.
5. Kim, D. H., H. S. Lee, Y.-H. Mun, S. Koh, J.-S. Park, S. M. Lee, N.-W. Kang, M. Y. Lee, C.-W. Cho and D.-D. Kim. "An overview of chondrosarcoma with a focus on nanoscale therapeutics." *Journal of Pharmaceutical Investigation* 50 (2020): 537-52.
6. Shield III, W. P., A. Cellini, H. Tian, K. Wilson, Y. Dan, J. M. Abzug, S. Garcia, N. Moritani, I. Alferiev and M. Chorny. "Selective agonists of nuclear retinoic acid receptor gamma inhibit growth of hcs-2/8 chondrosarcoma cells." *Journal of Orthopaedic Research®* 38 (2020): 1045-51.
7. Wentworth, K. L., U. Masharani and E. C. Hsiao. "Therapeutic advances for blocking heterotopic ossification in fibrodysplasia ossificans progressiva." *British journal of clinical pharmacology* 85 (2019): 1180-87.
8. Pacifici, M. "Retinoid roles and action in skeletal development and growth provide the rationale for an ongoing heterotopic ossification prevention trial." *Bone* 109 (2018): 267-75.
9. Şahin, Ş., E. Bilgiç, K. Salimi, A. Tuncel, B. Karaosmanoğlu, E. Z. Taşkıran, P. Korkusuz and F. Korkusuz. "Development, characterization and research of efficacy on in vitro cell culture of glucosamine carrying hyaluronic acid nanoparticles." *Journal of Drug Delivery Science and Technology* 52 (2019): 393-402.
10. Trucco, M. M., C. F. Meyer, K. A. Thornton, P. Shah, A. R. Chen, B. A. Wilky, M. A. Carrera-Haro, L. C. Boyer, M. F. Ferreira and U. Shafique. "A phase ii study of temsirolimus and liposomal doxorubicin for patients with recurrent and refractory bone and soft tissue sarcomas." *Clinical sarcoma research* 8 (2018): 1-9.
11. Jafari, D., S. Shajari, R. Jafari, N. Mardi, H. Gomari, F. Ganji, M. F. Moghadam and A. Samadikuchaksaraei. "Designer exosomes: A new platform for biotechnology therapeutics." *BioDrugs* (2020): 1-20.
12. Pullan, J. E., M. I. Confeld, J. K. Osborn, J. Kim, K. Sarkar and S. Mallik. "Exosomes as drug carriers for cancer therapy." *Molecular Pharmaceutics* 16 (2019): 1789-98.
13. Elliott, R. O. and M. He. "Unlocking the power of exosomes for crossing biological barriers in drug delivery." *Pharmaceutics* 13 (2021): 122.
14. Doyle, L. M. and M. Z. Wang. "Overview of extracellular vesicles, their origin, composition, purpose, and methods for exosome isolation and analysis." *Cells* 8 (2019): 727.
15. Kidd, S., E. Spaeth, J. L. Dembinski, M. Dietrich, K. Watson, A. Klopp, V. L. Battula, M. Weil, M. Andreeff and F. C. Marini. "Direct evidence of mesenchymal stem cell tropism for tumor and wounding microenvironments using in vivo bioluminescent imaging." *Stem cells* 27 (2009): 2614-23.
16. Di Trapani, M., G. Bassi, M. Midolo, A. Gatti, P. T. Kamga, A. Cassaro, R. Carusone, A. Adamo and M. Krampera. "Differential and transferable modulatory effects of mesenchymal stromal cell-derived extracellular vesicles on t, b and nk cell functions." *Scientific Reports* 6 (2016): 1-13.
17. Ono, M., N. Kosaka, N. Tominaga, Y. Yoshioka, F. Takeshita, R.-u. Takahashi, M. Yoshida, H. Tsuda, K. Tamura and T. Ochiya. "Exosomes from bone marrow mesenchymal stem cells

contain a microrna that promotes dormancy in metastatic breast cancer cells." *Science signaling* 7 (2014): ra63-ra63.
18. Keerthikumar, S., D. Chisanga, D. Ariyaratne, H. Al Saffar, S. Anand, K. Zhao, M. Samuel, M. Pathan, M. Jois and N. Chilamkurti. "Exocarta: A web-based compendium of exosomal cargo." *Journal of molecular biology* 428 (2016): 688-92.
19. Burrello, J., S. Monticone, C. Gai, Y. Gomez, S. Kholia and G. Camussi. "Stem cell-derived extracellular vesicles and immune-modulation." *Frontiers in cell and developmental biology* 4 (2016): 83.
20. Lai, R. C., R. W. Y. Yeo and S. K. Lim. "Mesenchymal stem cell exosomes." Presented at Seminars in cell & developmental biology, 2015. Elsevier, 40, 82-88.
21. Batsali, A. K., A. Georgopoulou, I. Mavroudi, A. Matheakakis, C. G. Pontikoglou and H. A. Papadaki. "The role of bone marrow mesenchymal stem cell derived extracellular vesicles (msc-evs) in normal and abnormal hematopoiesis and their therapeutic potential." *Journal of clinical medicine* 9 (2020): 856.
22. Li, T., Y. Yan, B. Wang, H. Qian, X. Zhang, L. Shen, M. Wang, Y. Zhou, W. Zhu and W. Li. "Exosomes derived from human umbilical cord mesenchymal stem cells alleviate liver fibrosis." *Stem cells and development* 22 (2013): 845-54.
23. Tan, C. Y., R. C. Lai, W. Wong, Y. Y. Dan, S.-K. Lim and H. K. Ho. "Mesenchymal stem cell-derived exosomes promote hepatic regeneration in drug-induced liver injury models." *Stem cell research & therapy* 5 (2014): 1-14.
24. Bordanaba-Florit, G., I. Madarieta, B. Olalde, J. M. Falcón-Pérez and F. Royo. "3d cell cultures as prospective models to study extracellular vesicles in cancer." *Cancers* 13 (2021): 307.
25. Perut, F., F. V. Sbrana, S. Avnet, A. De Milito and N. Baldini. "Spheroid-based 3d cell cultures identify salinomycin as a promising drug for the treatment of chondrosarcoma." *Journal of Orthopaedic Research®* 36 (2018): 2305-12.
26. Goh, W. J., C. K. Lee, S. Zou, E. C. Woon, B. Czarny and G. Pastorin. "Doxorubicin-loaded cell-derived nanovesicles: An alternative targeted approach for anti-tumor therapy." *International journal of nanomedicine* 12 (2017): 2759.
27. Wei, H., J. Chen, S. Wang, F. Fu, X. Zhu, C. Wu, Z. Liu, G. Zhong and J. Lin. "A nanodrug consisting of doxorubicin and exosome derived from mesenchymal stem cells for osteosarcoma treatment in vitro." *International journal of nanomedicine* 14 (2019): 8603.
28. Tian, Y., S. Li, J. Song, T. Ji, M. Zhu, G. J. Anderson, J. Wei and G. Nie. "A doxorubicin delivery platform using engineered natural membrane vesicle exosomes for targeted tumor therapy." *Biomaterials* 35 (2014): 2383-90.
29. Dubbelboer, I. R., N. Pavlovic, F. Heindryckx, E. Sjögren and H. Lennernäs. "Liver cancer cell lines treated with doxorubicin under normoxia and hypoxia: Cell viability and oncologic protein profile." *Cancers* 11 (2019): 1024.
30. Zhong, Y., Y. Li, J. Qu, X. Zhang, S. A. Seytahmetovna, A. Blennow and D. Guo. "Structural features of five types of maize starch granule subgroups sorted by flow cytometry." *Food Chemistry* 356 (2021): 129657.
31. Voissiere, A., E. Jouberton, E. Maubert, F. Degoul, C. Peyrode, J.-M. Chezal and É. Miot-Noirault. "Development and characterization of a human three-dimensional chondrosarcoma culture for in vitro drug testing." *PLoS One* 12 (2017): e0181340.
32. Lv, D., Z. Hu, L. Lu, H. Lu and X. Xu. "Three-dimensional cell culture: A powerful tool in tumor research and drug discovery." *Oncology letters* 14 (2017): 6999-7010.
33. Weigelt, B., C. M. Ghajar and M. J. Bissell. "The need for complex 3d culture models to unravel novel pathways and identify accurate biomarkers in breast cancer." *Advanced drug delivery reviews* 69 (2014): 42-51.

34. Bovée, J. V., P. C. Hogendoorn, J. S. Wunder and B. A. Alman. "Cartilage tumours and bone development: Molecular pathology and possible therapeutic targets." *Nature Reviews Cancer* 10 (2010): 481-88.
35. Skryabin, G., A. Komelkov, E. Savelyeva and E. Tchevkina. "Lipid rafts in exosome biogenesis." *Biochemistry (Moscow)* 85 (2020): 177-91.
36. Haraszti, R. A., M.-C. Didiot, E. Sapp, J. Leszyk, S. A. Shaffer, H. E. Rockwell, F. Gao, N. R. Narain, M. DiFiglia and M. A. Kiebish. "High-resolution proteomic and lipidomic analysis of exosomes and microvesicles from different cell sources." *Journal of extracellular vesicles* 5 (2016): 32570.
37. Skotland, T., K. Sagini, K. Sandvig and A. Llorente. "An emerging focus on lipids in extracellular vesicles." *Advanced drug delivery reviews* 159 (2020): 308-21.

Chapter 4

Exosomes stability in biological environment: comparison with polymeric Nanoparticles

Introduction

Upon contact with a biological milieu, the surface of Nanoparticles (NPs) tends to interact with biomolecules present in biological medium or body fluid. Consequentially, NPs are modified by the adsorption of biomolecules such as proteins and lipids, culminating in the formation of a layer called "protein corona" (PC) [1]. The PC has a dynamic nature since a limited number and specific type of biomolecules will compete for the NPs surface, resulting in a corona containing few identifiable proteins [2]. If the exchange kinetics is slow enough (depending on the coating proteins and the experimental setup), the corona will be biologically relevant, becoming the NPs biological identity [3]. For a given NP, only several dozen proteins interact with NPs surface in significant amounts and for long enough to be recognized by the cell. The recognition can either be generic or highly specific, involving receptor-ligand interactions and leading to the binding of NP to the cell [4]. In other words, the identity, organization and lifetime of these proteins adsorbed on NP surface affect their interaction, recognition and processing in the cells [5]. Lundqvist, Martin, et al. [6] hypothesized that once a NP is dispersed in any biological fluid, a cell will only "see" the system in which the NP core is surrounded by a "hard" corona (HC) of slowly exchanging proteins, tightly bound, and an outer layer of weakly interacting protein-protein complexes, rapidly exchanging with the proteins present in the environment, the so called "soft" corona (SC). Milani et al. [7] confirmed this theory through their study of reversible vs. irreversible binding of transferrin to polystyrene (PS) NPs. Between HC and SC, the inner HC is of high scientific relevance and also the most studied [8].

In recent decades, the corona of various NPs has been studied in detail, and a shared "core" proteome has been established, which comprises lipoproteins, complement and coagulation proteins, and immunoglobulins [9]. However, to date the growing interest in novel drug delivery system as EVs requires further investigation on uptake phenomena of these innovative nanovectors including PC formation.

To better understand the key mechanisms involved in Exos nanobiointeraction with biological environment, it is necessary to consider their proteo-lipid architecture. Indeed, unlike traditional NPs, EVs resemble liposomes in terms of size, shape and structure but have more complex bilayers, containing up to hundreds of different lipid, protein and carbohydrate types, as well as internal cargo and surface-associated molecules [10, 11].

At date very few studies clarified the mechanism of interaction between EVs membrane proteins and other biomolecules naturally present in biological compartments [12]. These protein layers may alter numerous membrane-related interactions and properties of natural systems, e.g., viral envelopes or EVs [13-16], as well as they do with traditional nanocarriers influencing their delivery or immunorecognition [17]. Since PC forms the first line in contact with other species, it is important for the better mechanistic understanding of both a diverse set of membrane active molecules, i.e., peptides, proteins, and the vesicular trafficking [18]. However, compared to standard membrane models, our knowledge is very poor on structural properties of biomembranes associated with PC. Typical model membrane systems in structural biophysics are Langmuir monolayers, vesicles, liposomes, and solid supported lipid bilayers [19]. Even though the provided systems can be easily produced, they may often limit the overall insight. Having an expanded set of complex membrane models is thus important for advanced membrane biophysics [20]. Related, EVs may also offer new model systems to address these problems.

So, in our work we propose a preliminary in vitro analysis of EVs stability in biological environment and interaction with other natural biomolecules.

To better understand their internalization mechanism, here we compare our natural nanovesicles to three different types of NPs: PS NPs, crosslinked hyaluronic acid (HA) NPs (cHANPs) and PEG-crosslinked hyaluronic acid NPs.

Materials

Atto 488 fluorescent label (Em/Ex 488/520) was purchased from ATTO-TEC GmbH (Germany). Dulbecco Modified Eagle Medium high glucose (DMEM), Fetal Bovine Serum (FBS), Phosphate Buffer Saline (PBS), Trypsin, Penicillin/Streptomycin, L-glutamine, Human Serum Albumin (HSA) for cell culture and in vitro study were purchased by Sigma Aldrich. For cell culture U-87 MG cell line (passage 15-36) was purchased from ATCC. Polystyrene NPs (PS NPs) were purchased from Sigma Aldrich. Crosslinked hyaluronic acid nanoparticles (cHANPs) and Polyethylene glycol crosslinked hyaluronic acid nanoparticles (PEG-cHANPs) were synthesized using a flow-focused nanoprecipitation approach in a microfluidic platform, as previously described [21, 22]. Briefly, a non-solvent phase (i.e. acetone or ethanol with stabilizing compounds) flows from two side channels, focusing a solvent phase (a hydrogel aqueous solution) in the central channel.

Methods

Protein Corona formation

NP dispersions and Exos were prepared by diluting the concentrated stock solutions in DMEM medium supplemented with different % of sera, 10% FBS or 20% Human Serum Albumin (HSA) [23] used for cell culture at 37°C, immediately prior to the experiments on cells, with an identical time delay between diluting and introducing NPs to the cells for all experiments. Before sampling, NPs were vigorously mixed by vortexing for 30 seconds. After the addition of the NPs to the different incubation solutions, these were also vortexed for 15 seconds to ensure maximum NPs dispersion. Concentration of protein corona adsorbed on NPs surface was determined using a bicinchoninic acid (BCA) assay (Thermo Fisher Scientific). Previously, unbound, and weakly bound soft-corona proteins were removed from the protein-NP mixture by Corning Spin-x (cut off 50 KDa) centrifugation (3000 rpm, 10 min, 4°C) for cHANPs and PEG-cHANPs, by Corning Spin-x (cut off 10 KDa) centrifugation (5000 rpm, 30 min, 4°C) for Exos, while UltraCentrifugation (70000rpm, 30min, 4°C) was performed for PS NPs.

Characterization of NPs: Size, charge and morphological stability

The particle size, PDI, ZP of PS NPs, cHANPs, PEG-cHANPs compared with U87-Exos were measured using the DLS technique. NPs were dispersed in 1 mL of double distilled deionized water at a concentration of 20 μg/mL and measurements were performed using Malvern Zetasizer Nano ZS90 (Malvern Instruments, Malvern, UK) at 37°C. All measurements were replicated three times and reported results are the mean value of all measurements.

Tecnai FEI® transmission electron Microscope was used to evaluate NPs stability and architecture after protein corona adsorption. Sample preparation consisted in placing 10 μL of NPs suspension on a

Formvar/Carbon 200 mesh Cu Agar® filter. After drying overnight under hood, samples were ready to be analyzed.

Flow cytometry

U87 cells were seeded in 48-well plates (Falcon®) at a density of 0.5 x 10^5 cells/well and incubated for 24 hrs prior to the addition of NPs to assure cell attachment. Afterwards, cells were incubated in two different sera conditions (10% FBS and 20% HSA) and three different NPs conditions (PS NPs, cHANPs and PEG-cHANPs) at specific time points (1, 2, 4, 24 and 48 hrs). The final concentration of NPs used in the incubation solution was 20 μg/mL for all three NPs. Negative controls consisted in the complete medium condition (medium, FBS, L-glutamine and penicillin/streptomycin) without NPs. After different time points contacts, medium was removed, and samples were washed three times with PBS (1x) to ensure particle removal from the outer cell membrane. Cells were then trypsinized for 5 min at 37°C. After cell detachment confirmation at optical microscope, complete medium was added to neutralize trypsin and cells were transferred to polystyrene round-bottomed tubes (Falcon®), before samples were immediately analyzed by flow cytometry. Every flow cytometry study has been conducted in triplicate, and the average of the three samples is considered for the percentage of fluorescence intensity (FI %) and SSC in order to obtain reliable results in terms of cell viability and internalization information.
Measurements were performed using a BDFACSCelesta™ (BD®) flow cytometer. 488nm laser wavelength was used to excite NPs fluorescence, which was collected using the 595–660 nm spectral detection channel. Results are reported as the mean of the distribution of cell fluorescence intensity obtained by measuring 10000 events averaged between three independent replicas. Error bars correspond to the standard deviation between the triplicates. Data analysis was performed using CytoFlow software.

Results

Qualitative analysis of protein corona formation on Polymeric NPs and Exos

DLS analysis gives information about dispersity and size of PS NPs, cHANPs, PEG-cHANPs and Exos in presence and absence of biological fluids. After protein-NPs contact for 1 hr, an increase in mean size was registered for all NPs as a result of PC formation. Figure 1 shows PDS of PS NPs, cHANPs, PEG-cHANPs and Exos in three different sera condition. On average, bare carboxylated PS NPs showed a slight increase in PDS with the formation of a PC as shown in Figure 1a. Interestingly Figures 1 b-c show that the PC affects more cHANPs than PEG-cHANPs PDS. Indeed, in line with literature, the PDS of PEG-cHANPs exhibited little change (Figure 1c) due to the hydrophilic nature of PEG that reduced the surface energy of the NP-solvent interface to minimize proteins adsorption [5, 24-26].
However, in all samples it is possible to observe a slight broadening, hence indicating increased heterogeneity in the NPs population due to NPs clustering or protein agglomeration. Nonetheless, Exos samples show a more pronounced peak around 10 nm in both FBS and HSA conditions, indicative of protein aggregate due to a still ongoing SC dissociation phenomenon (Figure 2d). Notably, in all samples the increasing in size is more pronounced in presence of FBS. Indeed, the most prominent difference between plasma and serum is the

presence of clotting factors in plasma; this will have an inherent effect on the PC structure and resulting interactions with the particle surface [27].

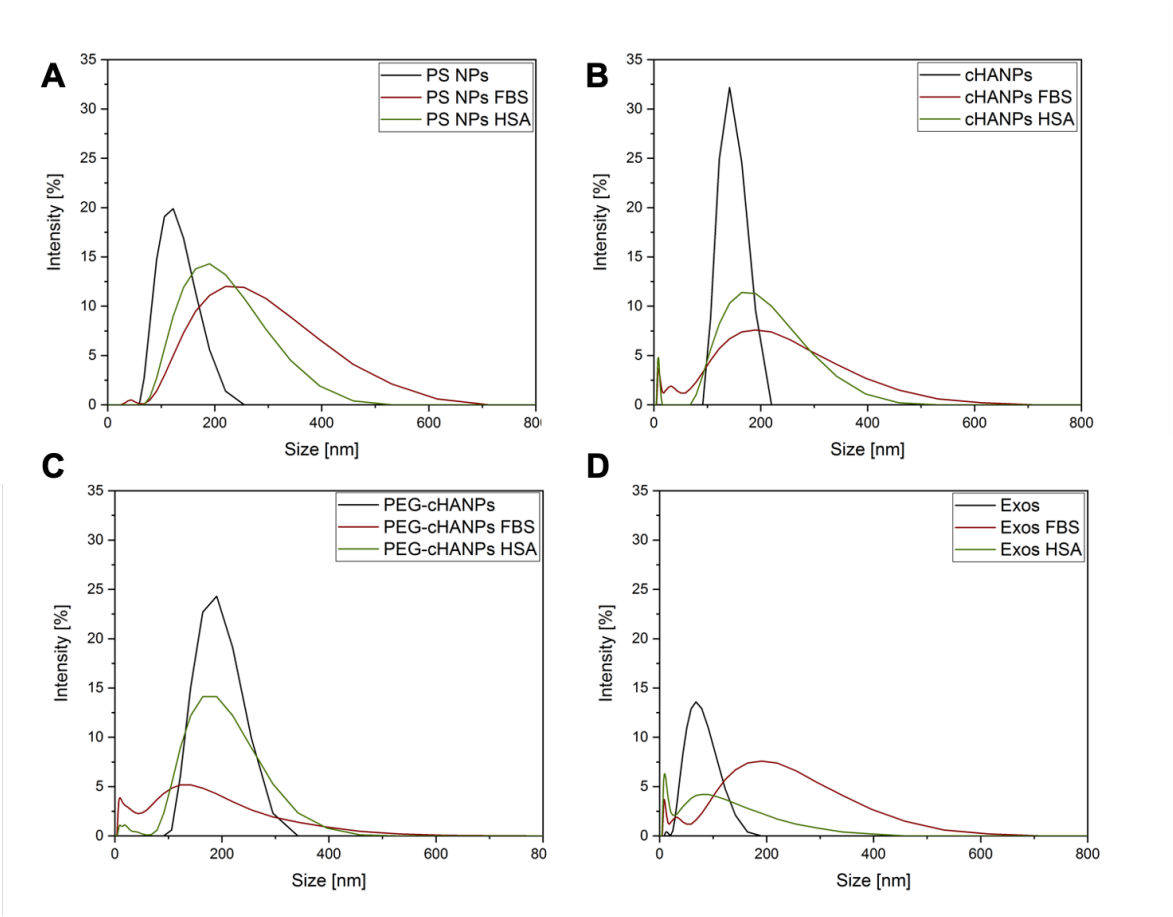

Figure 1 PSD in absence of serum and with FBS and HSA PC before and after 1 hr of contact. (a) PS NPs, (b) cHANPs and (c) PEG-cHANPs and (d) Exos.

ZP of all bare NPs decrease in absolute value after 1 hr of contact with different *sera*, as a confirmation of protein adsorption on NPs surface. Interestingly, in PS NPs, cHANPs and PEG-cHANPs we notice a decrease in the surface charge at values between -10 and -8 mV (Figure 2). cHANPs and PEG-cHANPs showed a relatively small change of mean ZP after incubation in sera condition, while the ZP of carboxyl PS NPs shows a drastically decrease due to their higher negative charge and affinity with FBS and HSA. Moreover, comparing cHANPs and PEG-cHANPs, it is visible that bare PEG-cHANPs have closer to zero ZP than bare cHANPs, and the ZP decrease is lower in PEG-cHANPs than cHANPs, demonstrating a thinner PC due to the presence of crosslinked-PEG. This data seems in line with DLS analysis, indeed PEG-cHANPs show a lower increase in size, suggesting less affinity to FBS and HSA proteins because of the presence of PEG chains in the HA network. These data are further confirmed for Exos ZP.

As for PEG-cHANPs also Exos show a stable surface charge after contact with different sera indicating the absence of a stable PC structure over their surface. Indeed, exosomal proteo-lipid architecture confers immune-stealth properties and protects Exos cargo from interaction with other protein in body fluids and degradation in the bloodstream similarly to PEGylated NPs. It is widely known that PEGylation increases biodistribution

in human body [28]. One of the reasons why PEG can prolong the circulation time of drugs and nanocarriers is the de-opsonization effect [29], that inhibits - or drastically reduces - adsorption of proteins and complements normally present in biological fluids, and so reducing recognition by cells of the RES [30]. Despite Exos de-opsonization effect and in vivo biodistribution need further investigation, several studies confirmed a stealth effect due to the presence of genetic material and ubiquitinated proteins over their surface.

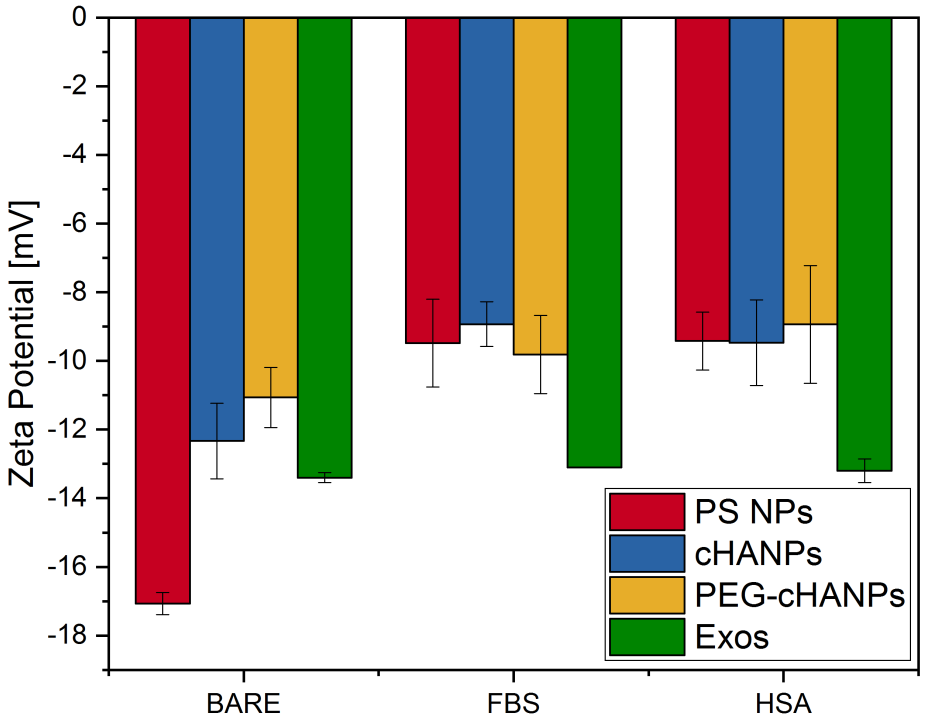

Figure 2. ZP of bare PS NPs, cHANPs, PEG-cHANPs and Exos compared to Z-P after 1 hr of contact with FBS and HSA.

Particle Type	Serum Condition	Mean Size (nm)	PDI	ZP (mV)
PS NPs	Bare	105.673 ± 6.139	0.032	-17.067 ± 0.322
	FBS	234.605 ± 35.288	-	-9.480 ± 1.279
	HSA	159.959 ± 20.430	-	-9.427 ± 0.845
cHANPs	Bare	150.027 ± 13.832	0.068	-12.333 ± 1.102
	FBS	165.558 ± 46.349	-	-8.930 ± 0.648
	HSA	162.608 ± 49.489	-	-9.473 ± 1.244
PEG-cHANPs	Bare	161.380 ± 15.626	0.075	-11.067 ± 0.873
	FBS	175.554 ± 11.459	-	-9.813 ± 1.142
	HSA	185.736 ± 47.852	-	-8.937 ± 1.712

Exos	Bare	68.06	-	-13.432 ± 0.145
	FBS	105.07	-	-13.1 ± 0.476
	HSA	78.82	-	-13.2 ± 0.476

Table 1 Size, PDI and ZP of bare PS NPs, cHANPs and PEG-cHANPs compared to ZP of NPs after 1 hr of contact with FBS and HSA.

The PC morphology and the NPs structural stability have been assessed by TEM analysis. Figure 2 shows that all polymeric NPs were surrounded by a protein cloud, which appeared to be narrower than the diameter of the NPs. Given the average diameter of 105 nm for bare PS NPs, 150 nm for cHANPs and 161 nm for PEG-cHANPs (Table 1), the average additional corona was estimated to be very variable depending on the type of NP but not over 50 nm thick (Figure 2) and referred to as a HC. Indeed, PC could be considered as a dynamic multi-layered structure formed by proteins adsorbed onto a NPs surface upon contact with the physiological environment and consequent interaction with proteins. This structure can be generally divided in two parts, HC and SC [1]. While the inner layer of tightly bound proteins with a longer lifetime has been termed as HC, the outer layer of weakly bound proteins with a shorter lifetime is considered a SC [31]. HC is known to be formed in less than 10 min over NPs surface and is constituted by high affinity proteins with a low dissociation constant [32]. In our case, experiments were performed after 1 hr of co-incubation of NPs with different sera in order to achieve the formation of both HC and SC. However, TEM analysis was performed after two steps of purification per each type of NPs in order to remove all unbounded or weakly-bounded proteins. Interestingly, all images show a dense and stable protein complex over NPs surface. However, PS NPs in FBS serum and PEG-cHANPs in HSA serum do not show a well-rounded structure over their surface but a non-uniform network that could be ascribe to the SC.

Generally [33, 34] SC is described as highly dynamic layer of proteins which have high exchange rates and low binding affinities towards the NPs. While there is extensive literature dealing with the subject of HC, only limited analytic methods used to study the SC are available. Consequently, determining the biological relevance of the soft corona need further investigation.

However independently from the type of interaction between our NPs and the PC, despite it increases NPs surface rugosity, structural integrity of NPs is still maintained.

Otherwise, the analysis carried out on Exos samples are not perfectly comparable with the other NPs. First, we decided to not investigate the Exos morphology in FBS serum. Indeed, FBS is widely enriched in Exos from bovine serum that might be similar to our exosomal sample [35]. Moreover, unlike the polymeric NPs, the preparation of samples for TEM needs different staining sand washing steps. As a result, structural artifacts caused by negative staining cannot be excluded.

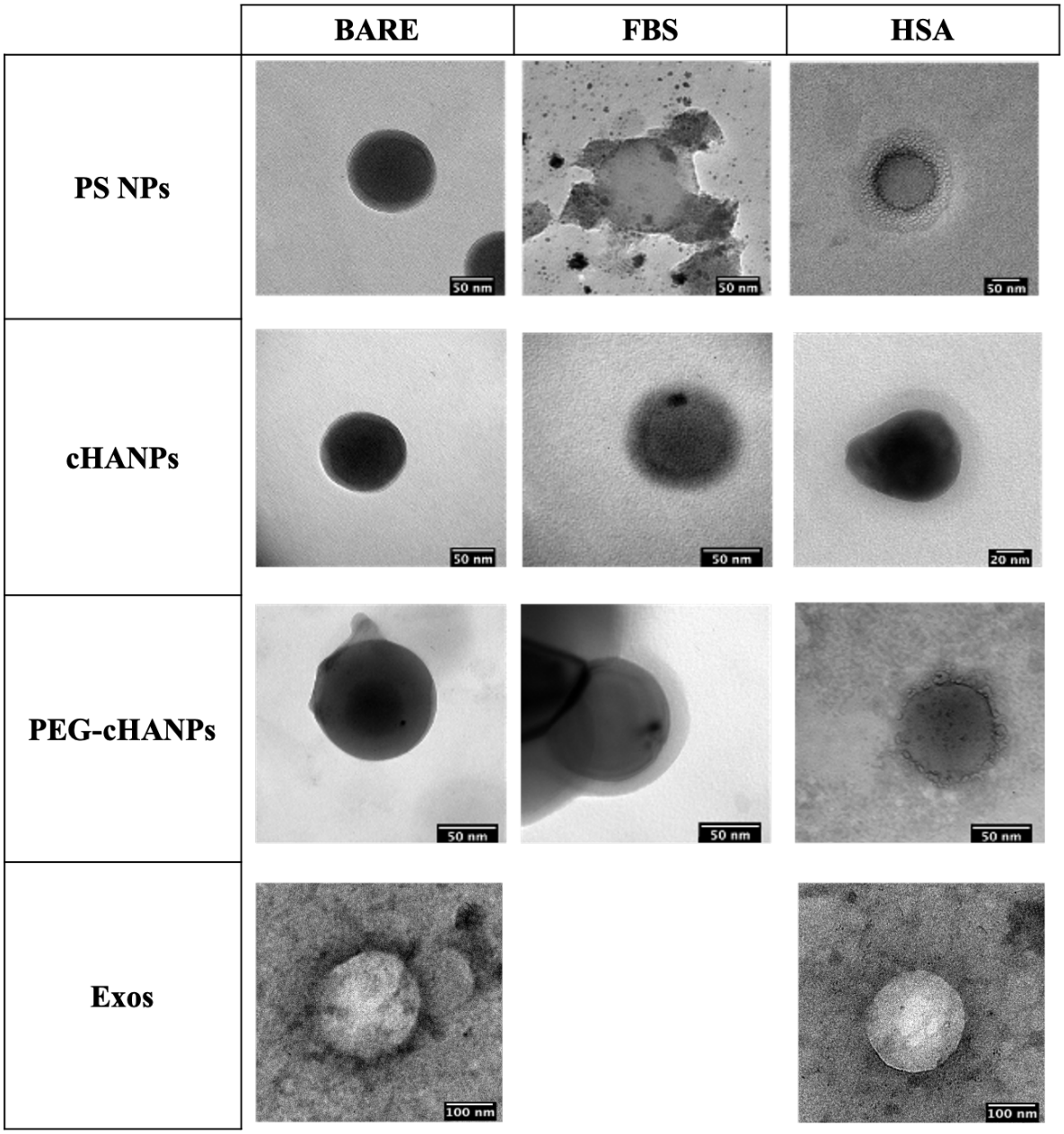

Figure 2 TEM images of bare PS NPs, cHANPs, PEG-cHANPs and Exos after 1 hr of contact with FBS and HSA, respectively. Protein corona is clearly adsorbed on the surface.

In vitro preliminary analysis of uptake and internalization phenomena of NPs in different sera condition

Owing to its high binding affinity to CD44, which is abundant in the tumor tissue, HA has been extensively investigated for the development of tumor-targeted imaging agents [36, 37] and drug delivery systems.
To make a comparison between HA and PS NPs and furthermore to observe the effect of HA-PEGylation on the receptor-mediated cellular uptake, our NPs were incubated with U87-MG cancer cell lines. Indeed, the cancer cells used in this study, have been widely demonstrated to over-express CD44 on their surfaces, compared to normal cells [38-40].

As shown in Figure 3 a-b, fluorescent signals were detected from U87-MG cells treated with bare PS NPs, cHANPs and PEG-cHANPs for 48 hrs in two different sera condition. Percentage was calculated with respect to fluorescence of the total volume of NPs exposed to cells.

Figure 3a show the internalization phenomena in the presence of FBS. Interestingly, PS NPs demonstrate a delay in uptake process compared to HA-NPs. Indeed, PS NPs FI slowly increase in the first 4 hrs to less than 15% while cHANPs and PEG-cHANPs have an almost 30% FI already after 1 hr of co-incubation.

This result proves that, in line with literature [41-43], NPs uptake by living cells is governed by chemical interactions between functional groups on the NPs as well as the receptors on cell surfaces. The much lower rate of uptake of PS NPs in comparison to HA-NPs indicates that the surface charge strongly affects the probability of approaching the cell surface. The negative potential of the cell surface is unfavorable for the interaction with negatively charged particles. However, once PS NPs have reached the cell membrane, their specific functional groups on the particle surface play an important role in binding to receptors that activate the endocytosis machinery. Indeed after 24 hrs internalization values are quite comparable with them of cHANPs.

Notably Figure 3a-b show that up to 4 hrs PS NPs uptake mechanism is completely different compared to cHANPs. Moreover, PS NPs after 24 hrs of contact have a drastically reduction of Internalization value, over 30%. On the other hand, cHANPs shifted their maximum peak of internalization from 24 to 48 hrs.

In both sera condition PEG-cHANPs show lower cellular uptake than cHANPs especially in FBS after 24 hrs of contact with a drastic reduction of FI % (34.212% against 76.009 % of cHANPs).

This behavior suggests that PEG chains play a critical role in the internalization, resulting in a stealth effect due to PEG blocks present in the architecture of PEG-cHANPs.

Nevertheless, in presence of HSA both cHANPs and PEG-cHANPs have a similar internalization behavior. So, in this case we may hypothesize a similar affinity for plasma proteins present in Human serum.

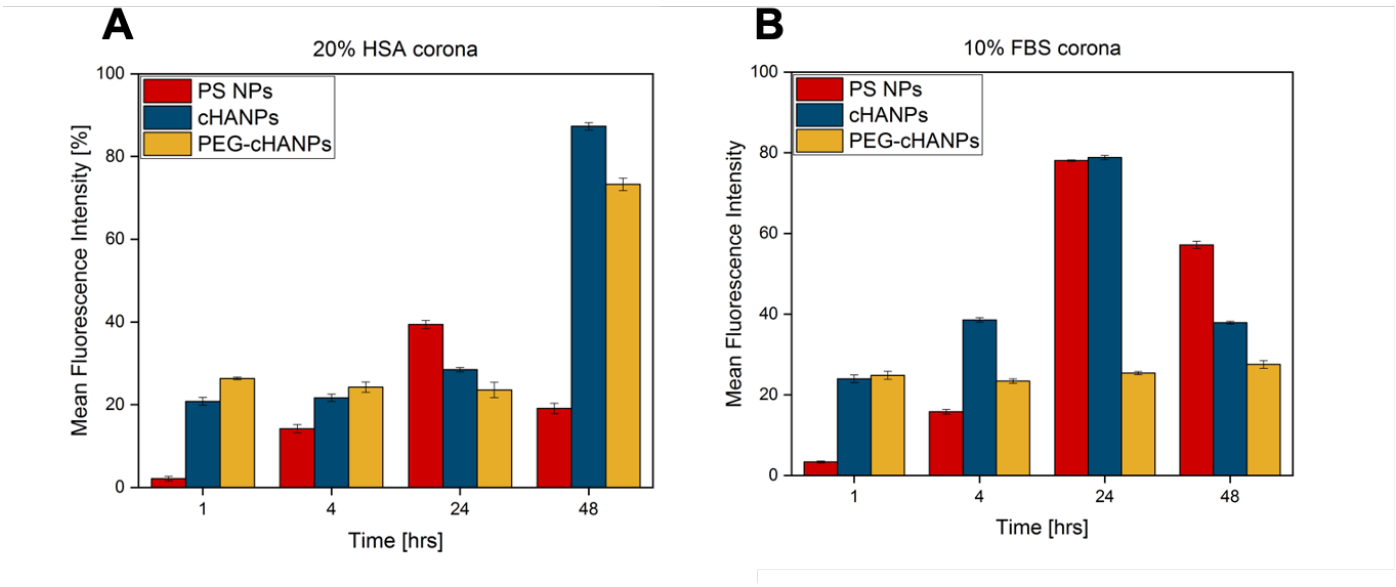

Figure 3 Mean Fluorescence Intensity % showing cell uptake phenomena of U87 MG glioma cells after contact with PS NPs, cHANPs and PEG-cHANPs in different serum conditions (a) HSA and (b) FBS and time points (1-4-24-48hrs).

SSC Signal Intensity is reported as a value of cell granularity. Indeed, it is proportional to the intracellular density. As shown in figure 4 a-b regardless of the sera conditions it shows a slightly increasing trends for all three types of particles.

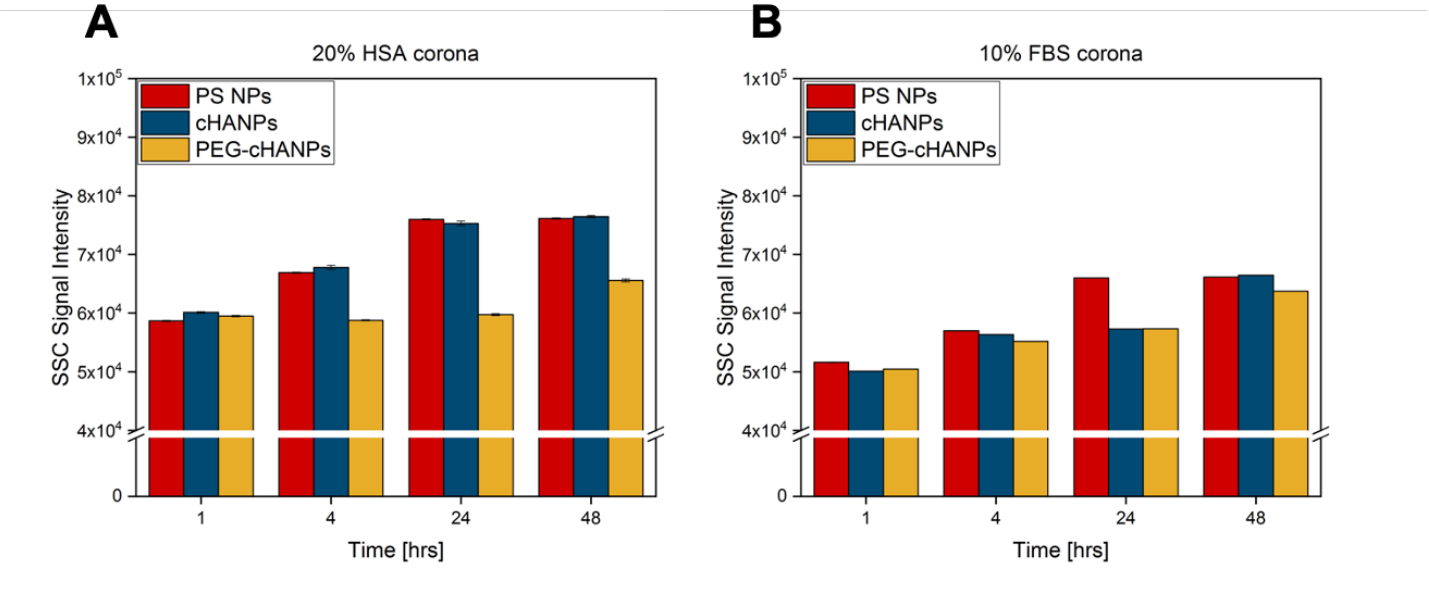

Figure 4 SSC showing cell uptake phenomena of U87 MG glioma cells after contact with PS NPs, cHANPs and PEG-cHANPs in different serum conditions (a) HSA and (b) FBS and time points (1-4-24-48hrs).

Discussion

After the administration of NPs in biological fluids, an NP-protein complex is formed, which represents the "true identity" of NP in our body. This protein-NP interaction should be carefully studied to predict and control the fate of drug-loaded NPs, including systemic circulation, biodistribution and bioavailability.

In the last decades considerable studies for both organic and inorganic NPs fate elucidated some unknown mechanisms. However, there are still different features that influence the PC as NPs shape, charge, size, biomaterials. So, elucidating all the mechanisms related to PC formation and of interaction with the biological environment seems almost impossible.

With the advent of new natural nanovectors such as EVs in the field of nanotechnologies, the urgency to answer some questions about the biodistribution, uptake phenomena and intercellular communication in the surrounding environment has become increasingly necessary.

To date, very few studies have been conducted on the biodistribution of Exos and possible phenomena of interaction with circulating proteins. The presence of a lipid coating layer and an innumerable amount of surface proteins already overexpressed in progenitor cells, has long led to assume that Exos do not have any type of interaction with the PC. Although it is not clear whether PC is formed on Exos, it could change the properties of these nanocarriers such as mechanisms of cellular uptake, interaction with the target area, and clearance from blood circulation.

For this reason, here for the first time we investigated this phenomenon by comparing different NPs systems. We studied the PC formation and internalization mechanisms of PS NPs, a traditional and widely studied

nanovector, HA-based NPs and PEG-crosslinked-HA-based NPs. These polymeric vectors were compared to Exos naturally extracted from U87-MG tumor cells. Although our study is a very preliminary analysis and requires further investigations, here we directly evaluated for the first time the formation of a PC on Exos surfaces by further discriminating between SC and HC.

Even though polymeric NPs and Exos are not totally comparable, it has emerged a very similar mechanism of interaction with FBS and HSA protein between PEG-cHANPs and Exos. Notably, in both cases it was detected an increase in the average size after 1 hr of incubation in sera condition. However, unlike PS NPs and cHANPs, the surface charge was almost stable in both sera conditions. So, we may hypothesize a reversible phenomenon of SC dissociation in progress. Conversely, PS NPs and cHANPs showed a drastically reduction in surface charge and increasing in mean size almost attributable to a thicker layer of proteins over their surfaces. Further analysis in flow cytometry also revealed a delay in the internalization process of the PEG-cHANPs in all serum conditions confirming their widely known stealth mechanism.

In conclusion, our study partially corroborates the hypotheses of possible interactions between circulating proteins and the proteolipid structure of the EVs. Once in circulation, the phenomena of both a protein-protein interaction and SC formation can not be completely excluded. However, as demonstrated for PEG-cHANPs, even Exos could be involved in deopsonization and favor a specific interaction with the target area. So further studied are needed to elucidate these key role mechanisms.

Once administrated, how far Exos can travel in the body, and how long they can maintain stability? Substantial investigations about their uptake and key mechanisms in their biological environment, pharmacokinetics, pharmacodynamics, and toxicity profiles should be conducted to obtain a reliable and stable delivery system and prevent potential side effects.

References

1. García-Álvarez, R. and M. Vallet-Regí. "Hard and soft protein corona of nanomaterials: Analysis and relevance." *Nanomaterials* 11 (2021): 888.
2. Lima, T., K. Bernfur, M. Vilanova and T. Cedervall. "Understanding the lipid and protein corona formation on different sized polymeric nanoparticles." *Scientific reports* 10 (2020): 1-9.
3. Lynch, I. and K. A. Dawson. "Protein–nanoparticle interactions." *Nano-Enabled Medical Applications* (2020): 231-50.
4. Dos Santos, T., J. Varela, I. Lynch, A. Salvati and K. A. Dawson. "Quantitative assessment of the comparative nanoparticle-uptake efficiency of a range of cell lines." *Small* 7 (2011): 3341-49.
5. Ho, Y. T., R. D. Kamm and J. C. Y. Kah. "Influence of protein corona and caveolae-mediated endocytosis on nanoparticle uptake and transcytosis." *Nanoscale* 10 (2018): 12386-97.
6. Lundqvist, M., J. Stigler, T. Cedervall, T. Berggard, M. B. Flanagan, I. Lynch, G. Elia and K. Dawson. "The evolution of the protein corona around nanoparticles: A test study." *ACS nano* 5 (2011): 7503-09.
7. Milani, S., F. Baldelli Bombelli, A. S. Pitek, K. A. Dawson and J. Radler. "Reversible versus irreversible binding of transferrin to polystyrene nanoparticles: Soft and hard corona." *ACS nano* 6 (2012): 2532-41.
8. Lee, Y. K., E.-J. Choi, T. J. Webster, S.-H. Kim and D. Khang. "Effect of the protein corona on nanoparticles for modulating cytotoxicity and immunotoxicity." *International journal of nanomedicine* 10 (2015): 97.
9. Rampado, R., S. Crotti, P. Caliceti, S. Pucciarelli and M. Agostini. "Recent advances in understanding the protein corona of nanoparticles and in the formulation of "stealthy" nanomaterials." *Frontiers in Bioengineering and Biotechnology* 8 (2020): 166.
10. Sperelakis, N. *Cell physiology source book: Essentials of membrane biophysics*. Elsevier, 2012,
11. Nickels, J. D., S. Chatterjee, C. B. Stanley, S. Qian, X. Cheng, D. A. Myles, R. F. Standaert, J. G. Elkins and J. Katsaras. "The in vivo structure of biological membranes and evidence for lipid domains." *PLoS biology* 15 (2017): e2002214.
12. Van Hong Nguyen, B.-J. L. "Protein corona: A new approach for nanomedicine design." *International journal of nanomedicine* 12 (2017): 3137.
13. Monopoli, M. P., C. Åberg, A. Salvati and K. A. Dawson. "Biomolecular coronas provide the biological identity of nanosized materials." *Nature nanotechnology* 7 (2012): 779-86.
14. Bros, M., L. Nuhn, J. Simon, L. Moll, V. Mailänder, K. Landfester and S. Grabbe. "The protein corona as a confounding variable of nanoparticle-mediated targeted vaccine delivery." *Frontiers in immunology* 9 (2018): 1760.
15. Buzás, E. I., E. Á. Tóth, B. W. Sódar and K. É. Szabó-Taylor. "Molecular interactions at the surface of extracellular vesicles." Presented at Seminars in immunopathology, 2018. Springer, 40, 453-64.
16. Ezzat, K., M. Pernemalm, S. Pålsson, T. Roberts, P. Järver, A. Dondalska, B. Bestas, M. Sobkowiak, B. Levänen and M. Sköld. *The viral protein corona directs viral pathogenesis and amyloid aggregation. Nat. Commun. 10 (1), 2331*. 2019,
17. Oh, J. *Cloaking nanoparticles with protein corona shield for targeted drug delivery nat*. Commun, 2018,
18. Pattipeiluhu, R., S. Crielaard, I. Klein-Schiphorst, B. I. Florea, A. Kros and F. Campbell. "Unbiased identification of the liposome protein corona using photoaffinity-based chemoproteomics." *ACS central science* 6 (2020): 535-45.

19. Palivan, C. G., R. Goers, A. Najer, X. Zhang, A. Car and W. Meier. "Bioinspired polymer vesicles and membranes for biological and medical applications." *Chemical society reviews* 45 (2016): 377-411.
20. Stone, T. A. and C. M. Deber. "Therapeutic design of peptide modulators of protein-protein interactions in membranes." *Biochimica Et Biophysica Acta (BBA)-Biomembranes* 1859 (2017): 577-85.
21. Tammaro, O., A. C. di Polidoro, E. Romano, P. A. Netti and E. Torino. "A microfluidic platform to design multimodal peg-crosslinked hyaluronic acid nanoparticles (peg-chanps) for diagnostic applications." *Scientific reports* 10 (2020): 1-11.
22. Russo, M., P. Bevilacqua, P. A. Netti and E. Torino. "A microfluidic platform to design crosslinked hyaluronic acid nanoparticles (chanps) for enhanced mri." *Scientific reports* 6 (2016): 1-10.
23. Partikel, K., R. Korte, D. Mulac, H.-U. Humpf and K. Langer. "Serum type and concentration both affect the protein-corona composition of plga nanoparticles." *Beilstein journal of nanotechnology* 10 (2019): 1002-15.
24. Jain, A., R. Liu, Y. K. Xiang and T. Ha. "Single-molecule pull-down for studying protein interactions." *Nature protocols* 7 (2012): 445-52.
25. Michel, R., S. Pasche, M. Textor and D. G. Castner. "Influence of peg architecture on protein adsorption and conformation." *Langmuir* 21 (2005): 12327-32.
26. Larson, T. A., P. P. Joshi and K. Sokolov. "Preventing protein adsorption and macrophage uptake of gold nanoparticles via a hydrophobic shield." *Acs Nano* 6 (2012): 9182-90.
27. Blundell, E. L., M. J. Healey, E. Holton, M. Sivakumaran, S. Manstana and M. Platt. "Characterisation of the protein corona using tunable resistive pulse sensing: Determining the change and distribution of a particle's surface charge." *Analytical and bioanalytical chemistry* 408 (2016): 5757-68.
28. Veronese, F. M. and G. Pasut. "Pegylation, successful approach to drug delivery." *Drug discovery today* 10 (2005): 1451-58.
29. Jokerst, J. V., T. Lobovkina, R. N. Zare and S. S. Gambhir. "Nanoparticle pegylation for imaging and therapy." *Nanomedicine* 6 (2011): 715-28. 10.2217/nnm.11.19. <Go to ISI>://WOS:000292994300019.
30. Suk, J. S., Q. G. Xu, N. Kim, J. Hanes and L. M. Ensign. "Pegylation as a strategy for improving nanoparticle-based drug and gene delivery." *Advanced Drug Delivery Reviews* 99 (2016): 28-51. 10.1016/j.addr.2015.09.012. <Go to ISI>://WOS:000374370700004.
31. Ke, P. C., S. Lin, W. J. Parak, T. P. Davis and F. Caruso. "A decade of the protein corona." *ACS nano* 11 (2017): 11773-76.
32. Kokkinopoulou, M., J. Simon, K. Landfester, V. Mailänder and I. Lieberwirth. "Visualization of the protein corona: Towards a biomolecular understanding of nanoparticle-cell-interactions." *Nanoscale* 9 (2017): 8858-70.
33. Carrillo-Carrion, C., M. Carril and W. J. Parak. "Techniques for the experimental investigation of the protein corona." *Current opinion in biotechnology* 46 (2017): 106-13.
34. Ahsan, S. M., C. M. Rao and M. F. Ahmad. "Nanoparticle-protein interaction: The significance and role of protein corona." *Cellular and Molecular Toxicology of Nanoparticles* (2018): 175-98.
35. Yu, G., H. Jung and H. Mok. "Indocyanine green-incorporated exosomes for improved in vivo imaging of sentinel lymph node." *Applied Biological Chemistry* 59 (2016): 71-76.
36. Lee, Y., H. Lee, Y. B. Kim, J. Kim, T. Hyeon, H. Park, P. B. Messersmith and T. G. Park. "Bioinspired surface immobilization of hyaluronic acid on monodisperse magnetite nanocrystals for targeted cancer imaging." *Advanced Materials* 20 (2008): 4154-57.
37. Lee, H., K. Lee, I. K. Kim and T. G. Park. "Synthesis, characterization, and in vivo diagnostic applications of hyaluronic acid immobilized gold nanoprobes." *Biomaterials* 29 (2008): 4709-18.

38. Lim, S., D. Kim, S. Ju, S. Shin, I.-j. Cho, S.-H. Park, R. Grailhe, C. Lee and Y. K. Kim. "Glioblastoma-secreted soluble cd44 activates tau pathology in the brain." *Experimental & molecular medicine* 50 (2018): 1-11.
39. Yusupov, M., A. Privat-Maldonado, R. M. Cordeiro, H. Verswyvel, P. Shaw, J. Razzokov, E. Smits and A. Bogaerts. "Oxidative damage to hyaluronan–cd44 interactions as an underlying mechanism of action of oxidative stress-inducing cancer therapy." *Redox biology* 43 (2021): 101968.
40. Wang, H.-H., C.-C. Liao, N.-H. Chow, L. L.-H. Huang, J.-I. Chuang, K.-C. Wei and J.-W. Shin. "Whether cd44 is an applicable marker for glioma stem cells." *American journal of translational research* 9 (2017): 4785.
41. Jiang, X., A. Musyanovych, C. Röcker, K. Landfester, V. Mailänder and G. U. Nienhaus. "Specific effects of surface carboxyl groups on anionic polystyrene particles in their interactions with mesenchymal stem cells." *Nanoscale* 3 (2011): 2028-35.
42. Sun, R., J. Dittrich, M. Le-Huu, M. M. Mueller, J. Bedke, J. Kartenbeck, W. D. Lehmann, R. Krueger, M. Bock and R. Huss. "Physical and biological characterization of superparamagnetic iron oxide-and ultrasmall superparamagnetic iron oxide-labeled cells: A comparison." *Investigative radiology* 40 (2005): 504-13.
43. Arbab, A. S., L. A. Bashaw, B. R. Miller, E. K. Jordan, J. W. Bulte and J. A. Frank. "Intracytoplasmic tagging of cells with ferumoxides and transfection agent for cellular magnetic resonance imaging after cell transplantation: Methods and techniques." *Transplantation* 76 (2003): 1123-30.

Major findings and Future perspectives

The therapeutic efficacy of any pharmacological treatment depends on achieving an optimal drug concentration at the targeted site of action. This is strongly influenced by the absorption, biodistribution, metabolism and excretion of the active compound. Moreover, these processes do not exert a constant and predictable influence on the drug concentration at the site of action but are subjected to pathophysiological mechanisms and dynamic regulation changing among patients.

The use of nanotechnology in medicine and more specifically of nanovectors as drug delivery systems is considered as a promising tool to carry therapeutic agents efficiently into the specific targeted area. However, in the last decades also RNA Therapeutics comprise a rapidly expanding category of drug delivery system. Recent advances in the generation, purification and cellular delivery of RNA allowed the RNA-based therapeutics application in a wide range of diseases. These new strategies would contribute to the already on-going passage from a single therapy for all the patients with the same disease to a new paradigm where each patient receives a personalized treatment. Even though the clinical investigation of EV-based personalized therapy is at an early stage it could offer a significant advantage in the delivery of drugs to specific targets enabling the biocamouflage of theranostic agents. So it seems clear that there is an urgent unmet need to move the EV-based personalized therapy to the clinical practice. Actually, the main issues related to their clinical translation consist in the absence of cost-effective, standardized methods for EV production and loading in a scale-up perspective. Furthermore, up to date, several studies were conducted to understand the key mechanisms related to their natural biogenesis, release in intercellular space, and engineering them for an efficient therapeutic application. However, no one resulted advantageously due to laborious purification, loss of membrane integrity and biological activity and poor Encapsulation Efficiency. Moreover, cost-effective and industrially scalable methodologies, avoiding time-consuming steps, are still missing.

In our study, we proposed for the first time the principle of Dynamic High-Pressure Homogenization applied on both cell and Exos membrane to overcame two of the main criticisms related to EVs application in nanomedicine field.
So in the present work, we were able to control and increase both the production and loading of EVs from different biological sources and with several active compounds. Furthermore, our studies in different biological environments point out some unclarified mechanisms related to their fate after release in the extracellular space.

In detail, this work of thesis is divided in 4 main sections: the first chapter presents an innovative large-scale procedure for Exos production. Here we investigated the Exos biogenesis under Pressure stimuli applied on cell sources. Using a large-scale High Pressure Homogenizer, we demonstrated that Hydrostatic Pressure is able to improve the biological release of nanovesicles. Setting some relevant parameters as Pressure, Temperature, Cycles, Volume and cell concentration we were able to fine-tune the shape, size, protein and RNA amount of EVs. In the second chapter, we applied the Hydrostatic Pressure directly on vesicle membrane curvature to entrap different active compounds. Interestingly, at three different pressure values, we found a critical step that induces break up and permanent deformation phenomena on Exos bilayer, thus affecting their

stability. On the other hand, we further demonstrate that, through an accurate process set-up of Pressure, Temperature and Cycles, it is possible to generate a temporary permeability on phospholipidic bilayer without affecting exosomal shape, size and endogenous cargo. This manipulation of membrane curvature could be applied as a novel encapsulation method to allow the entrapment of both hydrophilic and hydrophobic small molecules in a Pressure-depend manner, with high efficacy and less time-consuming procedure. In the third chapter, we validate our theory, demonstrating its feasibility on Exos generated from different cell sources. As widely known from the literature, lipids and proteins tend to aggregate and reassembly in various ways, mainly depending on their composition. Our novel nanomixing procedure is reliable on phospholipidic bilayer with different percentage of cholesterol, SM, glycosphingolipids, and phosphatidylserine. Finally, in the fourth chapter we further investigate the intercellular communication and internalization phenomena in a relevant biological environment. In detail, we conducted a preliminary in vitro analysis on tumoral cells, focusing our attention on PC phenomenon by comparing EVs with polymeric NPs behavior. In theory, even less is known regarding the PC, Exos should not have any interaction with other protein in circulation than specific receptors for their surface antigens. However, as suggested by our analysis it cannot be excluded that circulating proteins in the body could modify the outer proteolipid architecture of Exos leading to the interaction with a SC.

However, we are still at an early stage of understanding. So, the future perspectives of this research work are:

- Application of HPH nanomixing for the loading of active compound into Exos generated under Pressure stimuli
- In vitro and in vivo testing of their uptake and intercellular communication with the target area
- Optimization of Exos co- loading with more complex structure such as CeO_2NPs and Co-encapsulation of active compounds
- In vivo testing of Engineered Exos biodistribution pharmacokinetics, pharmacodynamics, and toxicity profiles

-

Appendix

List of total proteins that were identified from the extract obtained from U87-MG-Exos.

UP REGULATION

ID	NAME PROTEINS		FC
P47914	60S ribosomal protein L29	RPL29	57.30
P10412	Histone H1.4	HIST1H1E	53.74
Q8TCJ2	Dolichyl-diphosphooligosaccharide--protein glycosyltransferase	STT3B	21.02
P49327	Fatty acid synthase	FASN	15.52
Q03135	Caveolin-1	CAV1	14.49
P38606	V-type proton ATPase catalytic subunit A	ATP6V1A	13.12
P17931	Galectin-3	LGALS3	12.44
O14828	Secretory carrier-associated membrane protein 3	SCAMP3	12.36
Q86Y82	Syntaxin-12	STX12	12.24
P16403	Histone H1.2	HIST1H1C	11.78
O14617	AP-3 complex subunit delta-1	AP3D1	11.62
P62841	40S ribosomal protein S15	RPS15	9.77
P08670	Vimentin	VIM	9.04
P61769	Beta-2-microglobulin	B2M	9.00
P84243	Histone H3.3	H3F3A	8.96
P46776	60S ribosomal protein L27a	RPL27A	8.88
Q86UE4	Protein LYRIC	MTDH	8.86
O43169	Cytochrome b5 type B	CYB5B	8.71
P31943	Heterogeneous nuclear ribonucleoprotein H	HNRNPH1	8.65
O95169	NADH dehydrogenase 1 beta subcomplex subunit 8	NDUFB8	8.49
Q15293	Reticulocalbin-1	RCN1	8.45
O00194	Ras-related protein Rab-27B	RAB27B	8.37
O95831	Apoptosis-inducing factor 1, mitochondrial	AIFM1	8.33
P62750	60S ribosomal protein L23a	RPL23A	8.17
P08621	U1 small nuclear ribonucleoprotein 70 kDa	SNRNP70	7.88
P50502	Hsc70-interacting protein	ST13	7.86
O43399	Tumor protein D54	TPD52L2	7.40
O43852	Calumenin	CALU	7.33
P84098	60S ribosomal protein L19	RPL19	7.23
Q9NQC3	Reticulon-4	RTN4	7.19

P47914	60S ribosomal protein L29	RPL29	57.30
P10412	Histone H1.4	HIST1H1E	53.74
Q8TCJ2	Dolichyl-diphosphooligosaccharide--protein glycosyltransferase	STT3B	21.02
P49327	Fatty acid synthase	FASN	15.52
Q03135	Caveolin-1	CAV1	14.49
P38606	V-type proton ATPase catalytic subunit A	ATP6V1A	13.12
P17931	Galectin-3	LGALS3	12.44
O14828	Secretory carrier-associated membrane protein 3	SCAMP3	12.36
Q86Y82	Syntaxin-12	STX12	12.24
P16403	Histone H1.2	HIST1H1C	11.78
O14617	AP-3 complex subunit delta-1	AP3D1	11.62
P62841	40S ribosomal protein S15	RPS15	9.77
P08670	Vimentin	VIM	9.04
P61769	Beta-2-microglobulin	B2M	9.00
P84243	Histone H3.3	H3F3A	8.96
P46776	60S ribosomal protein L27a	RPL27A	8.88
Q86UE4	Protein LYRIC	MTDH	8.86
O43169	Cytochrome b5 type B	CYB5B	8.71
P31943	Heterogeneous nuclear ribonucleoprotein H	HNRNPH1	8.65
O95169	NADH dehydrogenase 1 beta subcomplex subunit 8	NDUFB8	8.49
Q15293	Reticulocalbin-1	RCN1	8.45
O00194	Ras-related protein Rab-27B	RAB27B	8.37
O95831	Apoptosis-inducing factor 1, mitochondrial	AIFM1	8.33
P62750	60S ribosomal protein L23a	RPL23A	8.17
P08621	U1 small nuclear ribonucleoprotein 70 kDa	SNRNP70	7.88
P50502	Hsc70-interacting protein	ST13	7.86
O43399	Tumor protein D54	TPD52L2	7.40
O43852	Calumenin	CALU	7.33
P84098	60S ribosomal protein L19	RPL19	7.23
Q9NQC3	Reticulon-4	RTN4	7.19

Q15836	Vesicle-associated membrane protein 3	VAMP3	6.62
P60660	Myosin light polypeptide 6	MYL6	6.52
P06576	ATP synthase subunit beta, mitochondrial	ATP5F1B	6.50
O14979	Heterogeneous nuclear ribonucleoprotein D-like	HNRNPDL	6.32
Q99848	Probable rRNA-processing protein EBP2	EBNA1BP2	6.28
Q9BWM7	Sideroflexin-3	SFXN3	6.20
P62081	40S ribosomal protein S7	RPS7	6.18
P20645	Cation-dependent mannose-6-phosphate receptor	M6PR	6.08
Q9NX63	MICOS complex subunit MIC19	CHCHD3	6.06
O75569	Interferon-inducible double-stranded RNA-dependent protein	PRKRA	6.01
Q9H0U4	Ras-related protein Rab-1B	RAB1B	6.00
P38159	RNA-binding motif protein, X chromosome	RBMX	5.99
P62241	40S ribosomal protein S8	RPS8	5.63
P30101	Protein disulfide-isomerase A3	PDIA3	5.62
P49257	Protein ERGIC-53	LMAN1	5.59
O75367	Core histone macro-H2A.1	H2AFY	5.56
P17980	26S proteasome regulatory subunit 6A	PSMC3	5.52
P63173	60S ribosomal protein L38	RPL38	5.47
P19105	Myosin regulatory light chain 12A	MYL12A	5.45
P18621	60S ribosomal protein L17	RPL17	5.38
P62917	60S ribosomal protein L8	RPL8	5.37
Q04637	Eukaryotic translation initiation factor 4 gamma 1	EIF4G1	5.31
P48047	ATP synthase subunit O, mitochondrial	ATP5PO	5.31
O15118	NPC intracellular cholesterol transporter 1	NPC1	5.29
Q9HD33	39S ribosomal protein L47, mitochondrial	MRPL47	5.29
P43243	Matrin-3	MATR3	5.26
P36578	60S ribosomal protein L4	RPL4	5.26
P00387	NADH-cytochrome b5 reductase 3	CYB5R3	5.23
P49207	60S ribosomal protein L34	RPL34	5.14
P32969	60S ribosomal protein L9	RPL9	5.12
P62266	40S ribosomal protein S23	RPS23	5.11
P35998	26S proteasome regulatory subunit 7	PSMC2	5.07
Q8IWE2	Protein NOXP20	FAM114A1	5.06
P16401	Histone H1.5	HIST1H1B	5.04
P22626	Heterogeneous nuclear ribonucleoproteins A2/B1	HNRNPA2B1	4.87

P61019	Ras-related protein Rab-2A	RAB2A	4.85
Q14103	Heterogeneous nuclear ribonucleoprotein D0	HNRNPD	4.82
P25705	ATP synthase subunit alpha, mitochondrial	ATP5F1A	4.81
P62277	40S ribosomal protein S13	RPS13	4.81
P46821	Microtubule-associated protein 1B	MAP1B	4.73
P62910	60S ribosomal protein L32	RPL32	4.68
P07910	Heterogeneous nuclear ribonucleoproteins C1/C2	HNRNPC	4.65
P25786	Proteasome subunit alpha type-1	PSMA1	4.64
P40939	Trifunctional enzyme subunit alpha, mitochondrial	HADHA	4.61
O60506	Heterogeneous nuclear ribonucleoprotein Q	SYNCRIP	4.57
P52272	Heterogeneous nuclear ribonucleoprotein M	HNRNPM	4.56
Q12907	Vesicular integral-membrane protein VIP36	LMAN2	4.55
Q9ULV4	Coronin-1C	CORO1C	4.47
P62854	40S ribosomal protein S26	RPS26	4.44
Q9BUJ2	Heterogeneous nuclear ribonucleoprotein U-like protein 1	HNRNPUL1	4.38
P01903	HLA class II histocompatibility antigen, DR alpha chain	HLA-DRA	4.36
P07237	Protein disulfide-isomerase	P4HB	4.36
P14314	Glucosidase 2 subunit beta	PRKCSH	4.34
P62851	40S ribosomal protein S25	RPS25	4.31
P25398	40S ribosomal protein S12	RPS12	4.31
P45880	Voltage-dependent anion-selective channel protein 2	VDAC2	4.29
P24539	ATP synthase F(0) complex subunit B1, mitochondrial	ATP5PB	4.25
P46976	Glycogenin-1	GYG1	4.24
P54819	Adenylate kinase 2, mitochondrial	AK2	4.23
Q92542	Nicastrin	NCSTN	4.21
Q12906	Interleukin enhancer-binding factor 3	ILF3	4.17
Q93077	Histone H2A type 1-C	HIST1H2AC	4.17
Q6PIU2	Neutral cholesterol ester hydrolase 1	NCEH1	4.16
P14927	Cytochrome b-c1 complex subunit 7	UQCRB	4.16
Q9UJZ1	Stomatin-like protein 2, mitochondrial	STOML2	4.13
P68371	Tubulin beta-4B chain	TUBB4B	4.10
O60664	Perilipin-3	PLIN3	4.09
Q02818	Nucleobindin-1	NUCB1	4.07
P84103	Serine/arginine-rich splicing factor 3	SRSF3	4.06
Q9Y6N5	Sulfide:quinone oxidoreductase, mitochondrial	SQOR	4.05

P50454	Serpin H1	SERPINH1	3.98
Q16891	MICOS complex subunit MIC60	IMMT	3.91
Q8N6T3	ADP-ribosylation factor GTPase-activating protein 1	ARFGAP1	3.87
P27635	60S ribosomal protein L10	RPL10	3.87
P10606	Cytochrome c oxidase subunit 5B, mitochondrial	COX5B	3.87
P78559	Microtubule-associated protein 1A	MAP1A	3.86
P55084	Trifunctional enzyme subunit beta, mitochondrial	HADHB	3.83
P10620	Microsomal glutathione S-transferase 1	MGST1	3.82
O75396	Vesicle-trafficking protein SEC22b	SEC22B	3.80
Q5XKP0	MICOS complex subunit MIC13	MICOS13	3.79
P39019	40S ribosomal protein S19	RPS19	3.79
P68366	Tubulin alpha-4A chain	TUBA4A	3.77
Q9UI09	NADH dehydrogenase [ubiquinone] 1 alpha subcomplex 12	NDUFA12	3.75
Q71UI9	Histone H2A.V	H2AFV	3.74
Q9Y6M9	NADH dehydrogenase [ubiquinone] 1 beta subcomplex 9	NDUFB9	3.70
Q13509	Tubulin beta-3 chain	TUBB3	3.69
P19338	Nucleolin	NCL	3.67
P80303	Nucleobindin-2	NUCB2	3.67
Q13418	Integrin-linked protein kinase	ILK	3.63
P51665	26S proteasome non-ATPase regulatory subunit 7	PSMD7	3.62
Q99729	Heterogeneous nuclear ribonucleoprotein A/B	HNRNPAB	3.61
O75369	Filamin-B	FLNB	3.60
P83731	60S ribosomal protein L24	RPL24	3.60
Q16778	Histone H2B type 2-E	HIST2H2BE	3.60
P07919	Cytochrome b-c1 complex subunit 6, mitochondrial	UQCRH	3.59
Q9BRK5	45 kDa calcium-binding protein	SDF4	3.58
P43304	Glycerol-3-phosphate dehydrogenase, mitochondrial	GPD2	3.57
P08708	40S ribosomal protein S17	RPS17	3.56
P21796	Voltage-dependent anion-selective channel protein 1	VDAC1	3.54
Q12797	Aspartyl/asparaginyl beta-hydroxylase	ASPH	3.54
P27824	Calnexin	CANX	3.53
Q8TAE8	Growth arrest and DNA damage-inducible proteins	GADD45GIP1	3.51
P26373	60S ribosomal protein L13	RPL13	3.46
P61978	Heterogeneous nuclear ribonucleoprotein K	HNRNPK	3.46
Q9P015	39S ribosomal protein L15, mitochondrial	MRPL15	3.42

P04843	Dolichyl-diphosphooligosaccharide--protein	RPN1	3.42
Q9H9B4	Sideroflexin-1	SFXN1	3.41
P13073	Cytochrome c oxidase subunit 4 isoform 1, mitochondrial	COX4I1	3.41
P02792	Ferritin light chain	FTL	3.41
P02786	Transferrin receptor protein 1	TFRC	3.39
Q00839	Heterogeneous nuclear ribonucleoprotein U	HNRNPU	3.37
O95793	Double-stranded RNA-binding protein Staufen homolog 1	STAU1	3.33
Q9NS69	Mitochondrial import receptor subunit TOM22 homolog	TOMM22	3.32
Q07065	Cytoskeleton-associated protein 4	CKAP4	3.31
Q9BQE3	Tubulin alpha-1C chain	TUBA1C	3.30
P62333	26S proteasome regulatory subunit 10B	PSMC6	3.28
Q16718	NADH dehydrogenase [ubiquinone] 1 alpha subcomplex 5	NDUFA5	3.28
Q8N5N7	39S ribosomal protein L50, mitochondrial	MRPL50	3.27
P61353	60S ribosomal protein L27	RPL27	3.25
P22695	Cytochrome b-c1 complex subunit 2, mitochondrial	UQCRC2	3.25
O00264	Membrane-associated progesterone receptor component 1	PGRMC1	3.25
O76021	Ribosomal L1 domain-containing protein 1	RSL1D1	3.24
P61247	40S ribosomal protein S3a	RPS3A	3.24
Q9BUF5	Tubulin beta-6 chain	TUBB6	3.24
Q09666	Neuroblast differentiation-associated protein AHNAK	AHNAK	3.23
P55072	Transitional endoplasmic reticulum ATPase	VCP	3.20
P39656	Dolichyl-diphosphooligosaccharide--protein glycosyltransferase	DDOST	3.19
Q9NVP1	ATP-dependent RNA helicase DDX18	DDX18	3.18
P35232	Prohibitin	PHB	3.17
Q14204	Cytoplasmic dynein 1 heavy chain 1	DYNC1H1	3.15
Q9NX40	OCIA domain-containing protein 1	OCIAD1	3.14
P46940	Ras GTPase-activating-like protein IQGAP1	IQGAP1	3.14
P62244	40S ribosomal protein S15a	RPS15A	3.13
Q96PD2	Discoidin, CUB and LCCL domain-containing protein 2	DCBLD2	3.13
P02794	Ferritin heavy chain	FTH1	3.12
P51991	Heterogeneous nuclear ribonucleoprotein A3	HNRNPA3	3.11
P51149	Ras-related protein Rab-7a	RAB7A	3.10
P26640	Valine--tRNA ligase	VARS	3.08
P42892	Endothelin-converting enzyme 1	ECE1	3.07
P14866	Heterogeneous nuclear ribonucleoprotein L	HNRNPL	3.07

O76094	Signal recognition particle subunit SRP72	SRP72	3.06
P55327	Tumor protein D52	TPD52	3.05
O75380	NADH dehydrogenase [ubiquinone] iron-sulfur protein 6	NDUFS6	3.05
P31930	Cytochrome b-c1 complex subunit 1, mitochondrial	UQCRC1	3.05
P21333	Filamin-A	FLNA	3.03
Q10471	Polypeptide N-acetylgalactosaminyltransferase 2	GALNT2	3.02
Q96A33	Coiled-coil domain-containing protein 47	CCDC47	3.01
O75947	ATP synthase subunit d, mitochondrial	ATP5PD	3.01
P62805	Histone H4	HIST1H4A	3.00
Q9P0J0	NADH dehydrogenase [ubiquinone] 1 alpha subcomplex 13	NDUFA13	3.00
P0DP25	Calmodulin-3	CALM3	3.00
P38646	Stress-70 protein, mitochondrial	HSPA9	2.99
Q15366	Poly(rC)-binding protein 2	PCBP2	2.98
O00571	ATP-dependent RNA helicase DDX3X	DDX3X	2.98
Q15149	Plectin	PLEC	2.98
O00217	NADH dehydrogenase [ubiquinone] iron-sulfur protein 8	NDUFS8	2.96
P27797	Calreticulin	CALR	2.94
Q86V81	THO complex subunit 4	ALYREF	2.94
P46777	60S ribosomal protein L5	RPL5	2.92
P09651	Heterogeneous nuclear ribonucleoprotein A1	HNRNPA1	2.92
Q9P0L0	Vesicle-associated membrane protein-associated protein A	VAPA	2.91
O15400	Syntaxin-7	STX7	2.91
O75489	NADH dehydrogenase [ubiquinone] iron-sulfur protein 3	NDUFS3	2.91
Q14152	Eukaryotic translation initiation factor 3 subunit A	EIF3A	2.91
Q08211	ATP-dependent RNA helicase A	DHX9	2.91
Q6FI13	Histone H2A type 2-A	HIST2H2AA3	2.90
O43678	NADH dehydrogenase [ubiquinone] 1 alpha subcomplex 2	NDUFA2	2.90
Q00610	Clathrin heavy chain 1	CLTC	2.89
Q07955	Serine/arginine-rich splicing factor 1	SRSF1	2.88
Q14974	Importin subunit beta-1	KPNB1	2.87
P39023	60S ribosomal protein L3	RPL3	2.87
Q56VL3	OCIA domain-containing protein 2	OCIAD2	2.86
P50914	60S ribosomal protein L14	RPL14	2.85
P51970	NADH dehydrogenase [ubiquinone] 1 alpha subcomplex 8	NDUFA8	2.85
Q8IY17	Neuropathy target esterase	PNPLA6	2.84

O43707	Alpha-actinin-4	ACTN4	2.84
O75494	Serine/arginine-rich splicing factor 10	SRSF10	2.83
P20674	Cytochrome c oxidase subunit 5A, mitochondrial	COX5A	2.82
Q13200	26S proteasome non-ATPase regulatory subunit 2	PSMD2	2.81
P46778	60S ribosomal protein L21	RPL21	2.80
O43390	Heterogeneous nuclear ribonucleoprotein R	HNRNPR	2.79
Q99442	Translocation protein SEC62	SEC62	2.78
P16615	Sarcoplasmic/endoplasmic reticulum calcium ATPase 2	ATP2A2	2.78
P62191	26S proteasome regulatory subunit 4	PSMC1	2.77
P61604	10 kDa heat shock protein, mitochondrial	HSPE1	2.77
P62195	26S proteasome regulatory subunit 8	PSMC5	2.76
P37235	Hippocalcin-like protein 1	HPCAL1	2.75
P62424	60S ribosomal protein L7a	RPL7A	2.75
P46782	40S ribosomal protein S5	RPS5	2.74
Q13084	39S ribosomal protein L28, mitochondrial	MRPL28	2.73
P09874	Poly [ADP-ribose] polymerase 1	PARP1	2.71
Q16629	Serine/arginine-rich splicing factor 7	SRSF7	2.70
P46087	Probable 28S rRNA (cytosine(4447)-C(5))-methyltransferase	NOP2	2.70
Q9Y3E5	Peptidyl-tRNA hydrolase 2, mitochondrial	PTRH2	2.69
P13010	X-ray repair cross-complementing protein 5	XRCC5	2.69
Q99460	26S proteasome non-ATPase regulatory subunit 1	PSMD1	2.66
O95139	NADH dehydrogenase [ubiquinone] 1 beta subcomplex	NDUFB6	2.66
Q9Y3U8	60S ribosomal protein L36	RPL36	2.66
P40429	60S ribosomal protein L13a	RPL13A	2.65
P78527	DNA-dependent protein kinase catalytic subunit	PRKDC	2.64
P62280	40S ribosomal protein S11	RPS11	2.64
Q15365	Poly(rC)-binding protein 1	PCBP1	2.63
P36957	Dihydrolipoyllysine-residue succinyltransferase	DLST	2.63
P15880	40S ribosomal protein S2	RPS2	2.61
Q99613	Eukaryotic translation initiation factor 3 subunit C	EIF3C	2.61
P21964	Catechol O-methyltransferase	COMT	2.60
P17844	Probable ATP-dependent RNA helicase DDX5	DDX5	2.60
Q9UKM9	RNA-binding protein Raly	RALY	2.57
Q9HDC9	Adipocyte plasma membrane-associated protein	APMAP	2.57
Q92841	Probable ATP-dependent RNA helicase DDX17	DDX17	2.57

P07437	Tubulin beta chain	TUBB	2.57
P18077	60S ribosomal protein L35a	RPL35A	2.56
P10809	60 kDa heat shock protein, mitochondrial	HSPD1	2.54
P26641	Elongation factor 1-gamma	EEF1G	2.54
Q07020	60S ribosomal protein L18	RPL18	2.54
P53621	Coatomer subunit alpha	COPA	2.53
P05141	ADP/ATP translocase 2	SLC25A5	2.53
P02545	Prelamin-A/C	LMNA	2.53
P53007	Tricarboxylate transport protein, mitochondrial	SLC25A1	2.52
O43181	NADH dehydrogenase [ubiquinone] iron-sulfur protein 4	NDUFS4	2.52
P51572	B-cell receptor-associated protein 31	BCAP31	2.51
P31040	Succinate dehydrogenase [ubiquinone] flavoprotein subunit	SDHA	2.50
Q8IVF2	Protein AHNAK2	AHNAK2	2.50
Q9Y3I0	tRNA-splicing ligase RtcB homolog	RTCB	2.47
P60468	Protein transport protein Sec61 subunit beta	SEC61B	2.45
P18124	60S ribosomal protein L7	RPL7	2.45
P08133	Annexin A6	ANXA6	2.44
P62913	60S ribosomal protein L11	RPL11	2.43
Q96TA1	Niban-like protein 1	FAM129B	2.43
P26599	Polypyrimidine tract-binding protein 1	PTBP1	2.43
O75964	ATP synthase subunit g, mitochondrial	ATP5MG	2.42
O00303	Eukaryotic translation initiation factor 3 subunit F	EIF3F	2.42
P09382	Galectin-1	LGALS1	2.41
P62269	40S ribosomal protein S18	RPS18	2.40
Q9NVI7	ATPase family AAA domain-containing protein 3A	ATAD3A	2.39
P11717	Cation-independent mannose-6-phosphate receptor	IGF2R	2.39
Q9Y4P3	Transducin beta-like protein 2	TBL2	2.38
Q9Y4W6	AFG3-like protein 2	AFG3L2	2.38
P62701	40S ribosomal protein S4, X isoform	RPS4X	2.37
P62263	40S ribosomal protein S14	RPS14	2.37
P98179	RNA-binding protein 3	RBM3	2.36
P35579	Myosin-9	MYH9	2.36
Q99653	Calcineurin B homologous protein 1	CHP1	2.34
P62249	40S ribosomal protein S16	RPS16	2.33
Q02543	60S ribosomal protein L18a	RPL18A	2.33

P09525	Annexin A4	ANXA4	2.32
Q15084	Protein disulfide-isomerase A6	PDIA6	2.30
P49368	T-complex protein 1 subunit gamma	CCT3	2.28
P62899	60S ribosomal protein L31	RPL31	2.27
P62857	40S ribosomal protein S28	RPS28	2.27
Q96CW1	AP-2 complex subunit mu	AP2M1	2.27
Q9Y639	Neuroplastin	NPTN	2.27
P61313	60S ribosomal protein L15	RPL15	2.25
P30050	60S ribosomal protein L12	RPL12	2.23
P23284	Peptidyl-prolyl cis-trans isomerase B	PPIB	2.23
P48643	T-complex protein 1 subunit epsilon	CCT5	2.23
P17252	Protein kinase C alpha type	PRKCA	2.22
O75533	Splicing factor 3B subunit 1	SF3B1	2.22
P08574	Cytochrome c1, heme protein, mitochondrial	CYC1	2.22
P62847	40S ribosomal protein S24	RPS24	2.22
P14854	Cytochrome c oxidase subunit 6B1	COX6B1	2.21
P01911	HLA class II histocompatibility antigen, DRB1-15 beta chain	HLA-DRB1	2.21
O94826	Mitochondrial import receptor subunit TOM70	TOMM70	2.21
Q02878	60S ribosomal protein L6	RPL6	2.18
O94905	Erlin-2	ERLIN2	2.18
P60953	Cell division control protein 42 homolog	CDC42	2.15
P60866	40S ribosomal protein S20	RPS20	2.15
Q6NZI2	Caveolae-associated protein 1	CAVIN1	2.14
P46781	40S ribosomal protein S9	RPS9	2.14
Q9Y490	Talin-1	TLN1	2.13
P49585	Choline-phosphate cytidylyltransferase A	PCYT1A	2.13
P61106	Ras-related protein Rab-14	RAB14	2.11
P62753	40S ribosomal protein S6	RPS6	2.11
P00403	Cytochrome c oxidase subunit 2	MT-CO2	2.10
Q9NZM1	Myoferlin	MYOF	2.10
P35268	60S ribosomal protein L22	RPL22	2.09
O95292	Vesicle-associated membrane protein-associated protein B/C	VAPB	2.09
P12956	X-ray repair cross-complementing protein 6	XRCC6	2.09
P51571	Translocon-associated protein subunit delta	SSR4	2.08
P62820	Ras-related protein Rab-1A	RAB1A	2.06

P67809	Nuclease-sensitive element-binding protein 1	YBX1	2.05
Q99623	Prohibitin-2	PHB2	2.05
P62906	60S ribosomal protein L10a	RPL10A	2.04
P42704	Leucine-rich PPR motif-containing protein, mitochondrial	LRPPRC	2.04
Q99536	Synaptic vesicle membrane protein VAT-1 homolog	VAT1	2.03
Q13405	39S ribosomal protein L49, mitochondrial	MRPL49	2.01
Q13501	Sequestosome-1	SQSTM1	2.01
P60903	Protein S100-A10	S100A10	2.00
P49755	Transmembrane emp24 domain-containing protein 10	TMED10	1.98
O43242	26S proteasome non-ATPase regulatory subunit 3	PSMD3	1.98
Q9UJS0	Calcium-binding mitochondrial carrier protein Aralar2	SLC25A13	1.98
Q9NR30	Nucleolar RNA helicase 2	DDX21	1.97
P78371	T-complex protein 1 subunit beta	CCT2	1.97
Q9BS26	Endoplasmic reticulum resident protein 44	ERP44	1.93
Q7KZF4	Staphylococcal nuclease domain-containing protein 1	SND1	1.92
P11940	Polyadenylate-binding protein 1	PABPC1	1.92
Q71DI3	Histone H3.2	HIST2H3A	1.92
Q9Y224	RNA transcription, translation and transport factor protein	RTRAF	1.91
P68431	Histone H3.1	HIST1H3A	1.91
P11279	Lysosome-associated membrane glycoprotein 1	LAMP1	1.89
Q9NX14	NADH dehydrogenase [ubiquinone] 1 beta subcomplex subunit	NDUFB11	1.88
P07355	Annexin A2	ANXA2	1.88
P11021	Endoplasmic reticulum chaperone BiP	HSPA5	1.87
P14625	Endoplasmin	HSP90B1	1.87
O00541	Pescadillo homolog	PES1	1.85
Q9UKD2	mRNA turnover protein 4 homolog	MRTO4	1.84
Q14315	Filamin-C	FLNC	1.81
O94766	Galactosylgalactosylxylosylprotein	B3GAT3	1.80
P30481	HLA class I histocompatibility antigen, B-44 alpha chain	HLA-B	1.80
Q13641	Trophoblast glycoprotein	TPBG	1.79
P55209	Nucleosome assembly protein 1-like 1	NAP1L1	1.78
O75477	Erlin-1	ERLIN1	1.77
P17568	NADH dehydrogenase 1 beta subcomplex subunit 7	NDUFB7	1.77
P28331	NADH-ubiquinone oxidoreductase 75 kDa subunit,	NDUFS1	1.76
P05387	60S acidic ribosomal protein P2	RPLP2	1.76

P43686	26S proteasome regulatory subunit 6B	PSMC4	1.76
P11387	DNA topoisomerase 1	TOP1	1.76
O60313	Dynamin-like 120 kDa protein, mitochondrial	OPA1	1.74
P22087	rRNA 2-O-methyltransferase fibrillarin	FBL	1.71
O00461	Golgi integral membrane protein 4	GOLIM4	1.71
P50281	Matrix metalloproteinase-14	MMP14	1.70
P04844	Dolichyl-diphosphooligosaccharide--protein glycosyltransferase	RPN2	1.70
P50416	Carnitine O-palmitoyltransferase 1, liver isoform	CPT1A	1.70
Q5T9A4	ATPase family AAA domain-containing protein 3B	ATAD3B	1.69
P50995	Annexin A11	ANXA11	1.69
Q96AG4	Leucine-rich repeat-containing protein 59	LRRC59	1.69
P23396	40S ribosomal protein S3	RPS3	1.66
P62829	60S ribosomal protein L23	RPL23	1.66
Q9BZQ8	Protein Niban	FAM129A	1.63
Q06830	Peroxiredoxin-1	PRDX1	1.63
P53396	ATP-citrate synthase	ACLY	1.62
P20042	Eukaryotic translation initiation factor 2 subunit 2	EIF2S2	1.62
A5D8V6	Vacuolar protein sorting-associated protein 37C	VPS37C	1.62
Q9NX58	Cell growth-regulating nucleolar protein	LYAR	1.61
P23246	Splicing factor, proline- and glutamine-rich	SFPQ	1.61
P11233	Ras-related protein Ral-A	RALA	1.60
Q9H2W6	39S ribosomal protein L46, mitochondrial	MRPL46	1.59
Q15233	Non-POU domain-containing octamer-binding protein	NONO	1.58
P25787	Proteasome subunit alpha type-2	PSMA2	1.57
P17987	T-complex protein 1 subunit alpha	TCP1	1.57
P13639	Elongation factor 2	EEF2	1.56
Q92544	Transmembrane 9 superfamily member 4	TM9SF4	1.55
P26038	Moesin	MSN	1.53
O96000	NADH dehydrogenase [ubiquinone] 1 beta subcomplex 10	NDUFB10	1.53
P05388	60S acidic ribosomal protein P0	RPLP0	1.52
P62888	60S ribosomal protein L30	RPL30	1.52
P49458	Signal recognition particle 9 kDa protein	SRP9	1.49
P50991	T-complex protein 1 subunit delta	CCT4	1.49
P35637	RNA-binding protein FUS	FUS	1.47
Q8IXM3	39S ribosomal protein L41, mitochondrial	MRPL41	1.46

O95347	Structural maintenance of chromosomes protein 2	SMC2	1.45
Q13740	CD166 antigen	ALCAM	1.45
Q9NW13	RNA-binding protein 28	RBM28	1.44
Q99961	Endophilin-A2	SH3GL1	1.42
P29401	Transketolase	TKT	1.42
P35610	Sterol O-acyltransferase 1	SOAT1	1.42
P04792	Heat shock protein beta-1	HSPB1	1.41
P40227	T-complex protein 1 subunit zeta	CCT6A	1.41
P08195	4F2 cell-surface antigen heavy chain	SLC3A2	1.40
P06748	Nucleophosmin	NPM1	1.38
Q9BQG0	Myb-binding protein 1A	MYBBP1A	1.36
Q92520	Protein FAM3C	FAM3C	1.36
P08238	Heat shock protein HSP 90-beta	HSP90AB1	1.35
Q9NZN4	EH domain-containing protein 2	EHD2	1.35
Q9NVS2	39S ribosomal protein S18a, mitochondrial	MRPS18A	1.32
P07900	Heat shock protein HSP 90-alpha	HSP90AA1	1.32
Q00688	Peptidyl-prolyl cis-trans isomerase FKBP3	FKBP3	1.30
Q07666	KH domain-containing, RNA-binding, signal transduction	KHDRBS1	1.29
O43776	Asparagine--tRNA ligase, cytoplasmic	NARS	1.29
Q13724	Mannosyl-oligosaccharide glucosidase	MOGS	1.28
P36542	ATP synthase subunit gamma, mitochondrial	ATP5F1C	1.28
P15153	Ras-related C3 botulinum toxin substrate 2	RAC2	1.28
P54709	Sodium/potassium-transporting ATPase subunit beta-3	ATP1B3	1.26
P63241	Eukaryotic translation initiation factor 5A-1	EIF5A	1.24
Q92499	ATP-dependent RNA helicase DDX1	DDX1	1.24
P50990	T-complex protein 1 subunit theta	CCT8	1.23
Q99832	T-complex protein 1 subunit eta	CCT7	1.21
Q6DD88	Atlastin-3	ATL3	1.20
P13987	CD59 glycoprotein	CD59	1.20
O75844	CAAX prenyl protease 1 homolog	ZMPSTE24	1.19
Q1KMD3	Heterogeneous nuclear ribonucleoprotein U-like protein 2	HNRNPUL2	1.18
P42025	Beta-centractin	ACTR1B	1.17
P51148	Ras-related protein Rab-5C	RAB5C	1.17
P48307	Tissue factor pathway inhibitor 2	TFPI2	1.16

P08865	40S ribosomal protein SA	RPSA	1.15
Q9Y3C1	Nucleolar protein 16	NOP16	1.14
P05198	Eukaryotic translation initiation factor 2 subunit 1	EIF2S1	1.10
P01892	HLA class I histocompatibility antigen, A-2 alpha chain	HLA-A	1.09
P05023	Sodium/potassium-transporting ATPase subunit alpha-1	ATP1A1	1.09
Q9UBI6	Guanine nucleotide-binding protein G(I)/G(S)/G(O)	GNG12	1.08
P61586	Transforming protein RhoA	RHOA	1.08
O00487	26S proteasome non-ATPase regulatory subunit 14	PSMD14	1.08
P41091	Eukaryotic translation initiation factor 2 subunit 3	EIF2S3	1.07
P07814	Bifunctional glutamate/proline--tRNA ligase	EPRS	1.06
P11142	Heat shock cognate 71 kDa protein	HSPA8	1.05
P11586	C-1-tetrahydrofolate synthase, cytoplasmic	MTHFD1	1.05
Q15907	Ras-related protein Rab-11B	RAB11B	1.05
P68104	Elongation factor 1-alpha 1	EEF1A1	1.04
P35613	Basigin	BSG	1.02
P61224	Ras-related protein Rap-1b	RAP1B	1.02
Q96FQ6	Protein S100-A16	S100A16	0.99
P05106	Integrin beta-3	ITGB3	0.98
Q9NTJ3	Structural maintenance of chromosomes protein 4	SMC4	0.98
P60842	Eukaryotic initiation factor 4A-I	EIF4A1	0.97
Q8NBJ4	Golgi membrane protein 1	GOLM1	0.96
P31689	DnaJ homolog subfamily A member 1	DNAJA1	0.94
O94808	Glutamine--fructose-6-phosphate aminotransferase	GFPT2	0.94
Q92896	Golgi apparatus protein 1	GLG1	0.94
Q9Y285	Phenylalanine--tRNA ligase alpha subunit	FARSA	0.92
P62937	Peptidyl-prolyl cis-trans isomerase A	PPIA	0.91
O60884	DnaJ homolog subfamily A member 2	DNAJA2	0.91
Q07021	Complement component 1 Q subcomponent-binding protein	C1QBP	0.90
O60488	Long-chain-fatty-acid--CoA ligase 4	ACSL4	0.90
Q9Y2X3	Nucleolar protein 58	NOP58	0.89
Q6P2Q9	Pre-mRNA-processing-splicing factor 8	PRPF8	0.89
P62979	Ubiquitin-40S ribosomal protein S27a	RPS27A	0.89
Q9UQE7	Structural maintenance of chromosomes protein 3	SMC3	0.88
O14548	Cytochrome c oxidase subunit 7A-related protein	COX7A2L	0.87
Q9H4M9	EH domain-containing protein 1	EHD1	0.87

P14618	Pyruvate kinase PKM	PKM	0.87
O00567	Nucleolar protein 56	NOP56	0.86
P10599	Thioredoxin	TXN	0.86
O95182	NADH dehydrogenase [ubiquinone] 1 alpha subcomplex 7	NDUFA7	0.86
P19367	Hexokinase-1	HK1	0.85
P25445	Tumor necrosis factor receptor superfamily member 6	FAS	0.84
P61513	60S ribosomal protein L37a	RPL37A	0.84
P06756	Integrin alpha-V	ITGAV	0.83
Q58FF8	Putative heat shock protein HSP 90-beta 2	HSP90AB2P	0.79

DOWN REGULATION

ID	NAME PROTEINS		FC
O00159	Unconventional myosin-Ic	MYO1C	0.77
Q9Y512	Sorting and assembly machinery component 50 homolog	SAMM50	0.77
Q13283	Ras GTPase-activating protein-binding protein 1	G3BP1	0.77
Q15043	Zinc transporter ZIP14	SLC39A14	0.76
P04406	Glyceraldehyde-3-phosphate dehydrogenase	GAPDH	0.75
P08758	Annexin A5	ANXA5	0.74
P23528	Cofilin-1	CFL1	0.73
P24534	Elongation factor 1-beta	EEF1B2	0.73
P16070	CD44 antigen	CD44	0.71
P10301	Ras-related protein R-Ras	RRAS	0.70
P37108	Signal recognition particle 14 kDa protein	SRP14	0.70
Q9BVP2	Guanine nucleotide-binding protein-like 3	GNL3	0.69
Q15758	Neutral amino acid transporter B(0)	SLC1A5	0.69
P04083	Annexin A1	ANXA1	0.66
P00367	Glutamate dehydrogenase 1, mitochondrial	GLUD1	0.65
P61006	Ras-related protein Rab-8A	RAB8A	0.65
Q9UQ80	Proliferation-associated protein 2G4	PA2G4	0.65
P05556	Integrin beta-1	ITGB1	0.65
Q92616	eIF-2-alpha kinase activator GCN1	GCN1	0.64
P06703	Protein S100-A6	S100A6	0.63

Q10567	AP-1 complex subunit beta-1	AP1B1	0.62
O00560	Syntenin-1	SDCBP	0.60
P04899	Guanine nucleotide-binding protein G(i) subunit alpha-2	GNAI2	0.60
Q8TDD1	ATP-dependent RNA helicase DDX54	DDX54	0.59
Q01518	Adenylyl cyclase-associated protein 1	CAP1	0.56
Q9Y6M5	Zinc transporter 1	SLC30A1	0.56
P62873	Guanine nucleotide-binding protein G(I)/G(S)/G(T) subunit beta-1	GNB1	0.55
Q00341	Vigilin	HDLBP	0.55
Q9H444	Charged multivesicular body protein 4b	CHMP4B	0.53
P12236	ADP/ATP translocase 3	SLC25A6	0.53
Q01130	Serine/arginine-rich splicing factor 2	SRSF2	0.53
P11388	DNA topoisomerase 2-alpha	TOP2A	0.48
P09543	2,3-cyclic-nucleotide 3-phosphodiesterase	CNP	0.46
P27105	Erythrocyte band 7 integral membrane protein	STOM	0.46
Q9NVH1	DnaJ homolog subfamily C member 11	DNAJC11	0.45
O00161	Synaptosomal-associated protein 23	SNAP23	0.44
Q9NUM4	Transmembrane protein 106B	TMEM106B	0.43
P43307	Translocon-associated protein subunit alpha	SSR1	0.43
P63261	Actin, cytoplasmic 2	ACTG1	0.42
O00116	Alkyldihydroxyacetonephosphate synthase, peroxisomal	AGPS	0.41
Q13443	Disintegrin and metalloproteinase domain-containing protein 9	ADAM9	0.39
Q00325	Phosphate carrier protein, mitochondrial	SLC25A3	0.39
P29966	Myristoylated alanine-rich C-kinase substrate	MARCKS	0.38
P08648	Integrin alpha-5	ITGA5	0.37
P63000	Ras-related C3 botulinum toxin substrate 1	RAC1	0.35
P68032	Actin, alpha cardiac muscle 1	ACTC1	0.33
Q3ZCQ8	Mitochondrial import inner membrane translocase subunit	TIMM50	0.33
Q16698	2,4-dienoyl-CoA reductase, mitochondrial	DECR1	0.31
P31949	Protein S100-A11	S100A11	0.30
P18669	Phosphoglycerate mutase 1	PGAM1	0.30
Q14764	Major vault protein	MVP	0.29
P62879	Guanine nucleotide-binding protein G(I)/G(S)/G(T) subunit beta-2	GNB2	0.28
P51153	Ras-related protein Rab-13	RAB13	0.28
Q9NZZ3	Charged multivesicular body protein 5	CHMP5	0.27
P60174	Triosephosphate isomerase	TPI1	0.27

P37802	Transgelin-2	TAGLN2	0.27
P31946	14-3-3 protein beta/alpha	YWHAB	0.26
P35221	Catenin alpha-1	CTNNA1	0.26
P04075	Fructose-bisphosphate aldolase A	ALDOA	0.24
P04080	Cystatin-B	CSTB	0.24
P06733	Alpha-enolase	ENO1	0.23
P49748	Very long-chain specific acyl-CoA dehydrogenase, mitochondrial	ACADVL	0.22
P14209	CD99 antigen	CD99	0.22
P21589	5-nucleotidase	NT5E	0.22
P26006	Integrin alpha-3	ITGA3	0.22
P07737	Profilin-1	PFN1	0.21
Q99816	Tumor susceptibility gene 101 protein	TSG101	0.20
P48509	CD151 antigen	CD151	0.19
P00558	Phosphoglycerate kinase 1	PGK1	0.19
P18859	ATP synthase-coupling factor 6, mitochondrial	ATP5PF	0.19
P22392	Nucleoside diphosphate kinase B	NME2	0.16
P63104	14-3-3 protein zeta/delta	YWHAZ	0.13
Q8WUM4	Programmed cell death 6-interacting protein	PDCD6IP	0.13
P05026	Sodium/potassium-transporting ATPase subunit beta-1	ATP1B1	0.13
P80723	Brain acid soluble protein 1	BASP1	0.12
P61981	14-3-3 protein gamma	YWHAG	0.11
P62258	14-3-3 protein epsilon	YWHAE	0.11
P0DMV9	Heat shock 70 kDa protein 1B	HSPA1B	0.11
O14786	Neuropilin-1	NRP1	0.11
P43121	Cell surface glycoprotein MUC18	MCAM	0.09
P23634	Plasma membrane calcium-transporting ATPase 4	ATP2B4	0.09
Q9P2B2	Prostaglandin F2 receptor negative regulator	PTGFRN	0.06
O00299	Chloride intracellular channel protein 1	CLIC1	0.06
Q969P0	Immunoglobulin superfamily member 8	IGSF8	0.06
Q92743	Serine protease HTRA1	HTRA1	0.05
P09936	Ubiquitin carboxyl-terminal hydrolase isozyme L1	UCHL1	0.05
P24821	Tenascin	TNC	0.04
O43854	EGF-like repeat and discoidin I-like domain-containing protein 3	EDIL3	0.03
P02751	Fibronectin	FN1	0.02
P12111	Collagen alpha-3(VI) chain	COL6A3	0.02

List of abbreviation

NAME	ABBREVIATION
Arachidonic acid	AA
Atherosclerosis	AS
Atherosclerotic Placques	APs
Blood-Brain Barrier	BBB
cerebrospinal fluid	CSF
Cerium oxide nanoparticles	CeO_2NPs
Chondrosarcomas	CHS
Coronary atherosclerotic heart disease	CAD
Culture media	CM
Density gradient UC	DG
Differential Ultracentrifugation	dUC
Dioleoyl-phosphatidylcholine	DOPC
Docosahexaenoic acid	DHA
Doxorubicin	DXR
Encapsulation Efficiency	EE
Endosomal Sorting Complex	ESCRT
Exosomes	Exos
Exos-Mimetic Nanovesicles	EMNVs
Extracellular vesicles	EVs
Forward Scattering	FSC
Gd-diethylenetriamine penta-acetic acid	Gd-DTPA
Grade IV glioblastoma	GBM
Hard Corona	HA
High Pressure Homogenizer	HPH
Hyaluronic acid	HA
Hours	hrs
Human Serum Albumin	HSA
Human umbilical cord MSCs	hucMSC
Inductively Coupled Plasma	ICP-MS
Intraluminal vesicles	ILVs
Irinotecan	IRI
Lysophosphatidylcholine	LPC
Magnetic nanoparticles	MNP
Magnetic Resonance Imaging	MRI
Mesenchymal stem cells	MSC
Mesenchymal stem cells nanoghosts	MSC-NGs
Methotrexate	MTX
Multivesicular bodies	MVB

Nanoparticles	NPs
NPs Tracking Analysis	NTA
Paclitaxel	PTX
Paraformaldehyde	PFA
Plasma membrane	PM
Polydispersity index	PDI
Polyethylene glycol	PEG
Polystyrene	PS
Pressured-Cell EVs	PEVs
Scanning Electron Microscopy	SEM
Shedding MicroVesicles	SMVs
Side Scattering	SSC
Size exclusion chromatography	SEC
Soft Corona	SC
Sphingomyelina	SM
Transmission Electron Microscopy	TEM
Ultrafiltration	UF
Zeta Potential	ZP
1-palmitoyl-2-oleoyl-phosphatidylcholine	POPC
1,2-dimyristoyl-sn-glycero-3-phosphocholine	DMPC
4′,6- diamidino-2-phenylindole	DAPI

Collaborations

- Department of Molecular Medicine and Medical Biotechnologies, University of Naples Federico II, via S. Pansini 5, Naples 80131, Italy
- CEINGE Advanced Biotechnologies S.C. A R.L., via Gaetano Salvatore 486, Naples 80145, Italy
- Department of Public Health, University of Naples Federico II, via S. Pansini 5, Naples 80131, Italy
- Laboratory for Orthopaedic Pathophysiology and Regenerative Medicine, IRCCS Istituto Ortopedico Rizzoli, via di Barbiano 1/10, Bologna 40136, Italy,

Communications to Congress / Conference of the student in the three years of activity

School of Nanomedicine 3rd Course
Ettore Majorana Foundation and centre for scientific Culture Erice, 5-11 April 2018
"Nanofluidics, Nanoimaging and Nanomanipulation"
Poster Presentation

EIT Health Summer School 2019
Trinity College Dublin, 16-25 June 2019
"Biology of Brain Disorders: New Frontiers in Innovation"
Poster and Oral Presentation

International Conference ISEV 2021
International Society of Extracellular Vesicles
Poster Presentation

List of publications of the doctoral candidate

Tammaro, O., A. C. di Polidoro, E. Romano, P. A. Netti and E. Torino. "A microfluidic platform to design multimodal peg-crosslinked hyaluronic acid nanoparticles (peg-chanps) for diagnostic applications." Scientific reports 10 (2020): 1-11.

Romano, E., P. A. Netti and E. Torino. "Exosomes in gliomas: Biogenesis, isolation, and preliminary applications in nanomedicine." Pharmaceuticals 13 (2020): 319.

Costagliola di Polidoro, A., A. Grassia, F. De Sarno, P. Bevilacqua, V. Mollo, E. Romano, M. D. Di Taranto, G. Fortunato, U. M. Bracale and L. Tramontano. "Targeting nanostrategies for imaging of atherosclerosis." Contrast media & molecular imaging 2021 (2021):

A process based on Dynamic High-Pressure in microfluidics for the high throughput Encapsulation of active compounds in Exosomes for therapy and diagnosis– **Patent Pending**

A process based on Dynamic High-Pressure Homogenization in microfluidics for the high throughput isolation of Exosome from cell lines, mesenchymal stem cells and other biological entities- **Patent Pending**